Exchange bias effect of ferro-/antiferromagnetic heterostructures

Florin Radu[*]

BESSY GmbH, Albert-Einstein-Str. 15, 12489 Berlin, Germany

Hartmut Zabel[†]

Department of Physics, Ruhr-University Bochum, D 44780 Bochum, Germany

The exchange bias (EB) effect was discovered 60 years ago by Meiklejohn and Bean. Meanwhile the EB effect has become an integral part of modern magnetism with implications for basic research and for numerous device applications. The EB effect was the first of its kind which relates to an interface effect between two different classes of materials, here between a ferromagnet and an antiferromagnet. Here we review fundamental aspects of the exchange bias effect.

Contents

[*]Electronic address: florin.radu@rub.de
[†]Electronic address: Hartmut.Zabel@rub.de

I. INTRODUCTION

The exchange bias (EB) effect was discovered 60 years ago by Meiklejohn and Bean (92). Meanwhile the EB effect has become an integral part of modern magnetism with implications for basic research and for numerous device applications. The EB effect was the first of its kind which relates to an interface effect between two different classes of materials, here between a ferromagnet and an antiferromagnet. Later on the interlayer exchange coupling between ferromagnets interleaved by paramagnet layers was discovered (49), and the proximity effect between ferromagnetic and superconducting layers was described (127; 175). Recent reviews on these topics can be found in Refs: (8; 19; 20) and also in this book. The EB effect manifests itself in a shift of the hysteresis loop to negative or positive direction with respect to the applied field. Its origin is related to the magnetic coupling across the common interface shared by a ferromagnetic (F) and an antiferromagnetic (AF) layer. Extensive research is being carried out to unveil the details of this effect, which has resulted in more then 600 publications in the last five years and since the last comprehensive reviews by

Nogues and Schuller (109), Kiwi (72), Berkowitz (9), and Stamps (155).

An EB bilayer consists of two key elements, with rather different magnetic and structural properties: the ferromagnetic layer and the antiferromagnetic layer. While the ferromagnetic layer can be studied in detail by using laboratory equipment like SQUID, MOKE and MFM, this is not the case for the magnetic interface and for the antiferromagnetic layer. The interface embedded in between the F and AF layer has low volume, therefore it is difficult to separate its contribution from the F layer. Still, for the exchange bias effect the interfacial magnetic properties are essential for understanding the effect. For this purpose polarized neutron scattering and soft-xray magnetic scattering techniques can reveal some of the key magnetic properties of the interface. The AF layer has in principle no macroscopic magnetization, even so the magnetic moment of individual atoms are rather high. The magnetic properties of the AF materials are traditionally studied by neutron diffraction. In thin films, due to the reduced AF volume available for scattering, this method is rather difficult to apply. Here, soft-xray magnetic scattering through the linear dichroism can reveal information about the magnetic properties of the AF layer, therefore providing useful insights into the origin of the EB effect.

From the application point of view the situation appears to be less complex. The effect is being used in spin valves with one pinned and one free ferromagnetic layer which are embedded in devices such as storage media, readout sensors, and magnetic random access memory(MRAM). Nevertheless, robust, reliable and easy to control functional elements based on the exchange bias phenomenon require more understanding of the fundamentals of the effect, which is further motivating research in this field.

Because of recent experimental verifications of the existence of interfacial layers by several groups (54; 78; 118; 119; 120; 130; 131; 136; 137; 145; 170; 172), earlier models of EB need to be revisited and eventually modified to take into account the effects, which are introduced by this layer.

Here we first review some of the basic models for exchange bias. We focus on numerical calculations and analytical treatment of those models which are based on the Stoner-Wohlfarth model (159; 160). This has the advantage that analytical expressions can be derived and a numerical analysis can be much more efficiently performed as compared to micromagnetic simulations. It has, however, the disadvantage that only coherent magnetization reversal processes are described within this formalism. Nevertheless, for a large fraction of experimental situations the Stoner-Wolhfarth approach is adequate. The behavior of the F and AF spins during the magnetization reversal, as well as the dependence of the critical fields on the parameters of the F and AF layer are analyzed in detail. The Meiklejohn and Bean (91; 92; 93) model and the Mauri models (89) are revisited and numerical

and analytical expressions are compared. We continue with describing the main features of the Random Field model of Malozemoff (84; 85; 86) and Domain State(DS) model (5; 6; 98; 101; 115; 116; 117; 147). Then,we review the Kim and Stamp approach (69) which focuses on spring-like behavior of the AF layers and coercivity enhancement. We continue with one of the most recent models for exchange bias, the Spin Glass (SG) model (133). Assuming a realistic state of the interface between the F and AF layers, the SG model describes well most of the important features of EB heterostructures, including azimuthal dependence of exchange bias field and coercivity, AF and F thickness dependence, the inverse linear dependence on the lateral extension, and training effects. Finally we will discuss recent experiments in the light of the presented models. However, the main emphasis of this review is to describe the basic models in a systematic fashion and to compare them with recent experimental results.

II. STONER-WOHLFARTH MODEL

The term anisotropy refers to the orientation of the magnetic moments with respect to given geometrical directions. In bulk materials the crystal axes are the reference directions, while in thin films other reference systems become important. In order to account for the orientation of the magnetic moments in magnetic materials, the minimum energy state is provided by analysis of the different contributing terms to the total magnetic energy: Zeeman term, anisotropy terms, and exchange coupling terms. This evaluation is performed by minimization of the total magnetic energy with respect to various parameters.
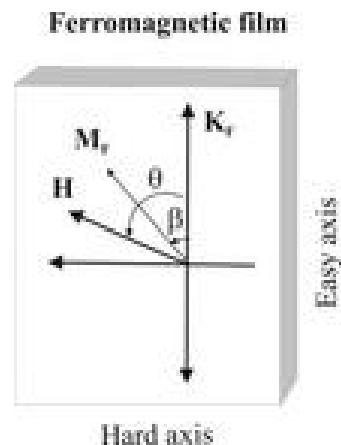

FIG. 1 Definition of angles and vectors used in Stoner-Wohlfarth type model calculations. The reference direction of the film is along the unidirectional anisotropy.

In the following we use the simplest possible expression for the total magnetic energy for a ferromagnetic thin film and calculate the magnetic hysteresis loops. We

assume that all spins are confined in the film plane and that the film has a uniaxial anisotropy. The response of the magnetization to an applied magnetic field is then uniform. Therefore the spins will coherently rotate during the variation of the external field. The direction of the magnetization can be described by only one parameter, namely the $(\theta - \beta)$ angle defining the direction of the magnetization with respect to the applied field (see Fig. 1). Many complexities of the magnetization reversal are neglected in this approach. Nevertheless, the Stoner-Wohlfarth (SW) model (25; 159; 160), named after the investigators who developed it for treating the magnetization reversal of a small single domain, is used with considerable success for various magnetic thin films and heterostructures.

FIG. 3 a) The azimuthal dependence of the normalized coercive field of a ferromagnetic film with uniaxial anisotropy. The curve is calculated with Eq. 5. b) The azimuthal dependence of the normalized irreversible switching field of a ferromagnetic film with uniaxial anisotropy. The curve is calculated using Eq. 7.

The minimization of the total magnetic energy with respect to the angle β and the stability equation:

$$\frac{\partial E_V(\beta)}{\partial \beta} = 0, \qquad \frac{\partial^2 E_V(\beta)}{\partial \beta^2} > 0 \qquad (2)$$

leads to the following equations:

$$-\mu_0 \, H \, M_F \, \sin(\theta - \beta) + K_F \, \sin(2\beta) = 0 \qquad (3)$$
$$\mu_0 \, H \, M_F \, \cos(\beta - \theta) + 2K_F \, \cos(2\beta) > 0 \qquad (4)$$

By solving Eq. 3 with the condition imposed by the Eq. 4 one obtains the β angle, which determines the longitudinal component ($m_{||} = \cos(\beta - \theta)$) and the transverse component ($m_\perp = \sin(\beta - \theta)$) of the magnetization. Both components are plotted in Fig. 2 for different in-plane orientations (θ). The evolution of the hysteresis loops for different angles θ between the applied magnetic field and the orientation of the uniaxial anisotropy is shown in the left column of Fig. 2 and reflects the typical behavior of thin films with in-plane uniaxial anisotropy. Along the easy axis the hysteresis loop is square shaped and the transverse component is zero. When the applied field is perpendicular to the anisotropy axis (hard axis), the hysteresis loop has a linear slope, whereas the transverse component is ovally shaped.

The expression for the coercive field can easily be inferred from
Eq. 3:

$$H_c(\theta) = \frac{2K_F}{\mu_0 \, M_F} \, |\cos\theta| \qquad (5)$$

For the hysteresis loops shown in Fig. 2, the coercive field follows in detail the expression above. At the position of the easy axis ($\theta = 0, \pi$) the coercive field is equal to the anisotropy field $H_a = 2K_F/\mu_0 M_F$, whereas along the hard axis ($\theta = \pm\pi/2$) the coercive field is zero. Experimentally, this is an often encountered situation. For instance, polycrystalline magnetic films grown on a-plane sapphire substrates show such uniaxial and growth induced anisotropy due to steps at the substrate surface.
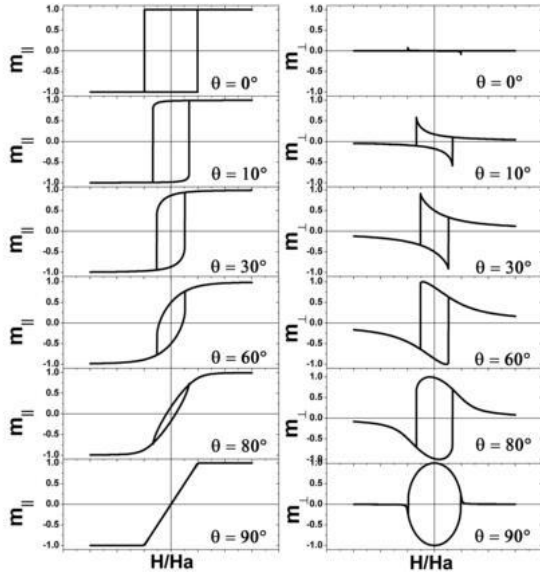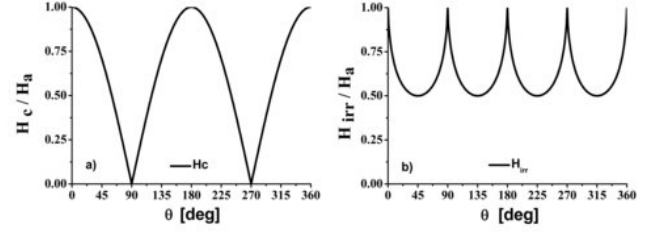

FIG. 2 The longitudinal (left column) and transverse (right column) components of the magnetization for a film with in-plane anisotropy. The curves are generated by numerical evaluation of Eq. 3.

The total magnetic energy per unit volume of a ferromagnetic film with in-plane uniaxial anisotropy reads:

$$E_V(\beta) = -\mu_0 \, H \, M_F \, cos(\theta - \beta) + K_F \, \sin^2(\beta), \qquad (1)$$

where the first term is the Zeeman energy contribution and the second term is the magnetic crystalline anisotropy (MCA), here assumed to have an uniaxial symmetry. The other parameters are: H for the applied field, M_F for the saturation magnetization of the ferromagnet, K_F for the volume anisotropy constant of the ferromagnet, and θ for the orientation of the applied magnetic field with respect to the uniaxial anisotropy direction, and β the orientation of the magnetization vector during the magnetization reversal.

Aside from the coercive field dependence as a function of the azimuthal angle θ, another critical field can be recognized in Fig. 2. This is the field where the magnetization changes irreversibly (i.e. where the hysteresis opens). This irreversible switching field H_{irr} can be extracted by solving both Eqs. 3 and 4. Expressing the applied magnetic field $\boldsymbol{H}$ by its components along the easy and hard axis directions: $\boldsymbol{H} = (H_x, H_y) = (H\cos\theta, H\sin\theta)$, the solution of the system of equations Eq. 3 and 4 gives: $H_x = -H_a\cos^3\beta$ and $H_y = +H_a\cos^3\beta$. Eliminating β from the previous two equations we obtain the asteroid equation (25; 153; 166):

$$|H_x|^{2/3} + |H_y|^{2/3} = H_a^{2/3} \qquad (6)$$

Now, introducing back into the equation above the expression for the field components we obtain for the irreversible switching field the following expression (25; 153; 166):

$$\frac{H_{irr}}{H_a} = \frac{1}{[(\sin^2\theta)^{2/3} + (\cos^2\theta)^{2/3}]^{3/2}} \qquad (7)$$
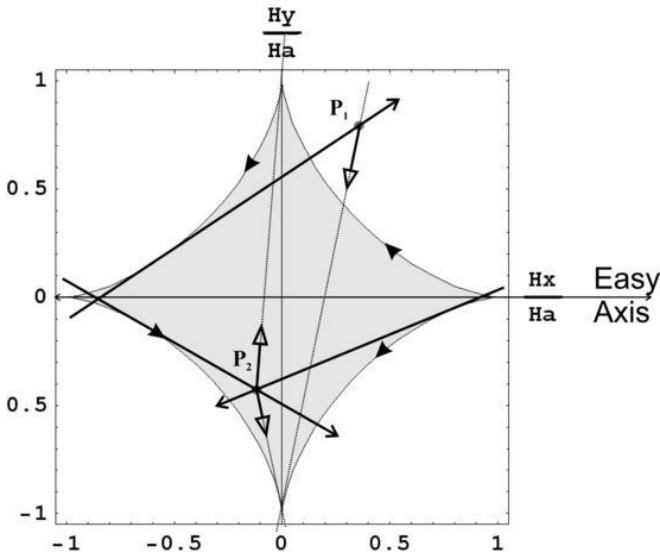

FIG. 4 The asteroid curve for a film with uniaxial anisotropy. Two situations are depicted for finding a geometrical solution to the Eq 6: a) The magnetic field represented as a point P1 lying outside the asteroid region exhibits one stable solution (solid line with filled arrow) and one unstable one (solid line with open arrow). b) A magnetic field P2 within the asteroid curve exhibits four solutions(see the tangent lines):two of them are stable (solid line with filled arrow) and the other two are unstable(solid line with open arrow).The dotted line show tangents for the unstable solutions (25; 153; 166).

This field is plotted in the right panel of Fig. 3. At the position of the easy axis ($\theta = 0, \pi$) the irreversible field is equal to the anisotropy field H_a, whereas at $\theta = \pi/4, 3\pi/4$, the irreversible field is equal to half of the anisotropy field ($H_{irr}(\pi/4) = H_a/2$). The irreversible switching field can be experimentally extracted from the transverse components of the magnetization, whereas the coercive field is extracted from the longitudinal component of the magnetization(see Fig. 2).

Fig. 4 shows the so called asteroid curve which defines stability criteria for the magnetization reversal(Eq. 6). The asteroid method refers to an elegant geometrical solution of Eq. 1 introduced by Slonczewski (153). An extended analysis can be found in Ref. (166). The field measured in units of H_a appears as a point in Fig. 4. Given a field P1 outside the asteroid curve, two solutions can be found by drawing tangent lines to the critical curve. Only one is a stable solution and is given by the tangent closest to the easy axis, orienting the magnetization towards the field. For fields inside the asteroid curve (P2) four tangents leading to four solutions can drawn. Two solutions are stable and the other two are unstable. The magnetization is stable oriented along the corresponding tangent (153; 166).

III. DISCOVERY OF THE EXCHANGE BIAS EFFECT

The exchange bias (EB) effect, also known as unidirectional anisotropy, was discovered in 1956 by Meiklejohn and Bean (91; 92; 93) when studying Co particles embedded in their native antiferromagnetic oxide CoO. It was concluded from the beginning that the displacement of the hysteresis loop is brought about by the existence of an oxide layer surrounding the Co particles. This implies that the magnetic interaction across their common interface is essential in establishing the effect. Being recognized as an interfacial effect, the studies of the EB effect have been performed mainly on thin films consisting of a ferromagnetic layer in contact with an antiferromagnetic one. Recently, however, the lithographically prepared structures as well as F and AF particles are studied with renewed vigor.

In Fig. 5 the original figures from Ref. (92; 93) show the shift of a hysteresis loop of Co-CoO particles. The system was cooled from room temperature down to 77 K through the Néel temperature of CoO(T_N (CoO) = 291 K). The magnetization curve is shown in Fig. 5a) as a dashed line. It is symmetrically centered around zero value of the applied field, which is the general behavior of ferromagnetic materials. When, however, the sample is cooled in a positive magnetic field, the hysteresis loop is displaced to negative values (see continuous line of Fig. 5a). Such displacement did not disappear even when extremely high applied fields of 70 000 Oe were used.

In order to get more insight into this unusual effect, the authors studied the anisotropy behavior by using a self-made torque magnetometer schematically shown in Fig. 5d). It consists of a spring connected to a sample placed in an external magnetic field. Generally, torque magnetometry is an accurate method for measuring the magnetocrystalline anisotropy (MCA) of single crystal
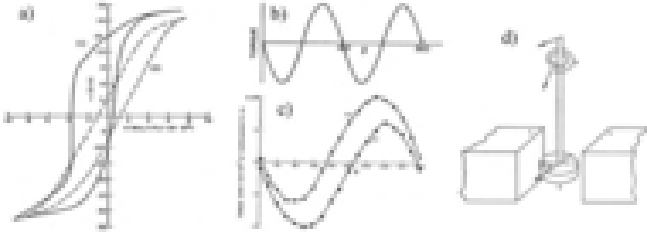
FIG. 5 a) Hysteresis loops of Co-CoO particles taken at 77° K. The dashed line shows the loop after cooling in zero field. The solid line is the hysteresis loop measured after cooling the system in a field of 10 kOe. b) Torque curve for Co particles at 300 K showing uniaxial anisotropy. b) Torque curve of Co-CoO particles taken at 77°K showing the unusual unidirectioal anisotropy. d) The torque magnetometer. The main component is a spring which measures the torque as a function of the θ angle on a sample placed in a magnetic field. (92; 93)

ferromagnets. The torque on a sample is measured as a function of the angle θ between certain crystallographic directions and the applied magnetic field. In strong external fields, when the magnetization of the sample is almost parallel to the applied field (saturation), the torque is equal to:

$$T = -\frac{\partial E(\theta)}{\partial \theta},$$

where $E(\theta)$ is the MCA energy. In the case of Co, which has a hexagonal structure, the torque about an axis perpendicular to the c-axis follows a $\sin(2\theta)$ function as seen in Fig. 5b). The torque and the energy density can then be written as:

$$T = -K_1 \sin(2\theta)$$

$$E_V = \int K_1 \sin(2\theta)\, d\theta = K_1 \sin^2(\theta) + K_0,$$

where K_1 is the MCA anisotropy and K_0 is an integration constant. It is clearly seen from the energy expression that along the c-axis, at $\theta = 0$ and $\theta = 180°$, the particles are in a stable equilibrium. This typical case of a uniaxial anisotropy is seen for the Co particles at room temperature, where the CoO is in a paramagnetic state. At 77°K, after field cooling, the CoO is in an antiferromagnetic state. Here, the torque curve of the Co-CoO system looks completely different as seen in Fig. 5c). The torque curve is a function of $\sin(\theta)$:

$$T = -K_u \sin(\theta), \tag{8}$$

hence,

$$E_V = \int K_u \sin(\theta)\, d\theta = -K_u \cos(\theta) + K_0, \tag{9}$$

The energy function shows that the particles are in equilibrium for one position only, namely $\theta = 0$. Rotating

the sample to any angle, it tries to return to the original position. This direction is parallel to the field cooling direction and such anisotropy was named *unidirectional anisotropy*.

Now, one can analyze whether the same unidirectional anisotropy observed by torque magnetometry is also responsible for the loop shift. In Fig. 1 are shown schematically the vectors involved in writing the energy per unit volume for a ferromagnetic layer with uniaxial anisotropy having the magnetization oriented opposite to the field. It reads:

$$E_V = -\mu_0 H M_F \cos(-\beta) + K_F \sin^2(\beta) \tag{10}$$

where H is the external field, M_F is the saturation magnetization of the ferromagnet per unit volume, and K_F is the MCA of the F layer. The two terms entering in the formula above are the Zeeman interaction energy of the external field with the magnetization of the F layer and the MCA energy of the F layer, respectively. Now, writing the stability conditions and assuming that the field is parallel to the easy axis, we find that the coercive field is:

$$H_c = 2\, K_F / \mu_0\, M_F \tag{11}$$

Next step is to cool the system down in an external magnetic field and to introduce in Eq. 10 the unidirectional anisotropy term. The expression for the energy density then becomes:

$$E_V = -\mu_0 H M_F \cos(-\beta) + K_F \sin^2(\beta) - K_u \cos(\beta) \tag{12}$$

We notice that the solution is identical to the previous case (Eq. 10) with the substitution of an effective field: $H' = H + K_u/M_F$. This causes the hysteresis loop to be shifted by $-K_u/\mu_0 M_F$. Thus, Meiklejohn and Bean concluded that the loop displacement is equivalent to the explanation for the unidirectional anisotropy.

Besides the shift of the magnetization curve and the unidirectional anisotropy, Meiklejohn and Bean have observed another effect when measuring the torque curves. Their experiments revealed an appreciable hysteresis of the torque (see Fig. 9 and Fig. 10 of Ref (93) and Fig. 2 of Ref (91)), indicating that irreversible changes of the magnetic state of the sample take place when rotating the sample in an external magnetic field. As the system did not display any rotational anisotropy when the AF was in the paramagnetic state, this provided evidence for the coupling between the AF CoO shell and the F Co core. Such irreversible changes were suggested to take place in the AF layer.

IV. IDEAL MODEL OF THE EXCHANGE BIAS: PHENOMENOLOGY

The macroscopic observation of the magnetization curve shift due to unidirectional anisotropy of a F/AF bilayer can qualitatively be understood by analyzing the microscopic magnetic state of their common interface.

Phenomenologically, the onset of exchange bias is depicted in Fig. 6. A ferromagnetic layer is in close contact to an antiferromagnetic one. Their critical temperatures should satisfy the condition: $T_C > T_N$, where T_C is the Curie temperature of the ferromagnetic layer and T_N is the Néel temperature of the antiferromagnetic layer. At a temperature which is higher than the Néel temperature of the AF layer and lower than the Curie temperature of the ferromagnet ($T_N < T < T_C$), the F spins align along the direction of the applied field, whereas the AF spins remain randomly oriented in a paramagnetic state (see Fig 6 1)). The hysteresis curve of the ferromagnet is centered around zero, not being affected by the proximity of the AF layer. Next, we saturate the ferromagnet by applying a high enough external field H_{FC} and then, without changing the magnitude or direction of the applied field, the temperature is decreased to a finite value lower then T_N (*field cooling procedure*).
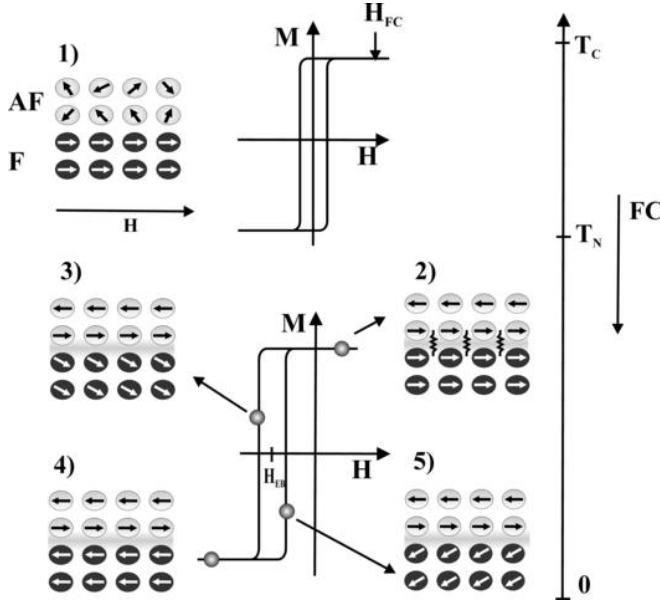

FIG. 6 Phenomenological model of exchange bias for an AF-F bilayer. 1) The spin configuration at a temperature which is higher than T_N and smaller than T_C. The AF layer is in a paramagnetic state while the F layer is ordered. Its magnetization curve (top-right) is centered around zero value of the applied field. Pannel 2): the spin configuration of the AF and F layer after field cooling the system through T_N of the AF layer in a positive applied magnetic field (H_{FC}). Due to uncompensated spins at the AF interface, the F layer is coupled to the AF layer. Panel 4): the saturated state at negative fields. Panel 3) and 5) show the configuration of the spins during the remagnetization, assuming that this takes place through in-plane rotation of the F spins. The center of magnetization curve is displaced at negative values of the applied field by H_{eb}. (The description is in accordance with Ref. (92; 93; 109))

After field cooling the system, due to exchange interaction at the interface the first monolayer of the AF layer will align parallel (or antiparallel) to the F spins. The next monolayer of the antiferromagnet will align antiparallel to the previous layer as to complete AF order, and so on (see Fig 6-2). Note that the spins at the AF interface are uncompensated, leading to a finite net magnetization of this monolayer. It is assumed that both the ferromagnet and the antiferromagnet are in a single domain state and that they will remain in this single domain state during the magnetization reversal process. When reversing the field, the F spins will try to rotate in-plane to the opposite direction. Being coupled to the AF spins, it takes a bigger force and therefore a stronger external field to overcome this coupling and to rotate the ferromagnetic spins. As a result, the first coercive field is higher than it used to be at $T > T_N$, where the F/AF interaction is not yet active. On the way back from negative saturation to positive field values (Fig 6 4)), the F spins require a smaller external force in order to rotate back (Fig 6 5)) to the original direction. A torque is acting on the F spins for all other angles, except the stable direction which is along the field cooling direction (unidirectional anisotropy). As a result, the magnetization curve is shifted to negative values of the applied field. This displacement of the center of the hysteresis loop is called *exchange bias field*, and is negative in relation to the orientation of the F spins after field cooling (*negative exchange bias*). It should be noted that in this simple description the AF spins are considered to be rigid and fixed to the field cooling direction during the entire reversal process.

V. THE IDEAL MEIKLEJOHN-BEAN MODEL: QUANTITATIVE ANALYSIS

Based on their observation about the rotational anisotropy, Meiklejohn and Bean proposed a model to account for the magnitude of the hysteresis shift. The assumptions made are the following (25; 92; 109):

- The F layer rotates rigidly, as a whole

- Both the F and AF are in a single domain state

- The AF/F interface is atomically smooth.

- The AF layer is magnetically rigid, meaning that the AF spins remain unchanged during the rotation of the F spins

- The spins of the AF interface are fully uncompensated: the interface layer has a net magnetic moment

- The F and the AF layers are coupled by an exchange interaction across the F/AF interface. The parameter assigned to this interaction is the interfacial exchange coupling energy per unit area J_{eb}

- The AF layer has an in-plane uniaxial anisotropy

In general, for describing the coherent rotation of the magnetization vector the Stoner-Wohlfarth (159; 160)

model is used. Different energy terms can be added as needed and to best account for the quantitative and qualitative behavior of the macroscopic magnetization reversal. In Fig. 7 is shown schematically the geometry of the vectors involved in the ideal Meiklejohn and Bean model. H is the applied magnetic field, which makes an angle θ with respect to the field cooling direction denoted by $\theta = 0$, K_F and K_{AF} are the uniaxial anisotropy directions of the F and the AF layer, respectively. They are assumed to be oriented parallel to the field cooling direction. M_F is the magnetization orientation of the F spins during the magnetization reversal. It is assumed that the AF spins are fixed to their orientation defined during the field cooling procedure (rigid AF). In the analysis below the angle $(\theta = 0)$ for the applied field is assumed to be parallel to the field cooling direction. This condition refers to the direction along which the hysteresis loops is measured , whereas $\theta \neq 0$ is used for torque measurements or for measuring the azimuthal dependence of the exchange bias field.
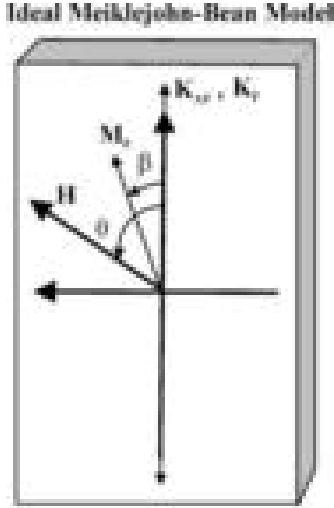
Ideal Meiklejohn-Bean Model

FIG. 7 Schematic view of the angles and vectors used in the ideal Meiklejohn and Bean model. The AF layer is assumed to be rigid and no deviation from its initially set orientation is allowed. K_{AF} and K_F are the anisotropy of the AF layer and F layer, respectively, which are assumed to be parallel oriented to the field cooling direction. β is the angle between magnetization vector M_F of the F layer and the anisotropy direction of the F layer. This angle is variable during the magnetization reversal. H is the external magnetic field which can be applied at any direction θ with respect to the field cooling direction at $\theta = 0$ (see Ref. (92; 93; 109)).

Within this model the energy per unit area assuming coherent rotation of the magnetization, can be written as (92; 109; 155):

$$E_A = -\mu_0 H M_F t_F \cos(-\beta) + K_F t_F \sin^2(\beta) - J_{eb} \cos(\beta) \tag{13}$$

where $J_{eb} [J/m^2]$ is the interfacial exchange energy per unit area, and M_F is the saturation magnetization of

the ferromagnetic layer. The interfacial exchange energy can be further expressed in terms of pair exchange interactions: $E_{int} = \sum_{ij} J_{ij} S_i^{AF} S_j^F$, where the summation includes all interactions within the range of the exchange coupling (43; 84; 85; 161).

The stability condition $\partial E_A / \partial \theta = 0$ has two types of solutions: one is $\beta = \cos^{-1}[(J_{eb} - \mu_0 H M_F t_F)/(2 K_F)]$ for $\mu_0 H M_F t_F - J_{eb} \leq 2 K_F$, ; the other one is $\beta = 0, \pi$ for $\mu_0 H M_F t_F - J_{eb} \geq 2 K_F$, corresponding to positive and negative saturation, respectively. The coercive fields H_{c1} and H_{c2} are extracted from the stability equation above for $\beta = 0, \pi$:

$$H_{c1} = -\frac{2 K_F t_F + J_{eb}}{\mu_0 M_F t_F} \tag{14}$$

$$H_{c2} = \frac{2 K_F t_F - J_{eb}}{\mu_0 M_F t_F} \tag{15}$$

Using the expressions above, the coercive field H_c of the loop and the displacement H_{eb} can be calculated according to:

$$H_c = \frac{-H_{c1} + H_{c2}}{2} \text{ and } H_{eb} = \frac{H_{c1} + H_{c2}}{2} \tag{16}$$

which further gives:

$$H_c = \frac{2 K_F}{\mu_0 M_F} \tag{17}$$

and

$$H_{eb} = -\frac{J_{eb}}{\mu_0 M_F t_F} \tag{18}$$

The equation Eq. 18 is the master formula of the EB effect. It gives the expected characteristics of the hysteresis loop for an ideal case, in particular the linear dependence on the interfacial energy J_{eb} and the inverse dependence on the ferromagnetic layer thickness. Therefore this equation serves as a guideline to which experimental values are compared. In the next section we will discuss some predictions of the model above.

A. The sign of the exchange bias

Eq. 18 predicts that the sign of the exchange bias is negative. Almost all hysteresis loops shown in the literature are shifted oppositely to the field cooling direction. The positive or negative exchange coupling across the interface produces the same sign of the exchange bias field. There are, however, exceptions. Positive exchange bias was observed for CoO/Co, $Fe_x Zn_{1-x} F_2/Co$ and $Cu_{1-x} Mn_x/Co$ bilayers when the measuring temperature was close to the blocking temperature (2; 48; 126; 130; 152). At low temperatures positive exchange bias was observed in Fe/FeF_2 (107) and Fe/MnF_2 (81) bilayers. Specific of the last two systems is the low anisotropy

of the antiferromagnet and the antiferromagnetic type of coupling between the F and AF layers. It was proposed that, at high cooling fields, the interface layer of the antiferromagnet aligns ferromagnetically with the external applied field and therefore ferromagnetically with the F itself. As the preferred orientation between the interface spins of the F layer and AF layer is the antiparallel one (AF coupling), the EB becomes positive. Further theoretical and experimental details of the positive exchange bias mechanism are presented in Ref. (61; 64; 71). In the original Meiklejohn and Bean model the interaction of the cooling field with the AF spins is not taken into account. However this interaction can be easily introduced in their model. The positive exchange bias could also be accounted for in the M&B model by simply changing the sign of J_{eb} in Eq. 13 from negative to positive.

B. The magnitude of the EB

Often the exchange coupling parameter J_{eb} is identified with the exchange constant of the AF layer (J_{AF}). For various calculations a value ranging from J_{AF} to J_F was assumed. For CoO, $J_{AF} = 21.6 K = 1.86$ meV (135). Using this value, the expected exchange coupling constant J_{eb} of a CoO(111)/F layer can be estimated as (84; 99):

$$J_{eb} = N J_{AF}/A = 4\, mJ/m^2, \qquad (19)$$

where $N = 4$ is the number of Co^{2+} ions at the uncompensated CoO interface per unit area $A = \sqrt{(3)}\, a^2$, and $a = 4.27$ Å is the CoO lattice parameter. With this number we would expect for a 100 Å thick Co layer, which shares an interface with a CoO AF layer, an exchange bias of:

$$H_{eb}\,[Oe] = \frac{J_{eb}\,[J/m^2]}{M_F\,[kA/m]\,t_F\,[\text{Å}]}\, 10^{11} \qquad (20)$$

$$H_{eb} = \frac{0.004}{1460 \times 100}\, 10^{11} = 2740\ Oe$$

This exchange bias field is by far bigger than experimentally observed. So far an ideal magnitude of the EB field as predicted by the Eq. 19 has not yet been observed, even so for some bilayers high EB fields were measured (see Table I). We encounter here two problems: first, we do not know how to evaluate the real coupling constant J_{eb} at the interfaces with variable degrees of complexity, and the second, in reality interfaces are never atomically smooth. The unknown interface was nicely labelled by Kiwi (72) as "a hard nut to crack". Indeed, the features of the interfaces may be complex regarding the structure, the roughness, the magnetic properties, and domain state of the AF and F layers.

TABLE I Experimental values related to Co/CoO exchange bias systems. The symbols used in the table are: *ebe*-electron-beam evaporation, *rsp*-reactive sputtering, *msp*-magnetron sputtering, *mbe*-molecular beam epitaxy, F-ferromagnet, AF antiferromagnet, t_{AF}-the thickness of the AF, t_F-the thickness of the F, H_{eb}-measured exchange bias field, H_c-measured coercive field, T_{mes}-measured blocking temperature, T_{mes}-the measuring temperature, J_{eb}-the coupling energy extracted from the experimental value of exchange bias field ($J_{eb} = H_{eb}\,(\mu_0 M_F t_F)$).

AF	F	t_{AF} [Å]	t_F [Å]	H_{eb} [Oe]	H_c [Oe]	T_B [K]	T_{mes} [K]	J_{eb} [mJ/m²]	Ref
CoO (air)	Co(rsp)	20	40	-3000	NA	-	4.2	1.75	(97)
CoO (air)	Co(rsp)	25	27	-2321	3683	180	10	0.91	(130)
CoO (air)	Co(rsp)	25	56	-1073	1751	180	10	0.88	(130)
CoO (air)	Co(rsp)	25	87	-675	1315	180	10	0.86	(130)
CoO (air)	Co(rsp)	25	119	-557	901	180	10	0.97	(130)
CoO (air)	Co(rsp)	25	153	-443	789	180	10	0.99	(130)
CoO (air)	Co(rsp)	25	260	-251	427	180	10	0.95	(130)
CoO (air)	Co(rsp)	25	320	-202	346	180	10	0.94	(130)
CoO (air)	Co(rsp)	25	398	-174	290	180	10	1.00	(130)
CoO (air)	Co(msp)	33	139	-145	325	-	5	0.29	(162)
CoO (air)	Co(msp)	33	139	-50	NA	-	30	0.1	(174)
CoO (rsp)	Co(rsp)	20	150	-25	295	-	20	0.055	(48)
[CoO (rsp)	Co(rsp)]$_{x25}$	70	37	-2500	5000	-	5	13.5!	(128)
CoO (in-situ)	Co(ebe)	20	160	-220	330	180	10	0.51	(51)
CoO(111)(mbe)	Fe(110)(mbe)	200	150	-150	520	291	10	0.4	sec. (114; 134)

In Table I are listed some EB data of systems with CoO as the AF layer. We focus on experimentally de-

termined interfacial exchange coupling constants using $J_{eb} = H_{eb}\,\mu_0\,M_F\,t_F$. The observed exchange coupling constant is usually smaller then the expected value of $4\,mJ/m^2$ for CoO/Co bilayers by a factor ranging from 3 to several orders of magnitude. One anomaly is seen for the multilayer system Co/CoO which is actually 3 times higher then the expected value of $4\,mJ/m^2$, and to our knowledge is the highest value observed experimentally (128). Such a variation of the experimental values for the interfacial exchange coupling constant is motivating further considerations of the mechanisms controlling the EB effect.

C. The $1/t_F$ dependence of the EB field

Eq. 18 predicts that the variation of the EB field is proportional to the inverse thickness of the ferromagnet:

$$H_{eb} \approx \frac{1}{t_F} \tag{21}$$

This dependence was subject of a large number of experimental investigations (109), because it is associated with the interfacial nature of the exchange bias effect. For the CoO/Co bilayers no deviation was observed (51), even for very low thicknesses (2 nm) of the Co layer(130). For other systems with thin F layers of the order of several nanometers it was observed that the $1/t_F$ law is not closely obeyed (109). It was suggested that the F layer is no longer laterally continuous (109). Deviations from $1/t_F$ dependence for the other extreme when the F layer is very thick were observed as well (109). For this regime it is assumed that for F layers thicker than the domain wall thickness (500nm for permalloy), the F spins may vary appreciably across the film upon the magnetization reversal (167).

D. Coercivity and exchange bias

According to Eq. 17 the coercivity of the magnetic layer is the same with and without exchange bias effect. This contradicts experimental observations. Usually an increase of the coercive field is observed.

VI. REALISTIC MEIKLEJOHN AND BEAN MODEL

In Ref. (93) a new degree of freedom for the AF spins was introduced: the AF is still rigid, but it can slightly rotate during the magnetization reversal as a whole as indicated in Fig. 8. This parameter was introduced in order to account for the rotational hysteresis observed during the torque measurements. Allowing the AF layer to rotate is not in contradiction to the rigid state of the AF layer, because it is allowed only to rotate as a whole. Therefore, the fourth assumption of the ideal M&B model in section V is removed. The new condition

for the AF spins is: $\alpha \neq 0$. With this new assumption, the equation Eq. 13 reads (91; 109):

$$\begin{aligned} E_A = {} & -\mu_0\,H\,M_F\,t_F\,\cos(\theta - \beta) \\ & + K_F\,t_F\,\sin^2(\beta) + K_{AF}\,t_{AF}\,\sin^2(\alpha) \\ & - J_{eb}\,\cos(\beta - \alpha), \end{aligned} \tag{22}$$

where t_{AF} is the thickness of the antiferromagnet, and K_{AF} is the MCA of the AF layer per unit area. The new energy term in the equation above as compared to Eq. 13 is the anisotropy energy of the AF layer.
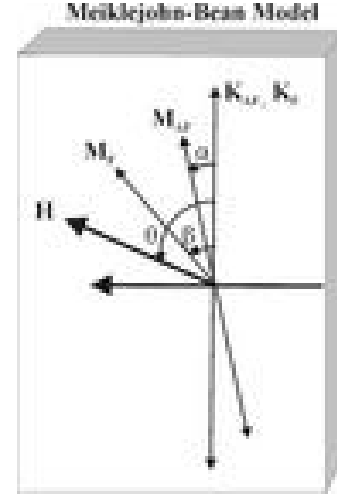

FIG. 8 Schematic view of the angles and vectors used for the Meiklejohn and Bean model, allowing a rotation α of the AF layer as a whole with respect to the initially set orientation. $\boldsymbol{M}_{AF}$ is the sublattice magnetization of the AF layer. $\boldsymbol{K}_{AF}$ and $\boldsymbol{K}_F$ are the anisotropy of the AF layer and F layer, respectively, which are assumed to be parallel oriented to the field cooling direction. β is the angle between F magnetization vector $\boldsymbol{M}_F$ and the anisotropy direction of the F layer. This angle is variable during the magnetization reversal. $\boldsymbol{H}$ is the external magnetic field which can be applied at any direction θ with respect to the field cooling direction at $\theta = 0$ (Ref. (91; 92; 93; 109)).

The Eq. 22 above can be analyzed numerically by minimization of the energy in respect to the α and the β angles. Below we will perform a numerical analysis of Eq. 23 and highlight a few of the conclusions discussed in Ref. (25; 91; 93). The minimization with respect to α and β leads to a system of two equations:

$$\begin{cases} \frac{H}{H_{eb}^{\infty}}\,\sin(\theta - \beta) + \sin(\beta - \alpha) = 0 \\ R\,\sin(2\,\alpha) - \sin(\beta - \alpha) = 0 \end{cases} \tag{23}$$

where

$$H_{eb}^{\infty} \equiv -\frac{J_{eb}}{\mu_0\,M_F\,t_F} \tag{24}$$

is the value of the exchange bias field when the anisotropy of the AF is infinitely large, and

$$R \equiv \frac{K_{AF}\, t_{AF}}{J_{eb}}, \qquad (25)$$

is the parameter defining the ratio between the AF anisotropy energy and the interfacial exchange energy J_{eb}. As we will see further below, exchange bias is only observed, if the AF anisotropy energy is bigger than the exchange energy. The unknown variables α and β are numerically extracted as a function of the applied field H. Note that for clarity reasons the anisotropy of the ferromagnet was neglected ($K_F = 0$) in the system of equation above. As a result the coercivity, which will be discussed further below, is not related to the F layer anymore, but to the AF layer alone. Also, in order to simplify the discussion we consider first the case $\theta = 0$, which corresponds to measuring a hysteresis loop parallel to the field cooling direction.
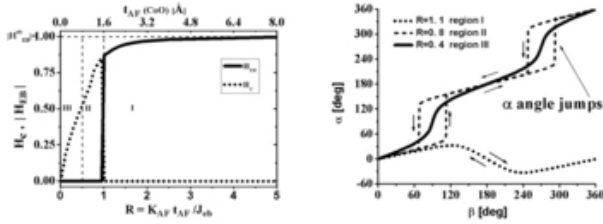

FIG. 9 Left: The phase diagram of the exchange bias field and the coercive fields as a function of the Meiklejohn-Bean parameter R. Right: Typical behavior of the antiferromagnetic angle α for the three different regions of the phase diagram. Only region I can lead to a shift of the hysteresis loop. In the other two regions a coercivity is observed but no exchange bias field.

Numerical evaluation of the Eqs. 23 yields the angles:

- α of the AF spins as a function of the applied field during the hysteresis measurement

- β of the F spins which rotate coherently during their reversal

The β angle defines completely the hysteresis loop and at the same time the coercive fields H_{c1} and H_{c2}. These fields, in turn, define the coercive field H_c and the exchange bias field H_{eb} (see Eq. 16). The α angle influences the shape of the hysteresis loops when the R-ratio has low values, as we will see below. For high R values the rotation angle of the antiferromagnet is close to zero, giving a maximum exchange bias field equal to H_{eb}^{∞}.

The properties of the EB system originate from the properties of the AF layer, which are accounted for by one parameter, the R-ratio. We will consider the effect of the R-ratio on the angels β and α which, as stated above, define the macroscopic behavior and the critical fields of the EB systems.
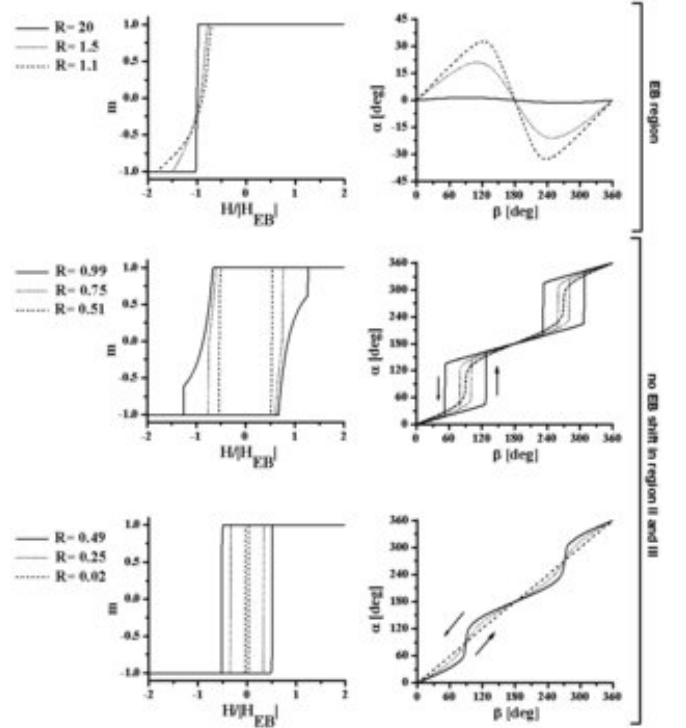

FIG. 10 Simulation of several hysteresis loops and antiferromagnetic spin orientations during the magnetization reversal. For the simulation we used the Meiklejohn-Bean formalism. Top row shows three hysteresis loops calculated for different R ratios within region I. The graph in the last column to the right shows the α angle of the AF layer for the three R values. The middle raw shows corresponding hysteresis loops and α angles for R values in region II. The bottom row shows simulations for region III. Note that the scales for the α angle in the top panel is enlarged compared to those in the lower two panels.

Numerical simulations of Eq. 23 as a function of R-ratio are shown in Fig. 9 and Fig.10. We distinguish three physically distinct regions (25; 35; 91; 93):

- I. $R \geq 1$
  In this region the coercive field is zero and the exchange bias field is finite, decreasing from the asymptotic value H_{eb}^{∞} to the lowest finite value at $R = 1$. The AF spins rotate reversibly during the complete reversal of the F spins. The α angle has a maximum value as a function of the R-ratio, ranging from approximatively zero for $R = \infty$ to $\alpha = 45°$ at $R = 1$. Notice that as the maximum angle of the AF spins increases, a slight decrease of the exchange bias field is observed. When the R-ratio approaches the critical value of unity, the exchange bias has a minimum. In the phase diagram, only range I can cause a shift of the magnetization curve. Simulated hysteresis loops for three different values of the R-ratio are shown in Fig. 10. One notices that not only the size of the exchange bias

field decreases when the R-ratio approaches unity, but also the shape of the hysteresis curve is changing. At high R-ratios the reversal is rather sharp, whereas for R-ratios close to unity it become more extended, almost resembling a spring-like behavior.

- II. $0.5 \leq R < 1$
  Characteristic for this region is that the AF spins are no more reversible. They follow the F spins and they change direction irreversibly, causing a coercive field at the expense of the exchange bias field, which becomes zero. Furthermore, depending on the field sweeping direction, there is a hysteresis-like behavior of the AF spin rotation. At a critical angle β of the F spin rotation, the AF spins cannot withstand the torque by the coupling to the F spins and they jump in a discontinuous fashion to another angle (*jump angle*). The hysteresis loops corresponding to this region (see Fig. 10) are drastically different from the previous case. The coercivity shows strong dependence as function of the R-ratio and they are not shifted at all. Moreover, the AF *jump angles* are clearly visible as kinks in the hysteresis shape during the reversal.

- III. $R < 0.5$
  This region preserves the features of the previous one with one exception, namely that the AF spins follow reversibly the F spins, without any jumps. Therefore, no hysteresis-like behavior of the α angle is seen. The exchange bias field is zero and the coercive field is finite, depending on the R-ratio. The hysteresis loops shown in Fig. 10 are quite similar to a ferromagnet with uniaxial anisotropy. Within the Stoner-Wohlfarth model the resultant coercive field can be roughly approximated as (25): $H_c \approx 2\, K_{AF}\, t_{AF}/(\mu_0\, M_F\, t_F)$.

It is easy to recognize that allowing the AF to rotate as a whole leads to an impressively rich phase diagram of the EB systems as a function of the parameters of the AF layer (and F layer). The R-ratio can be varied across the whole range from zero to infinity by changing the thickness of the AF layer (109), by varying its anisotropy (dilution of the AF layers with non-magnetic impurities (60; 66; 98)) , or by varying the interfacial exchange energy J_{eb} (low dose ion bombardment (23; 59; 102)). Recently (171), an almost ideal M&B behavior has been observed in $Ni_{80}Fe_{20}/Fe_{50}Mn_{50}$ bilayers. At high thicknesses of the AF layer the hysteresis loop is shifted to negative values and the coercivity is almost zero, whereas for reduced AF thicknesses a strong increase of the coercive field is observed together with a drastic decrease of exchange bias.

A. Analytical expression of the exchange bias field

First we calculate analytically the expression of the exchange bias field for $\theta = 0$ and $K_F = 0$. The exact analytical solution is obtained by solving the system of Eqs. 23 for $\beta = 0$, which leads to:

$$H_{eb} = \left\{ \begin{array}{cc} H_{eb}^{\infty}\sqrt{1-\frac{1}{4R^2}} & R \geq 1 \\[2mm] 0 & R < 1 \end{array} \right. \qquad (26)$$

This equation retains the $1/t_F$ dependence of the exchange bias field, but at the same time provides new features. The most important one is an additional term, which effectively lowers the exchange bias field when the R-ratio approaches the critical value of one. The R-ratio has three terms. One of them includes the thickness of the AF layer. The analytical expression for the exchange bias field (Eq. 26) predicts that there is a critical AF thickness t_{AF}^{cr} below which the exchange bias cannot exist. This is (88):

$$t_{AF}^{cr} = \frac{J_{eb}}{K_{AF}} \qquad (27)$$

Below this critical thickness the interfacial energy is transformed into coercivity. Above the critical thickness the exchange bias increases as a function of the AF layer thickness, reaching the asymptotic (ideal) value H_{eb}^{∞} when t_{AF} is infinite. Most recent observation of an AF critical thickness can be found in Ref. (75).

A similar expression as Eq. 26 was derived by Binek et al. (11) using a series expansion of Eq. 22 with respect to $\alpha = 0$: $H_{eb} \approx H_{eb}^{\infty}(1 - \frac{1}{8R^2})$ for $1/R \geq 0$. Note that close to the critical value of $R=1$ the α angle could reach high values up to $45°$. Therefore, the series expansion with respect to $\alpha=0$ is a good approximation for R>5.

B. Azimuthal dependence of the exchange bias field

In the following we consider the exchange bias field in region I, where it acquires non vanishing values. The coercive fields and the exchange bias field are extracted from the condition $\beta = \theta + \pi/2$ for both H_{c1} and H_{c2}. This gives $H_{c1} = H_{c2} = (-J_{eb}/\mu_0 M_F t_F)\cos(\alpha(R, \theta + \pi/2) - \theta)$, where $\alpha(R, \theta + \pi/2)$ is the value of the rotation angle of the AF spins at the coercive field. With the notation: $\alpha_0 \equiv \alpha(R, \theta + \pi/2)$, and using the expression 16, the angular dependence of the exchange bias field becomes:

$$H_{eb}(\theta) = \frac{-J_{eb}}{\mu_0\, M_F\, t_F}\cos(\alpha_0 - \theta) \qquad (28)$$

The equation above can be also written as:

$$H_{eb}(\theta) = -\frac{K_{AF}\, t_{AF}}{\mu_0\, M_F\, t_F}\ \sin(2\,\alpha_0) \qquad (29)$$

Interestingly, the exchange coupling parameter J_{eb} in Eq. 28 is missing in Eq. 29, leaving instead an explicit dependence of the exchange bias field on the parameters of the antiferromagnet and the ferromagnet. The exchange

coupling constant and the θ angle are accounted for by the AF angle α_0.

The Eq. 28 and Eq. 29 are the most general expressions for an exchange bias field. They include both, the influence of the rotation of the AF layer and the influence of the azimuthal orientation of the applied field. Moreover, the anisotropy and the thickness of the AF layer are explicitly shown in Eq. 29. To illustrate their generality we consider below two special cases for the Eq. 28:

- $\theta = 0$

  In this case the hysteresis loop is measured along the field cooling direction ($\theta = 0$) and Eq. 28 becomes equivalent to the Eq. 26.

- $R \to \infty$

  When R is very large ($R \gg 1$), α approximates zero, i.e. the rotation of the AF - layer becomes negligible. This is actually the original assumption of the Meiklejohn and Bean model. Such a condition ($R \to \infty$) is approximately satisfied for large thicknesses of the AF layer. Then the exchange bias field as function of θ can be written as (11; 13; 70):

$$H_{eb}^{\alpha=0}(\theta) = \frac{-J_{eb}}{\mu_0\,M_F\,t_F}\cos(\theta) \qquad (30)$$

In order to get more insight into the azimuthal dependence of the exchange bias field, we show in Fig. 11 the normalized exchange bias field $H_{eb}(\theta)\,/|H_{eb}^\infty(0)|$ as a function of the θ angle, according to Eq. 28 and Eq. 29, and for three different values of the R ratio ($R = 1.1$, $R = 1.5$, $R = 20$). The α_0 angle (see Fig. 10) was obtained by numerically solving the system of Eqs. 23. For large values of R, the azimuthal dependence of the exchange bias field follows closely a $\cos(\theta)$ unidirectional dependence. When, however, the R-ratio takes small values but larger then unity, the azimuthal behavior of the EB field deviates from the ideal unidirectional characteristic. There are two distinctive features: one is that at $\theta = 0$ the exchange bias field is reduced, and the other one is that the maximum of the exchange bias field is shifted from zero towards negative azimuthal angle values. According to Eq. 28 this shift angle is equal to α_0. In other words, the exchange bias field is not maximum along the field cooling direction. Another striking feature is that the shifted maximum of the exchange bias field with respect to the azimuthal angle θ does not depend on thickness and anisotropy of the AF layer:

$$H_{eb}^{MAX} = -\frac{J_{eb}}{\mu_0\,M_F\,t_F}. \qquad (31)$$

Summarizing we may state that, within the Meiklejohn and Bean model, a reduced exchange bias field is observed along the field cooling direction depending on the parameters of the AF layer (K_{AF} and t_{AF}). However, for $R \geq 1$ the maximum value for the exchange bias field which is reached at $\theta \neq 0$ does not depend on the anisotropy constant (K_{AF}) and thickness (t_{AF}) of the AF

layer. The azimuthal characteristic of the exchange bias allows to extract all three essential parameters defining the exchange bias field: J_{eb}, K_{AF} and, t_{AF}.

The condition for extracting the H_{c1} and H_{c2} from the same β angle hides an important property of the magnetization reversal of the ferromagnetic layer. This will be described next.
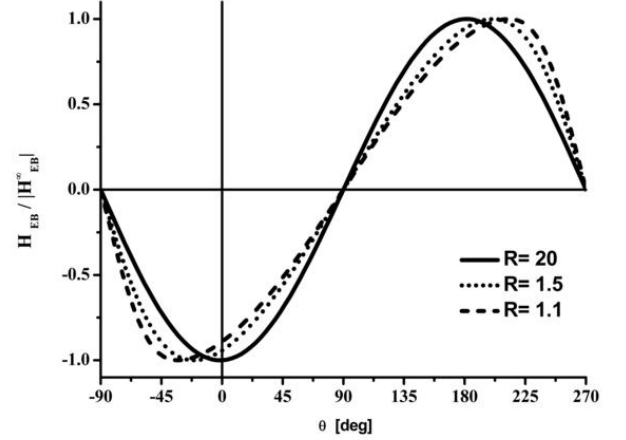

FIG. 11   Azimuthal dependence of exchange bias as a function of the θ angle. The curves are calculated by the Eq.28 and Eq.29.

C. Magnetization reversal

A distinct feature of exchange bias phenomena is the magnetization reversal mechanism. In Fig. 12 is shown the parallel component of the magnetization $m_{||} = \cos(\beta)$ versus the perpendicular component $m_\perp = \sin(\beta)$ for several R-ratios and for $\theta = 30°$. The geometrical conventions are the ones shown in Fig. 8. We see that for $R < 1$ the reversal of the F spins is symmetric, similar to typical ferromagnets with uniaxial anisotropy. Although the regions $0.5 \leq R < 1$ and $R < 0.5$ exhibit different reversal modes of the AF spins (see Fig.10), there is little difference with respect to the F spin rotation. For both regions $0.5 \leq R < 1$ and $R < 0.5$ the F spins do make a full rotation. Similar to the uniaxial ferromagnets. At the steep reversal branches one would expect magnetic domain formation.

When $R \geq 1$ another reversal mechanism is observed. The ferromagnetic spins first rotate towards the unidirectional axis as lowering the field from positive to negative values, and then the rotation proceeds continuously until the negative saturation is reached. On the return path, when the field is swept from negative to positive values, the ferromagnetic spins follow the same path towards the positive saturation. The rotation is continuous without any additional steps or jumps. A similar behavior was observed theoretically within the domain state
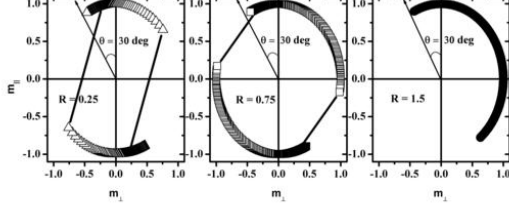
FIG. 12 Magnetization reversal for several values of the R ratio. The parallel component of the magnetization vector $m_{||} = \cos(\beta)$ is plotted as a function of the perpendicular component of the magnetization $m_{\perp} = \sin(\beta)$. The reversal for $R < 1$ resembles the typical reversal of ferromagnets with uniaxial anisotropy. For $R \geq 1$ the reversal proceeds along the same path for the increasing and decreasing branch of the hysteresis loop. The angle $\theta = 30°$ is chosen arbitrarily.

model (5; 6). The magnetization reversal modes can be accessed experimentally by using the Vector-MOKE technique (22; 27; 133; 144) which allows to follow both the magnetization vector and its angle during the reversal process.

D. Rotational hysteresis

We briefly discuss again the rotational hysteresis deduced from torque measurements (91; 92; 93), now in the light of the analysis provided above. The torque measurements were carried out in a strong applied magnetic field H. Therefore the applied field H and the magnetization M_F can be assumed to be parallel ($\beta = \theta$). The torque is given by:

$$T = -\frac{\partial E(\theta)}{\partial \theta} = J_{eb} \sin(\theta - \alpha(\theta))$$

This expression differs from Eq. 8 for the ideal model by the rotation of the AF spins through the α angle. However, this does not explain the energy loss during the torque measurements, as observed in the experiment (5(b)). The torque curve would only be a bit distorted but completely reversible. The integration of the energy curve predicts a rotational hysteresis $W_{rot} = 0$. In order to account for a finite rotational hysteresis, one can assume that a fraction p of particles at the F-AF interface are uniaxially coupled behaving as in region II, whereas the remaining fraction $(1 - p)$ of the F-AF particles are coupled unidirectionally, having the ideal behavior as described in regime I. As seen in Fig. 9(left), when the R-ratio of the uniaxial particle is in the range $0.5 \leq R < 1$, the AF spins will rotate irreversibly, showing hysteresis-like behavior due to α jumps indicated in the Fig. 9 (right). A rotational hysteresis is not expected for unidirectional particles with $R \geq 1$ because the AF structure changes reversibly with θ. With this assumption the uniaxial particles will contribute to the energy

loss during the torque measurements, while the unidirectional particles are responsible for the unidirectional feature of the torque curve. This argument was used by Meiklejohn and Bean (91) when studying the exchange bias in core-Co/shell-CoO. A fraction $p = 0.5$ was inferred from the torque curves shown in Fig. 5.

VII. NÉEL'S AF DOMAIN WALL - WEAK COUPLING

The rigid AF spin state and rigidly rotating AF spins concepts impose a restriction on the behavior of the antiferromagnetic spins, namely that the AF order is preserved during the magnetization reversal. Such restriction implies that the interfacial exchange coupling is found almost entirely in the hysteresis loop either as a loop shift or as coercivity. Experimentally, however, the size of the exchange bias does not agree with the expected value, being several orders of magnitude lower then predicted. In order to cope with such loss of coupling energy, one can assume that a partial domain wall develops in the AF layer during the magnetization reversal. This concept was introduced by Néel (72; 105) when considering the coupling between a ferromagnet and a low anisotropy antiferromagnet. The AF partial domain wall will store an important fraction of the exchange coupling energy, lowering the shift of the hysteresis loop.

Néel has calculated the magnetization orientation of each layer through a differential equation. The weak coupling is consistent with a partial AF domain wall which is parallel to the interface (Néel domain wall). His model predicts that a minimum AF thickness is required to produce hysteresis shift. More importantly the partial domain wall concept forms the basis of further models which incorporate either Néel wall or Bloch wall formation as a way to reduce the observed magnitude of exchange bias.

VIII. MALOZEMOFF RANDOM FIELD MODEL

Malozemoff (1987) proposed a novel mechanism for exchange anisotropy postulating a random nature of exchange interactions at the F-AF interface (84; 85; 86). He assumed that the chemical roughness or alloying at the interface, which is present for any realistic bilayer system, causes lateral variations of the exchange field acting on the F and AF layers. The resultant random field causes the AF to break up into magnetic domains due to the energy minimization. By contrast with other theories, where the unidirectional anisotropy is treated either microscopically (76; 148; 149) or macroscopically (89; 92; 93), the Malozemoff approach belongs to models on the mesoscopic scale for surface magnetism.

The general idea for estimating the exchange anisotropy is depicted in Fig. 13, where a domain wall in an uniaxial ferromagnet is driven by an applied in-plane magnetic field H (84). Assuming that the interfacial energy in one domain (σ_1) is different from the energy in
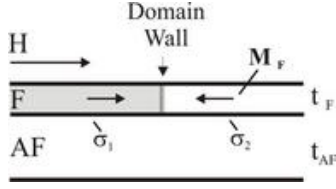
FIG. 13 Schematic side view of a F/AF bilayer with a ferromagnetic wall driven by an applied field **H** (84).

the neighboring domain σ_2, then the exchange field can be estimated by the equilibrium condition between the applied field pressure $2 H M_F t_F$ and the effective pressure from the interfacial energy $\Delta\sigma$:

$$H_{eb} = \frac{\Delta\sigma}{2 M_F t_F}, \qquad (32)$$

where M_F and t_F are the magnetization and thickness of the ferromagnet. When the interface is treated as ideally "compensated", then the exchange bias field is zero. On the other hand, if the AF/F interface is ideally uncompensated there is an interfacial energy difference $\Delta\sigma = 2J_i/a^2$, where J_i is the exchange coupling constant across the interface, and a is the lattice parameter of a simple cubic structure assigned to the AF layer. The EB field is $H_{eb} = J_i/a^2 M_F t_F$ (see Fig 14) [1].

Estimating numerically the size of the EB field using the equation above for an ideally uncompensated interface, results in a discrepancy of several orders of magnitude with respect to the experimental observation . Therefore, a novel mechanism based on random fields at the interface acting on the AF layer is proposed as to drastically reduce the resulting exchange bias field.
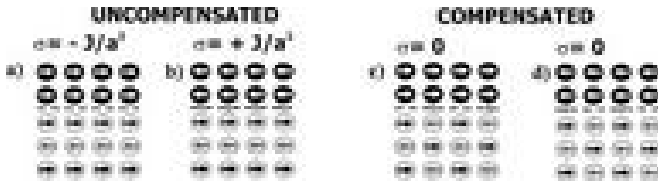

FIG. 14 Schematic view of possible atomic configurations in a F-AF bilayer with ideal interfaces. Frustrated bonds are indicated by crosses. Compensated configuration a) will result in configuration b) by reversing the ferromagnetic spins through domain wall movement. It gives an exchange bias field of $H_{eb} = J_i/a^2 M_F t_F$. The compensated configuration c) will result in the compensated configuration d). The exchange bias field for this case is zero ($H_{eb} = 0$). (84).

By simple and schematic arguments Malozemoff describes how roughness on the atomic scale of a "compensated" AF interface layer can lead to uncompensated

---

[1] For this example the energy is calculated as $E_{kl} = -J_i \boldsymbol{S}_k \boldsymbol{S}_l$ per pair of nearest neighbor spins kl at the interface

spins required for the loop to shift. An atomic rough interface depicted in Fig 15a) containing a single mono-atomic bump in a cubic interface gives rise to six net anti-ferromagnetic deviations from a perfect compensation. A bump shifted by one lattice spacing as shown in Fig. 15b), which is equivalent to reversing the F spins, provides six net ferromagnetic deviations from perfect compensation. Thus a net energy difference of $z_i J_i$ with $z_i = 12$ acts at the interface favoring one domain orientation over the other. Note that for an ideally uncompensated interface the energy difference is only $8J_i$ when reversing the F spins. This implies that an atomic step roughness at a compensated interface leads to a higher exchange bias field as compared to the ideally compensated interface.

The estimates of this local field can be further refined assuming a more detailed model. For example, by inverting the spin in the bump shown in Fig. 15c, the interfacial energy difference is reduced by $5 \times 2J_i$ at the cost of generating one frustrated pair in the AF layer just under the bump. This frustrated pair increases the energy difference by $2J_A$, where J_A is the AF exchange constant. Thus the energy difference between the two domains becomes $2J_i + 2J_A$ or roughly $4J$ if $J_i \approx J_A \approx J$. If one allows localized canting of the spins, one expects the energy difference to be reduced somewhat further.
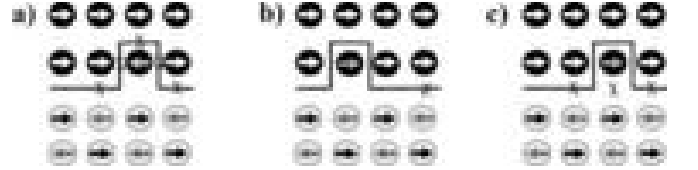

FIG. 15 Schematic side view of possible atomic moment configurations for a non-planar interface. The bump should be visualized on a two-dimensional interface. Configuration c) represents the lower energy state of a). The configuration b) is energetically equivalent to flipping the ferromagnetic spins of a). The x signs represent frustrated bonds. (84)

Each interface irregularity will give a local energy difference between domains whose sign depends on the particular location of the irregularity and whose magnitude is on the average $2zJ$, where z is a number of order unity. Furthermore, for an interface which is random on the atomic scale, the local unidirectional interface energy $\sigma_l = \pm zJ/a^2$ will also be random and its average σ in a region L^2 will go down statistically as $\sigma \approx \sigma_l/\sqrt{N}$, where $N = L^2/a^2$ is the number of sites projected onto the interface plane. Therefore the effective AF-F exchange energy per unit area is given by:

$$J_{eb} \approx \frac{1}{\sqrt{N}} J_i \approx \frac{1}{L} J_i,$$

where J_i is the exchange energy of a fully uncompensated AF-surface.

Given a random field provided by the interface roughness and assuming a region with a single domain of the

ferromagnet, it is energetically favorable for the AF to break up into magnetic domains, as shown schematically in Fig. 16. A perpendicular domain wall is the most preferable situation. This perpendicular domain wall is permanently present in the AF layer. It should be distinguished from a domain wall parallel to AF/F interface, which according to the Mauri model (89) develops temporarily during the rotation of the F layer.
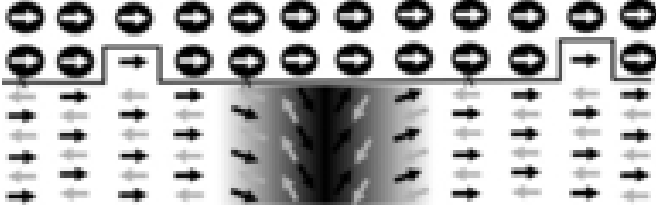

FIG. 16 Schematic view of a vertical domain wall in the AF layer. It appears as an energetically favorable state of F/AF systems with rough interfaces (26; 84).

By further analyzing the stability of the magnetic domains in the presence of random fields, a characteristic length L of the frozen-in AF domains and their characteristic height are obtained: $L \approx \pi\sqrt{A_{AF}/K_{AF}}$ and $h = L/2$, where A_{AF} is the exchange stiffness and h is the characteristic height of the AF domains. Once these domains are fixed, flipping the ferromagnetic orientation causes an energy change per unit area of $\Delta\sigma = 4zJ/\pi aL$, which further leads to the following expression for the EB field:

$$H_{eb} = \frac{2\,z\,\sqrt{A_{AF}K_{AF}}}{\pi^2\,M_F t_F} \tag{33}$$

Assuming a $CoO/Co(100\,\mathring{A})$ film, the calculated exchange bias using the Eq. 33 is:

$$
\begin{aligned}
H_{eb} &= \frac{2 \times 1\sqrt{\frac{0.0186 \times 1.6 \times 10^{-19}[J]}{4.27 \times 10^{-10}[m]}2.5 \times 10^7\,[J/m^3]}}{\pi^2 \times 1460\,[kA/m]\,100 \times 10^{-10}} \times 10 \\
&= 580\,Oe
\end{aligned}
\tag{34}
$$

For the estimations above we used for the exchange stiffness the following value: $A_{AF} = J_{AF}/a$, where a is the lattice parameter of CoO ($a = 4.27\mathring{A}$) and $J_{AF} = 1.86$ meV is the exchange constant for CoO (135).

The characteristic length of the AF domains is for CoO:

$$
\begin{aligned}
L &= \pi\sqrt{A_{AF}/K_{AF}} \\
&= \pi \times \sqrt{\frac{0.0186 \times 1.6 \times 10^{-19}[J]}{4.27 \times 10^{-10}[m] \times 2.5 \times 10^7\,[J/m^3]}} \\
&= 16.6\,\mathring{A}
\end{aligned}
\tag{35}
$$

The height of the AF domains is $h = L/2 = 8.3\,\mathring{A}$. Comparing this value to the experimental data on

CoO$(25\mathring{A})$/Co studied in (132), we notice that the calculated EB field agrees well with the value observed experimentally. For example, the exchange bias field for $CoO(25\,\mathring{A})/Co(119\,\mathring{A})$ is 557 Oe and the theoretical value calculated with Eq. 33 is 487 Oe. Also, the length and the height of the AF domains have enough space to develop. The difference between theory and experiment is, however, that experimentally AF domains occur after the very first magnetization reversal, whereas within the Malozemoff model the AF domains are assumed to develop during the field cooling procedure. Nevertheless, the agreement appears to be excellent.

IX. DOMAIN STATE MODEL

The Domain State model (DS) introduced by Usadel and coworkers (5; 98; 100; 101; 115; 117; 147) is a microscopic model in which disorder is introduced via magnetic dilution not only at the interface but also in the bulk of the AF layer as in Fig. 17. The key element in the model is that the AF layer is a diluted Ising antiferromagnet in an external magnetic field (DAFF) which exhibits a phase diagram like the one shown in Fig. 18 (117). In zero field the system undergoes a phase transition from a disordered, paramagnetic state to a long-range-ordered antiferromagnetic phase at the dilution dependent Néel temperature. In the low temperature region, for small fields, the long-range interaction phase is stable in three dimensions. When the field is increased at low temperature the diluted antiferromagnet develops a domain state phase with a spin-glass-like behavior. The formation of the AF domains in the DS phase originates from the statistical imbalance of the number of impurities of the two AF sublattices within any finite region of the DAFF. This imbalance leads to a net magnetization which couples to the external field. A spin reversal of the region, i. e., the creation of a domain, can lower the energy of the system. The formation of a domain wall can be minimized if the domain wall passes through nonmagnetic defects at a minimum cost of exchange energy.
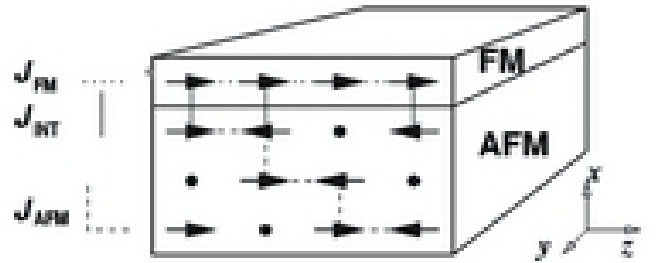

FIG. 17 Sketch of the domain state model with one ferromagnetic layer and three diluted antiferromagnetic layers. The dots mark defects (117).

Nowak et al. (117) further argue that during the field cooling below the irreversibility line $T_i(B)$, in an exter-
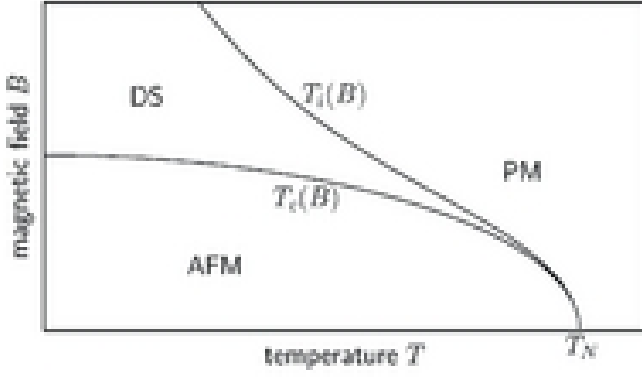
FIG. 18 Schematic phase diagram of a three-dimentional diluted antiferromagnet. AF is the antiferromagnetic phase, DS the domain state phase, and PM the paramagnetic phase (117).

nal field and in the presence of the interfacial exchange field of the ferromagnet, the AF develops a frozen domain state with an irreversible surplus of magnetization. This irreversible surplus magnetization controls then the exchange bias.

The F layer is described by a classical Heisenberg model with the nearest-neighbor exchange constant J_F. The AF is modelled as a magnetically diluted Ising system with an easy axis parallel to that of the F. The Hamiltonian of the system is given by (117):

$$
\begin{aligned}
H = & -J_F \sum_{<i,j>\epsilon F} \boldsymbol{S}_i.\boldsymbol{S}_j - \sum_{i\epsilon F}(d_z S_{iz}^2 + d_x S_{ix}^2 + \mu \boldsymbol{B}\boldsymbol{S}_i) \\
& -J_{AF} \sum_{<i,j>\epsilon AF} \epsilon_i\epsilon_j \boldsymbol{\sigma}_i\boldsymbol{\sigma}_j - \sum_{i\epsilon AF} \mu B_z \epsilon_i\sigma_i \\
& -J_{INT} \sum_{<i\epsilon AF,j\epsilon F>} \epsilon_i\sigma_i S_{jz},
\end{aligned} \tag{36}
$$

where the $\boldsymbol{S_i}$ and $\boldsymbol{\sigma_i}$ are the classical spin vectors at the ith site of the F and AF, respectively. The first line contains the energy contribution of the F, the second line describes the diluted AF layer, and the third line includes the exchange coupling across the interface between F and DAFF, where it is assumed that the Ising spins in the topmost layer of the DAFF interact with the z component of the Heisenberg spins of the F layer.

In order to obtain the hysteresis loop of the system, the Hamiltonian in Eq. 36 is treated by Monte Carlo simulations. Typical hysteresis loops are shown in Fig. 19 (101), where both the magnetization curve of the F layer and of the interface monolayer of the DAFF are shown. The coercive field extracted from the hysteresis curve depends on the anisotropy of the F layer, but it is also influenced by the DAFF. It, actually, depends on the thickness and anisotropy of the DAFF layer. The coercive field decreases with the increasing thickness of the DAFF layer (101), which can be understood as follows: the interface

magnetization tries to orient the F layer along its direction. The coercive field has to overcome this barrier, and the higher the interface magnetization of the DAFF, the stronger is the field required to reverse the F layer. The interface magnetization decreases with increasing DAFF thickness due to a coarsening of the AF domains accompanied by smoother domain walls.
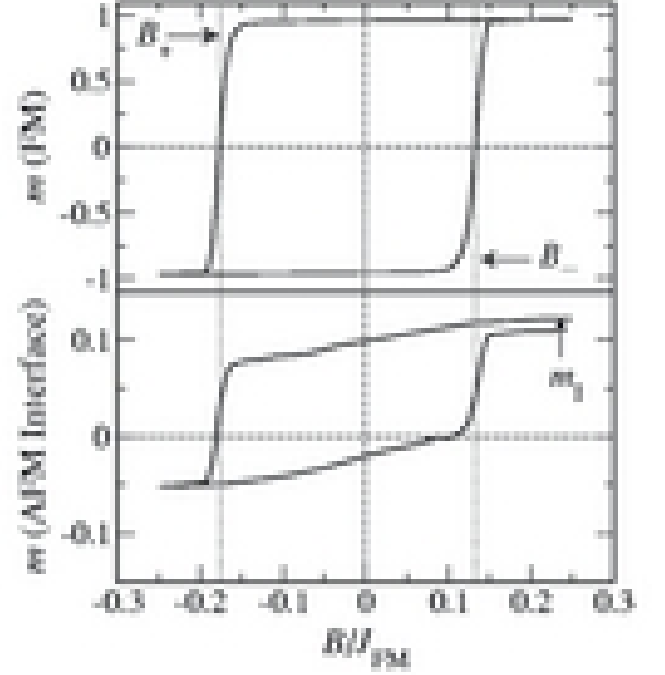

FIG. 19 Simulated hysteresis loops within the domain state model. The top hysteresis belongs to the ferromagnetic layer and the bottom hysteresis belongs to an AF interface monolayer (101).

The strength of the exchange bias field can be estimated from the Eq. 36 using simple ground state arguments. Assuming that all spins in the F remain parallel during the field reversal and some net magnetization of the interface layer of the DAFF remains constant during the reversal of the F, a simple calculation gives the usual estimate for the bias field (117):

$$
l\mu B_{eb} = J_{INT}m_{INT}, \tag{37}
$$

where l is the number of the F layers and m_{INT} is the interface magnetization of the AF per spin. B_{eb} is the notation for the exchange bias field in Ref. (117) and is equivalent to H_{eb} in this chapter. For an ideal uncompensated interface ($m_{INT} = 1$) the exchange bias is too high, whereas for an ideally compensated interface the exchange bias is zero. Within the DS model the interface magnetization $m_{INT} < 1$ is neither a constant nor is it a simple quantity (117). Therefore, it is replaced by m_{IDS}, which is a measure of the irreversible domain state magnetization of the DAFF interface layer and is responsible

for the EB field. With this, an estimate of exchange bias field for $l = 9$, $J_{INT} = -3.2 \times 10^{-22} J$, and $\mu = 1.7 \mu_B$ gives a value of about 300 Oe.

The exchange bias field depends also on the bulk properties of the DAFF layer as shown by Miltényi et al. (98). There the AF layer was diluted by substituting non-magnetic Mg in the bulk part and away from the interface. The representative results are shown in Fig. 20. It was shown experimentally that the EB field depends strongly on the dilution of the AF layer. As a function of concentration of the non-magnetic Mg impurities, the EB evolves as following: at zero dilution the exchange bias has finite values, whereas by increasing the Mg concentration, the EB field increases first, showing a broad peak-like behavior, and then, when the dilution is further increased the EB field decreases again. Simulations within the DS model showed an overall good qualitative agreement. The peak-like behavior of the EB as a function of the dilution is clearly seen in the simulations (see Fig. 20). However, it appears that at zero dilution, the DS gives vanishing exchange bias whereas experimentally finite values are observed. The exchange bias is missing at low dilutions because the domains in the AF cannot be formed as they would cost too much energy to break the AF bonds. This discrepancy (117; 122) is thought to be explained by other imperfections, such as grain boundaries in the AF layer which is similar to dilution and which can also reduce the domain-wall energy, thus leading to domain formation and EB even without dilution of the AF bulk.

An important property of the kinetics of the DAFF is the slow relaxation of the remanent magnetization, i.e., the magnetization obtained after switching off the cooling field (117). It is known that the remanent magnetization of the DS relaxes nonexponentially on extremely long-time scales after the field is switched off or even within the applied field. In the DS model the EB is related to this remanent magnetization. This implies a decrease of EB due to slow relaxation of the AF domain state. The reason for the training effect can be understood within DS model from Fig. 19 bottom panel, where it is shown that the hysteresis loop of the AF interface layer is not closed on the right hand side. This implies that the DS magnetization is lost partly during the hysteresis loop due to a rearrangement of the AF domain structure. This loss of magnetization clearly leads to a reduction of the EB.

The blocking temperature [2] within the DS model can be understood by considering the phase diagram of the DAFF shown in Fig 17. The frozen DS of the AF layer occurs after field cooling the system below the irreversibility temperature $T_i(b)$. Within this interpretation,
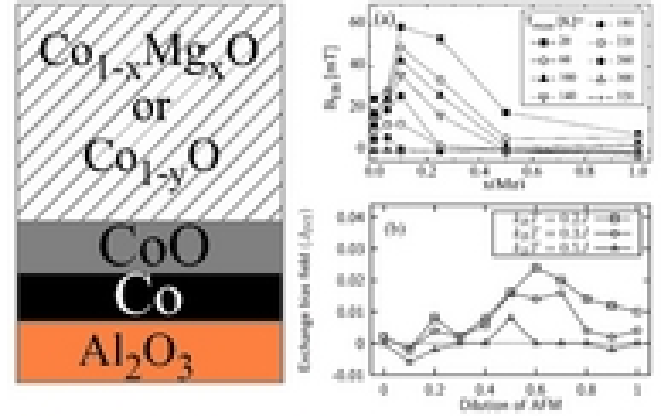

FIG. 20 In the right side of the figure is shown the film structure used to study the dilution influence on the exchange bias field. a) EB field as function of the Mg concentration x in the $Co_{1-x}Mg_xO$ layer for several temperatures. b) EB field as a function of different dilutions of the AF volume (98).

the blocking temperature corresponds to $T_i(b)$. Since $T_i(b) < T_N$, the blocking temperature should be always below the Néel temperature and should be dependent on the strength of the interface exchange field. The simulations within the DS model shows that EB depends linearly on the temperature, as observed experimentally in some Co/CoO systems, but no reason is given for this behavior (117). In Ref. (24) the blocking temperature of a DAFF system ($Fe_{1-x}Zn_xF_2(110)/Fe/Ag$ with x=0.4) exhibits a significant enhancement with respect to the global ordering temperature T_N=46.9 K, of the bulk antiferromagnet $Fe_0.6Zn_0.4F_2$.

Overall, it is believed that strong support for the DS model is given by experimental observations where non-magnetic impurities are added to the AF layer in a systematic and controlled fashion (60; 66; 94; 98; 102; 122; 151). Also, good agreement has been observed in Ref. (1), where the dependence of the EB as a function of AF thickness and temperature for IrMn/Co was analyzed. The asymmetry of the magnetization reversal mechanisms (5; 6) is shown to be dependent on the angle between the easy axis of the F and DAFF layers. It was found that either identical or different F reversal mechanisms (domain wall movement or coherent rotation) can occur as the relative orientation between the anisotropy axis of the F and AF is varied. This is discussed in more detail in sections XII.D and XIV.A.

X. MAURI MODEL

The model of Mauri *et al.* (89) renounces the assumption of a rigid AF layer and proposes that the AF spins develop a domain wall parallel to the interface. The motivation to introduce such an hypothesis was to explore a possible reduction of the exchange bias field resulting

---

[2] The blocking temperature of an exchange bias system is the temperature where the hysteresis loop acquires a negative or positive shift with respect to the field axis. It is always lower then the Néel temperature of the AF layer.

from the Meiklejohn and Bean model.

The assumptions of the Mauri model are:

- both the F and AF are in a single domain state;

- the F layer rotates rigidly, as a whole;

- the AF layer develops a domain wall parallel to the interface;

- the AF interface layer is uncompensated (or fully compensated);

- the AF layer has a uniaxial anisotropy;

- the cooling field is oriented parallel to the uniaxial anisotropy of the AF layer;

- the AF and F spins rotate coherently, therefore the Stoner-Wohlfarth model is used to describe the system.
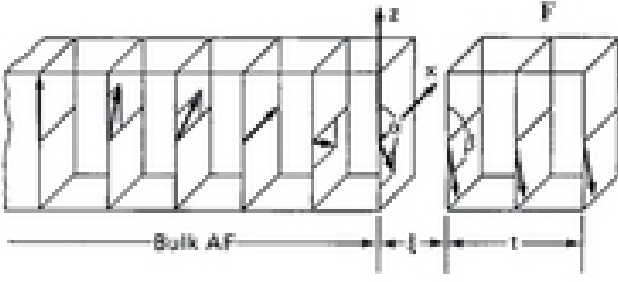

FIG. 21 Mauri model for the interface of a thin ferromagnetic film on a antiferromagnetic substrate (89).

Schematically the spin configuration within the Mauri model is shown in Fig. 21. The F spins rotate coherently, when the applied magnetic field is swept as to measure the hysteresis loop. The first interfacial AF monolayer is oriented away from the F spins making an angle α with the field cooling direction and with the anisotropy axis of the AF layer. The next AF monolayers are oriented away from the interfacial AF spins as to form a domain wall parallel to the interface. The spins of only one AF sublattice are depicted, the spins of the other sublattice being oppositely oriented for completing the AF order. At a distance ξ at the interface, a ferromagnetic layer of thickness t_F follows. Using the Stoner-Wohlfarth model, the total magnetic energy can be written as (89):

$$
\begin{aligned}
E = & -\mu_0 H M_F t_F \cos(\theta - \beta) \\
& + K_F t_F \sin^2(\beta) \\
& - J_{eb} \cos(\beta - \alpha) \\
& - 2\sqrt{A_{AF} K_{AF}}(1 - \cos(\alpha)),
\end{aligned} \tag{38}
$$

where the first term is the Zeeman energy of the ferromagnet in an applied magnetic field, the second term is the anisotropy term of the F layer, the third term is the

interfacial exchange energy and, the forth term is the energy of the partial domain wall. The new parameter in the equation above is the exchange stiffness A_{AF}. As in the case of the Meiklejohn and Bean model, the interfacial exchange coupling parameter J_{eb} $[J/m^2]$ is again undefined, assuming that it ranges between the exchange constant of the F layer to the exchange constant of the AF layer divided by an effective area (see section V.B).

The total magnetic energy can be written in units of $2\sqrt{A_{AF}K_{AF}}$, which is the energy per unit surface of a $90°$ domain wall in the AF layer:

$$
\begin{aligned}
e = & \ k(1 - \cos(\beta)) + \mu \cos(\beta)^2 \\
& + \lambda[1 - \cos(\alpha - \beta)] + (1 - \cos(\alpha)), \tag{39}
\end{aligned}
$$

where $\lambda = J_{eb}/(2\sqrt{A_{AF}K_{AF}})$, is the interface exchange, with J_{eb} being redefined as $J_{eb} \equiv A_{12}/\xi$, where A_{12} is the interfacial exchange stiffness and ξ is the thickness of the interface (see Fig. 21), $\mu = K_F t_F/2\sqrt{A_{AF}K_{AF}}$ is the reduced ferromagnet anisotropy, and $k = \mu_0 H M_F t_F/2\sqrt{A_{AF}K_{AF}}$ is the reduced external magnetic field.

Mauri *et al.* (89) have calculated the magnetization curves by numerical minimization of the reduced total magnetic energy Eq. 39. Several values of the λ and μ parameters were considered providing quite realistic hysteresis loops. Their analysis highlights two limiting cases with the following expressions for the exchange bias field:

$$
H_{eb} = \begin{cases} -(A_{12}/\xi)/\mu_0 M_F t_F & for \ \lambda \ll 1 \\ -2\sqrt{A_{AF}K_{AF}}/\mu_0 M_F t_F & for \ \lambda \gg 1 \end{cases} \tag{40}
$$

In the strong coupling limit $\lambda \ll 1$, the expression for the exchange bias field is similar to the value given by the Meiklejohn and Bean model. For this situation, practically no important differences between the predictions of the two models exist. When the coupling is weak ($\lambda \gg 1$), the Mauri model delivers a reduced exchange bias field which is practically independent of the interfacial exchange energy. It depends on the domain wall energy and the parameters of the F layer. In either case the "$1/t_F$" dependence is preserved by the Mauri-model.

A. Analytical expression of exchange bias field

In order to compare the predictions of the Mauri model and the Meiklejohn and Bean approach, we reconsider the analysis of the free energy. Starting from the expression of the free energy Eq. 38, the minimization with respect to the α and β angle leads to the following system of equations:

$$
\begin{cases} \frac{H}{-\frac{J_{eb}}{\mu_0 M_F t_F}} \sin(\theta - \beta) + \sin(\beta - \alpha) = 0 \\ \frac{2\sqrt{A_{AF}K_{AF}}}{J_{eb}} \sin(\alpha) - \sin(\beta - \alpha) = 0 \end{cases} \tag{41}
$$

Similar to the Meiklejohn and Bean model we define the parameters $P \equiv \frac{2\sqrt{A_{AF}\,K_{AF}}}{J_{eb}}$ and $H_{eb}^\infty \equiv -\frac{J_{eb}}{\mu_0\,M_F\,t_F}$. Also we set $\theta = 0$, meaning that the applied field is swept along the easy axis of the AF layer. Also, we do not take into account the anisotropy of the ferromagnet ($K_F = 0$), for two reasons. For one the coercive fields of the exchange bias systems are usually much higher then the coercive field of the isolated F layer, and secondly it is easier to compare the results of the Mauri model and the M&B model when the anisotropy of the F layer is disregarded. From inspection of the equations Eq. 41 and Eq. 23 one can clearly see that the first equations of the two systems are identical, while the second ones are different in two respects. The first difference is related to the term P, which includes the domain wall energy instead of the AF anisotropy term in the R ratio. The second difference is that instead of a $\sin(2\,\alpha)$ term in the second equation of Eq. 23, the Mauri model has a $\sin(\alpha)$ term, which influences strongly the phase diagram shown in Fig. 22.
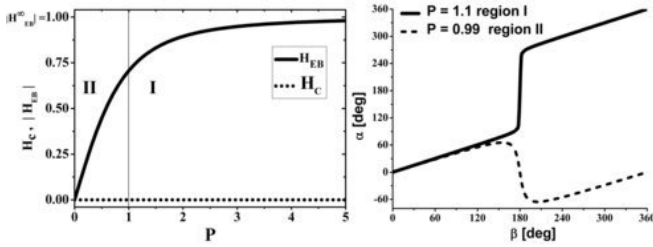

FIG. 22 Left: The phase diagram of the exchange bias field and the coercive fields given by the Mauri formalism. Right: Typical behavior of the antiferromagnetic angle α for the two different regions of the phase diagram. In both regions I and II a shift of the hysteresis loop can exist. The coercive field is zero in both regimes.

The analytical expression for the exchange bias are obtained by solving the system of Eqs. 41. First step in solving the Eq. 41 is to extract the α angle ($\alpha = \pm \arccos(\pm \frac{P - \cos(\beta)}{\sqrt{1 + P^2 - 2\,P\,\cos(\beta)}})$) from the second equation and to introduce it in the first equation. Next we use the condition that at the coercive field $\beta = -\pi/2$ to obtain both coercive fields $H_{c1} = H_{c2}$. Then, inserting them into the general expressions of Eq. 16, the coercive field H_c is zero and the exchange bias field becomes (155):

$$
\begin{aligned}
H_{eb} &= -\frac{J_{eb}}{\mu_0\,M_F\,t_F}\,\frac{2\sqrt{A_{AF}\,K_{AF}}}{\sqrt{J_{eb}^2 + 4\,A_{AF}\,K_{AF}}} \\
&= -\frac{J_{eb}}{\mu_0\,M_F\,t_F}\,\frac{P}{\sqrt{1 + P^2}}
\end{aligned}
\tag{42}
$$

This equation is plotted as a function of $H/|H_{EB}|$ and for different P values ranging from $P = 0$ to $P = 5$. (compare Fig. 22 left panel). The behavior of the EB field according to the Eq. 42 is monotonic with respect to the stiffness and anisotropy of the AF spins. At $P \gg 1$ the exchange bias is equal to $H_{eb}^{P\to\infty} = -\frac{J_{eb}}{\mu_0\,M_F\,t_F}$, which is
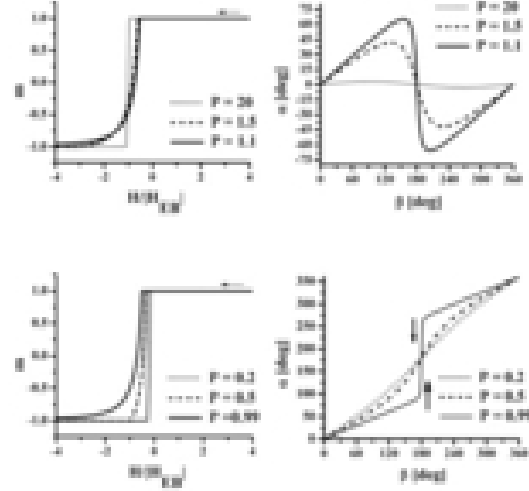

FIG. 23 Several hysteresis loops and antiferromagnetic spin orientations as plotted during the magnetization reversal. For the simulation we used the Mauri formalism. Top row shows three hysteresis loops calculated for different P ratios of the region I shown in Fig. 22. The right hand panel in the top row shows the α angle of the antiferromagnetic layer for the three P parameters of the hysteresis loop. The bottom raw are the corresponding hysteresis loops and α angles for the P values within region II.

the well known expression given by M&B model. When, however, the P-ratio approaches low values, the exchange bias decreases, vanishing at $P = 0$, provided that the thickness of the AF layer is sufficiently thick to allow a $180°$ wall. With some analytical analysis of the Eq. 42 one can easily reach the limiting cases of weak coupling ($P \ll 1$) and strong coupling ($P \gg 1$) discussed by Mauri et al. (88) (see Eq. 40). In Fig. 22 right column is shown the representative behavior of the α angle of the first interfacial AF monolayer as a function of the β orientation of the F spins during the magnetization reversal and for two representative P values (see the discussion below).

In Fig. 23 the hysteresis loops ($m_{||} = \cos(\beta)$) and the corresponding AF angle rotation during the magnetization reversal are plotted for several P-ratios. They were obtained by solving numerically the system of Eqs. 41. For all the values of the P-ratio the magnetization curves are shifted to negative values of the applied magnetic field. We distinguish two different regions with respect to the behavior of the α angle of the first AF monolayer. In the first region , for $P \geq 1$ (region I), the AF monolayer in the proximity of the F layer behaves similar to the Meiklejohn and Bean, namely the α angle deviates reversibly from the anisotropy direction as function of β. The maximum value of the α angle acquired during the rotation of the F layer is two times higher for the Mauri model as compared to the M&B model, reaching a maximum value of $90°$ at $P = 1$. The coercive field in

this region is zero. The angle α in the region II where $P < 1$ has a completely different behavior. It rotates with the ferromagnet following the general behavior depicted in Fig. 23. Notice that α follows monotonically the rotation of the F spins, with no jumps or hysteresis-like behavior in contrast to the M&B model(see Fig. 9). Very importantly, the exchange bias field does not vanish in this region and therefore no additional coercive field related to the AF is observed, provided that the AF layer is sufficiently thick to allow for a domain wall as shown in Fig. 21. In this region (II) the EB field is smaller as compared to the M&B model. This reduction is more clearly seen further below, when analyzing the azimuthal dependence of the EB field within the Mauri model.

Comparing the phase diagram of the Mauri model Fig. 22 left to the corresponding one given by the M&B model Fig. 9 left one can clearly see that region I of both models is very similar with respect to the qualitative behavior of the exchange bias field as a function of the R-ratio and, respectively, P-ratio. However, we can compare those curves only when accounting for the variation of the EB field as a function of the anisotropy of the AF layer. Both models predict that the EB field depends on the anisotropy of the AF layer in a similar qualitative manner. Additionally, within the M&B model the EB field includes also the dependence on the thickness of the AF layer, which is not visible in the Mauri model. The other regions of both phase diagrams are completely different. Within the Mauri model, the exchange bias does not vanish at $P < 1$, but it continuously decreases, whereas the M&B model predicts that the exchange bias field vanishes for $R < 1$ leading to enhanced coercivity. Also note that for the weak coupling region (II) of the Mauri model, the exchange bias would strongly depend on the temperature through the anisotropy constant of the AF layer (31).

B. Azimuthal dependence of the exchange bias field

Next we analyze the azimuthal dependence of the EB field by deriving an analytical expression of the EB field as a function of the rotation angle θ. By solving the second equation of the system of equation Eqs. 41 with respect to β, one finds the angle α as function of β. Using the condition for the coercive field as $\beta = \theta - \pi/2$, and introducing it in the first line of Eq. 41, one obtains the coercive fields $H_{c1} = H_{c2}$. It follows that the coercive field $H_c(\theta) = 0$ and the exchange bias field as function of the azimuthal angle is (155):

$$H_{eb}(\theta) = -\frac{J_{eb}}{\mu_0\, M_F\, t_F}\frac{2\sqrt{A_{AF}K_{AF}}\cos(\theta)}{\sqrt{J_{eb}^2 + 4A_{AF}K_{AF} - 4J_{eb}\sqrt{A_{AF}K_{AF}}\sin(\theta)}}$$

$$(43)$$

In Fig. 24 is plotted the EB bias field calculated by the expression above for different values of the P-ratio, which was also confirmed numerically. In region I the EB

field is maximum parallel to the field cooling directions ($\theta = 0$) only for very large P-ratios. When P approaches the unity, the maximum of the EB field is shifted away from $\theta = 0$, to higher azimuthal angles and has the value:

$$H_{eb}^{MAX,P\geq 1} = -\frac{J_{eb}}{\mu_0\, M_F\, t_F} \qquad (44)$$

This expression is identical to Eq. 31 of the M&B model and shown in Fig. 11. The shape of the curves evolves from an ideal unidirectional shape at $P \to \infty$ to a skewed shape at $P \geq 1$.
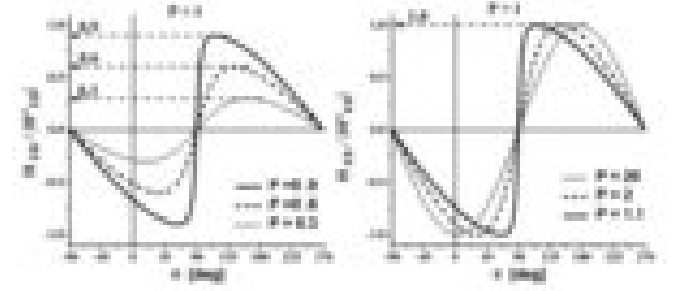

FIG. 24 Azimuthal dependence of exchange bias as a function of the θ angle. The dotted line for $P = 20$ can be considered an "ideal" case. The curves are plotted according to Eq. 43.

In region II (Fig. 24 left) a drastic change as compared to region I is seen for the maximum of the exchange bias field as a function of azimuthal angle. Its value decreases monotonically towards zero according to the following expression:

$$H_{eb}^{MAX,P<1} = -P = -\frac{2\sqrt{A_{AF}K_{AF}}}{J_{eb}}. \qquad (45)$$

In this region the shape of the curves is also skewed for P-ratios close to unity, but as P decreases towards zero, the curves acquire a more ideal unidirectional behavior. Similar to region I, the maximum EB value is shifted away from the field cooling direction to higher azimuthal angles, whereas in M&B it is shifted to lower azimuthal angles.

In the limit of strong R and P-ratios ($R, P \gg 1$) the Mauri and M&B models give similar results. The differences appear for the R and P-ratios which are close to but higher than one. This region ($0 < R, P \leq 5$) can be experimentally explored in order to decide in favor of one or the other model. In order to distinguish between the Mauri and the M&B model, the azimuthal dependence of the exchange bias offers an excellent tool because it is visibly different for the two models (shift to higher or lower azimuthal angles).

The presence of the planar domain wall as described by Mauri et al. appears to have been confirmed experimentally for first time in Ref. (145). Although the Co/NiO system studied by Scholl et al. did not exhibit a hysteresis loop shift, the rotation angle α of the AF planar

wall was deduced as function of field. Also, in a recent publication by Gornakov *et al.* (45) show experimental results that are similar to the characteristic curves for the α angle shown in Fig. 22. An AF critical thickness which is often observed experimentally do not appear explicitly in the Mauri model. To account for the AF thickness dependence, Xi and White (177) proposed a model which assumes a helical structure for the AF spins during the magnetization reversal. The temperature dependence of EB is accounted for by the Mauri model through the anisotropy of the AF ($H_{EB} \approx \sqrt{K_{AF}}$). Since the anisotropy constant is rather difficult to measure for thin films, the evidence for the predicted temperature dependence remains elusive (31). One insufficiency of the Mauri model is the inability to predict any changes in coercivity. The domain wall produces only shifted reversible magnetization curves (69). Therefore, further refinements of the model were introduced which is described in the next section.

XI. KIM-STAMPS APPROACH - PARTIAL DOMAIN WALL

The approach of Kim and Stamps (67; 68; 69; 70; 154; 155) follows from the work of Néel and Mauri *et al.* extending the model of an extended planar domain wall to the concept of a partial domain wall in the AF layer. Biquadratic (spin-flop) and bilinear coupling energies are used to describe exchange biased system, where the bias is created by the formation of partial walls in the AF layer. The model applies to compensated, partially compensated, and uncompensated interfaces.

A typical hysteresis loop indicative for a partial domain wall in the AF layer is shown in Fig. 25 (69). In saturation at $h > 0$, the F spins are aligned with the external field while the AF spins are in a perfect Néel state, collinear with the easy axis. The interface spins are antiparallel to the F layer due to a presumably antiparallel coupling. As the field is reduced and reversed, the AF pins the F layer by interfacial exchange coupling until the critical value of the reversal field is reached at h_c, where the magnetization begins to rotate. When it is energetically more favorable to deform the AF, rather than breaking the interfacial coupling, a partial wall twists up as the F rotates. The winding and unwinding of the partial domain wall in the AF is reversible, therefore the magnetization is reversible (no coercivity). This mechanism is only possible if the AF is thick enough to support a partial wall. The magnitude of the exchange bias is similar to the one given by the Mauri model. Neiter the partial-wall theory nor the Mauri model account, however, for the coercivity enhancement that accompanies the hysteresis loop shift in single domain materials, which is usually observed in experiments.

The enhanced coercivity observed experimentally, is proposed to be related to the domain wall pinning at magnetic defects. The presence of an attractive domain-
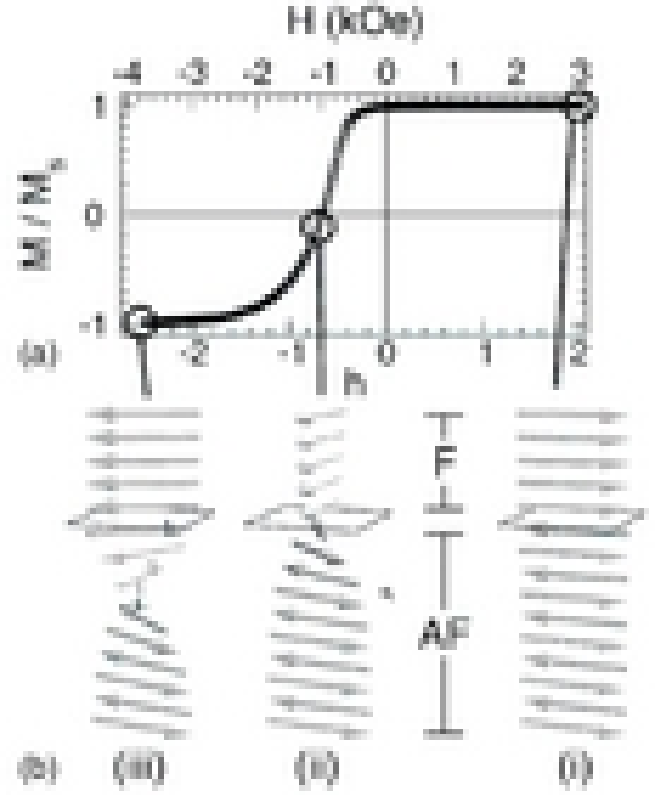

FIG. 25   (a) Magnetization curve for the ferromagnet/antiferromagnet system. (b) Calculated spin structure at three different points of the magnetization curve. The creation of a partial antiferromagnet domain wall can be seen in (iii). Only the spins close to the F/AF interface are shown. From Ref. (69).

wall potential in the AF layer, arising from magnetic impurities can provide an energy barrier for domain-wall processes that controls coercivity. Following the treatment of pinning in magnetic materials by Braun et. al. (16), Kim and Stamps examined the influence of a pointlike impurity at an arbitrary position in the AF layer. As a result, the AF energy acquires, besides the domain wall energy, another term which depends on the concentration of the magnetic defects. These defects decrease the anisotropy locally and lead to an overall reduction of the AF energy. This reduction of the AF energy gives rise to a local energy minimum for certain defect positions relative to the interface. The domain walls can be pinned at such positions and contribute to the coercivity.

Kim and Stamps argue that irreversible rotation of the ferromagnet due to a combination of wall pinning an depinning transitions, give rise to asymmetric hysteresis loops. Some examples are given in Fig. 26 (69). The loops are calculated with an exchange defect at $x_L = 5$, for three different values of defect concentration ρ_J, where x_L denotes the defect positions in the antiferromagnet, with $x_L = 0$ corresponding to the interface
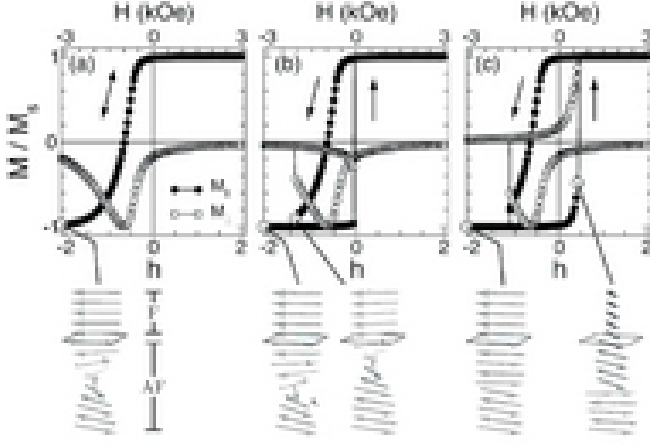
FIG. 26 Defect-induced asymmetry in hysteresis loops. The hysteresis loops are shown for a reduced exchange defect at $x_L = 5$ for three concentrations: (a) $\rho_J = 0.15$,. (b) $\rho_J = 0.45$, and (c) $\rho_J = 0.75$. The components of magnetization parallel ($M_\parallel$) (dots) and perpendicular ($M_\perp$) (open circles) to the field direction are shown. The arrows indicate the directions for reversal and remagnetization. The spin configuration near the interface is shown for selected field values below the hysteresis curves (69).

layer and $x_L = t_{AF} - 1$ being the free surface. At low defect concentrations, the pinning potential is insufficient to modify partial-wall formation. The resulting magnetization curve, as shown in Fig. 26(a), is reversible and resembles the curve obtained with the absence of impurities. Pinning of the partial wall occurs during reversal for moderate concentrations, which appears as a sharp rotation of the magnetization at negative fields, as shown in Fig. 26(b). During remagnetization the wall is released from the pinning center at a different field, thus resulting in an asymmetry in the hysteresis loop. The release of the wall is indicated by a sharp transition in M. The energy barrier between wall pinning and release increases with defect concentration, resulting in a larger coercivity and reduced bias as in Fig. 26(c).

Within this model, the asymmetry of the hysteresis loops is interpreted in terms of domain-wall pinning processes in the antiferromagnet. This explanation appears to be consistent with some recent work by Nikitenko *et al.* and Gornakov *et al.* on a NiFe/FeMn system (45; 106) who concluded that the presence of an antiferromagnetic wall at the interface is necessary to explain their hysteresis measurements.

XII. THE SPIN GLASS MODEL OF EXCHANGE BIAS

To overcame the theoretical difficulties in explaining interconnection between the exchange bias and coercivity, in Ref. (133; 134) is considered a magnetic state of the interface between F and AF layer which is magnetically disordered behaving similar to a spin glass system. The assumptions of the spin glass(SG) model are:

- the F/AF interface is a frustrated spin system (spin-glass like)

- frozen-in uncompensated AF spins are responsible for the EB shift

- low anisotropy interfacial AF spins contribute to the coercivity

Within this model, the AF layer is assumed to contain, in a first approximation, two types of AF statesv(see Fig. 27). One part has a large anisotropy with the orientation ruled by the AF spins and another part with a weaker anisotropy which allows some spins to rotate together with the F spins. This interfacial part of the AF is a frustrated region (spin-glass-like) and gives rise to an increased coercivity. The presence of a low anisotropy AF region can be rationalized as follows: the interface between the F and AF layer is never perfect, therefore one may assume chemical intermixing, deviations from stoichiometry, structural inhomogeneities, low coordination, etc, at the interface to take place. This leads to the formation of a transition region from the pure AF state to a pure F state. On average, the anisotropy of such an interfacial region is reduced. In addition, structural and magnetic roughness can provide a weak AF interface region. Therefore, we assume that a fraction of the frustrated interfacial spins do rotate almost in phase with the F spins and that they mediate enhanced coercivity. We describe them by an effective uniaxial anisotropy K_{SG}^{eff}, because they are coupled to the presumably uniaxial AF layer.

Generally, one can visualize a spin glass system (10) as a collection of spins which remains in a frozen disordered state even at low-temperatures. In order to achieve such a state, two ingredients are necessary: a) there must be a competition among the different interactions between the moments, in the sense that no single configuration of the spins is uniquely favored by all interactions (this is commonly called 'frustration'); b) these interactions must be at least partially random. This partial random state will be introduced in the M&B model as an effective uniaxial anisotropy.

Adding this effective anisotropy to the M&B model, the free energy reads (133):

$$
\begin{aligned}
E = & -\mu_0\,H\,M_F\,t_F\,\cos(\theta - \beta) \\
& + K_F\,t_F\,\sin^2(\beta) \\
& + K_{AF}(t_{AF})\,t_{AF}\,\sin^2(\alpha) \\
& + K_{SG}^{eff}\,\sin^2(\beta - \gamma) - J_{eb}^{eff}\,\cos(\beta - \alpha) \quad (46)
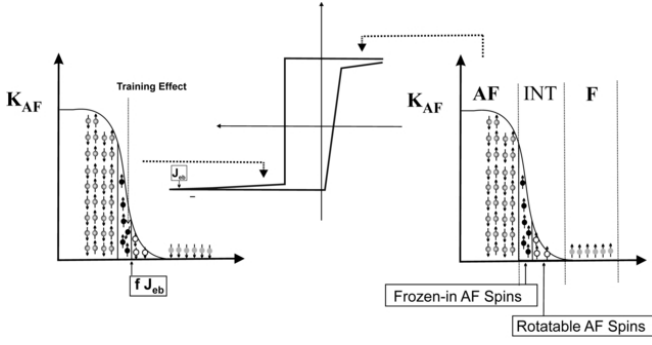\end{aligned}
$$

FIG. 27 Schematic view of the SG Model. At the interface between the AF and the F layer the AF anisotropy is assumed to be reduced leading to two types of AF states after field cooling the system: frozen-in AF spins and rotatable AF spins. After reversing the magnetic field, the rotatable spins follows the F layer rotation mediating coercivity. The frozen-in spins remain largely unchanged in moderate fields. But some of them will also deviate from the original cooling state. This could lead to training effects and also to an open loop in the right side of the hysteresis loop. At larger applied fields in the negative direction, the frustrated frozen-in spins can further reverse leading to a slowly decreasing slope of the hysteresis loop. A more complex antiferromagnetic state consisting of frozen magnetic domains or/and AF grains can be also reduced to the basic concepts depicted here.

where, K_{SG}^{eff} is an effective uniaxial SG anisotropy related to the frustrated AF spins with reduced anisotropy at the interface, J_{eb}^{eff} is the reduced interfacial exchange energy, and γ is the average angle of the effective SG anisotropy. $K_{AF}(t_{AF})$ is the anisotropy constant of AF layer. To avoid further complications for the numerical simulations, we neglect the thickness dependence of the K_{AF} anisotropy ($K_{AF}(t_{AF}) \equiv K_{AF}$). We mention though, that this dependence could become important for low AF thicknesses due to finite size effects and due to structurally non-ideal very thin layers. From now on, the MCA anisotropy of the ferromagnetic layer ($K_F = 0$) will also be neglected as to highlight more clearly the influences of AF layer and the SG interface onto the general properties of the EB systems. Note that the Zeeman energies of the ferromagnetic-like AF interfacial spins are neglected in the model since they are usually much smaller as compared to Zeeman energy of the F layer. Nevertheless, they can be seen as a vertical shift of the hysteresis loop (frozen-in AF spins in Fig. 27) and as an additional contribution to the total magnetization (rotatable AF spins in Fig. 27).

The model is depicted schematically in Fig. 27. At the interface two rather distinct AF phases are assumed to occur in an EB system: the rotatable AF spins, depicted as open circles and frozen-in AF spins shown as filled circles. After field cooling, a presumably collinear arrangement is depicted in the right hand panel. After reversing the magnetic field, the rotatable AF spins follow the F layer rotation mediating coercivity. The frozen-in

spins remain largely unchanged in moderate fields. But some of them could also deviate from the original cooling state. Irreversible changes of the frustrated AF spins lead to training effects and also to an open loop in the right side of the hysteresis loop. At larger negative applied fields, the frustrated frozen-in spins could further reverse leading to a slowly degresing slope of the hysteresis loop. A more complex antiferromagnetic state consisting of frozen magnetic domain state or/and AF grains can be also reduced to the basic two spin components depicted in Fig. 27. Basically, additional frozen-in spins can occur in the AF layer extending to the interface and, therefore, leading to an even more interfacial disorder.

Next, we evaluate numerically the resulting hysteresis loops and azimuthal dependence of the exchange bias within the SG model. When the K_{SG}^{eff} parameter is zero, the system behaves ideally as described by the M&B model discussed in Sec.VI: the coercive field is zero and the exchange bias is finite. In the other case, when the interface is disordered we relate the SG effective anisotropy to the available interfacial coupling energy as follows:

$$K_{eff} = (1 - f)\, J_{eb}$$
$$J_{eb}^{eff} = f\, J_{eb} \tag{47}$$

where J_{eb} is the total available exchange energy and f is a conversion factor describing the fractional order at the interface, with $f = 1$ for a perfect interface and $f = 0$ for perfect disorder. Some basic models to calculate the available exchange energy were discussed in the previous sections. For even more complicated situations when the AF consists of AF grains and/or AF domains the exchange energy can be further estimated as described in Ref. (161).

With these notations we write the system of equations resulting from the minimization of the Eq. 46 with respect to the angles α and β:

$$h \sin(\theta - \beta) + \frac{(1 - f)}{f} \sin(2\,(\beta - \gamma)) + \sin(\beta - \alpha) = 0$$
$$R \sin(2\,\alpha) - \sin(\beta - \alpha) = 0 \tag{48}$$

where,

$$h = \frac{H}{-\dfrac{J_{eb}^{eff}}{\mu_0\, M_F\, t_F}} = \frac{H}{-\dfrac{f\, J_{eb}}{\mu_0\, M_F\, t_F}}$$

is the reduced applied field and

$$R \equiv \frac{K_{AF}\, t_{AF}}{J_{eb}^{eff}} = \frac{K_{AF} t_{AF}}{f\, J_{eb}}$$

is the R-ratio defining the strength of the AF layer.

The system of equations above can easily be solved numerically, but it does provide simple analytical expressions for the exchange bias. Numerical evaluation provides the α and β angles as a function of the applied magnetic field H. The reduced longitudinal component of magnetization along the field axis follows from

$m_{||} = cos(\beta - \theta)$ and the transverse component from $m_\perp = sin(\beta - \theta)$.

With the assumptions made above the absolute value of the exchange bias field is directly proportional to f. The parameter f can be called *conversion factor*, as it describes the conversion of interfacial energy into coercivity. For example, in the M&B phase diagram in the region II and III corresponding to reduced R-ratios, the exchange bias field is zero and the coercive field is enhanced as a result of such a conversion of the interfacial energy into coercive field.

The idea of reduced interfacial anisotropy at the interface can be traced back to the the Néel weak ferromagnetism at the surface of AF particles. Néel (105) discussed the training effect as a tilting of the superficial magnetization of the AF domains. Later, Schlenker *et al.* (143) suggested that successive reversals of the F magnetization could lead to changes of the interface uncompensated AF magnetization and therefore provide means of going from one ground state to another. Such multiple interface configurations are similar to a spin glass system. The spin-glass interface is further discussed by other authors (2; 73; 77; 87; 96; 125; 138; 157; 173). Exchange bias has been observed recently for spin-glass/F system (176). The interfacial magnetic disorder was observed through hysteresis loop widening below a critical temperature point (7). Non-collinearity have been observed at the AF/F even in saturation (18; 128; 129). The frozen spins at the interface were also observed by MFM (65). Using element specific techniques such as soft x-ray resonant magnetic dichroism (XMCD) and of x-ray resonant magnetic scattering (XRMS), both frozen and rotatable AF spins can be studied (21; 29; 118; 119; 120; 131; 137; 141; 180). The frozen-in spins appear as a shift of the hysteresis loop along magnetization axis, whereas the AF rotatable spins exhibit a hysteresis loop. Moreover, an evidence for SG behavior is recently reported in thin films (50) and AF nanoparticles (140). Therefore, we believe that there is enough experimental evidence to consider the interface between the AF/F layer as a disordered state behaving similar to a spin-glass system.

A. Hysteresis loops as a function of the conversion factor f

If Fig. 28 we show simulations of several hysteresis loops as a function of the conversion factor f. We assume a strong antiferromagnet in contact with a ferromagnet, where the interface has different degrees of disorder depicted in the right column of Fig. 28. For the R ratio we assume the following value: $R = \frac{K_{AF} t_{AF}}{f J_{eb}} = 62.5/f$ which corresponds to a 100 Å thick CoO antiferromagnetic layer. The field cooling direction and the measuring field direction are parallel to the anisotropy axis of the AF. The anisotropy of the ferromagnet is neglected in the simulations below. For the interface we have chosen a SG anisotropy oriented 10 degrees away from the unidirectional anisotropy orientation ($\gamma = 10°$). On the

abscissa the reduced exchange bias field $h = H/|H_{eb}^\infty|$ ($H_{eb}^\infty \equiv -\frac{J_{eb}^{eff}}{\mu_0 M_F t_F}$)is plotted, which then can easily be compared to the M&B model. With this assumption the system of Eqs. 48 was solved numerically.
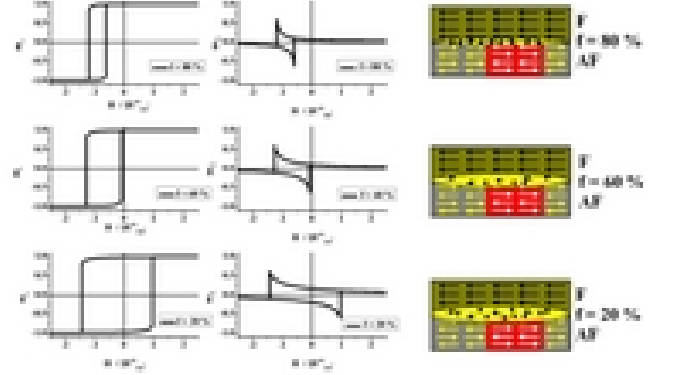

FIG. 28 Longitudinal ($m_{||} = cos(\beta)$) and transverse ($m_\perp = sin(\beta)$) components of the magnetization for a F($K_F = 0$)/AF($R = 62.5/f, \gamma = 10°, \theta = 0$) bilayer for different values of the conversion factor f ($f = 80$ %, 60 %, 20 %). We observe, that when the AF layer is strong ($R \gg 1$) the hysteresis loops are symmetric when measured along the field cooling direction. The hysteresis loops are simulated by solving numerically the Eqs. 48. In the right column is schematically depicted the layer structure, here the emphasis is given to the disorder state at the interface. The AF layer is depicted as consisting of magnetic domains which also contribute to interface disorder.

The left column shows the longitudinal component of the magnetization (parallel to the measuring field direction) ($m_{||} = cos(\beta)$) whereas the middle column shows the transverse component of the magnetization ($m_\perp = sin(\beta)$).

We observe that with decreasing conversion factor f the exchange bias vanishes linearly. The reduction of the EB field is accompanied by an increased coercivity. The shape of the hysteresis loop is close to the results found in literature. For instance the hysteresis loop with $f = 60\%$ is similar to the data shown in Refs. (44; 51). The hysteresis loop with $f = 20\%$ is similar to the data shown in Refs. (7; 130). The longitudinal and transverse components of the magnetization show that the reversal mechanism is symmetric. The symmetry is directly related to the strength of the AF layer, when no training effect is involved. For the examples depicted in Fig. 28, the R-ratio is much larger than 1 ($R \gg 1$), and therefore the hysteresis loops are symmetric when measured along the field cooling direction and along anisotropy axis of the AF layer. The asymmetry of the hysteresis loops is discussed further below.

B. Phase diagram of exchange bias and coercive field within the spin glass model

In this section we discuss the phase diagram for the exchange field and coercive field as a function of the R-value within the SG-model. The additional parameter is the conversion factor f. In Fig. 29 phase diagrams are shown for reduced exchange bias and reduced coercive fields as a function of the R-ratio for four different values of the conversion factor f. This allows us to compare directly the behavior of exchange bias fields as predicted in the SG model and the M&B model. The reduced exchange bias field plotted in Fig. 29 (left panel) is defined:

$$h_{eb} = \frac{H_{eb}}{\frac{J_{eb}^{eff}}{\mu_0 \, M_F \, t_F}} = \frac{H_{eb}}{f \, H_{eb}^{\infty}},$$

where the H_{eb} is the absolute value of the exchange bias within the SG model and the denominator term $\frac{J_{eb}}{\mu_0 \, M_F \, t_f}$ is the exchange bias field within the ideal M&B model.
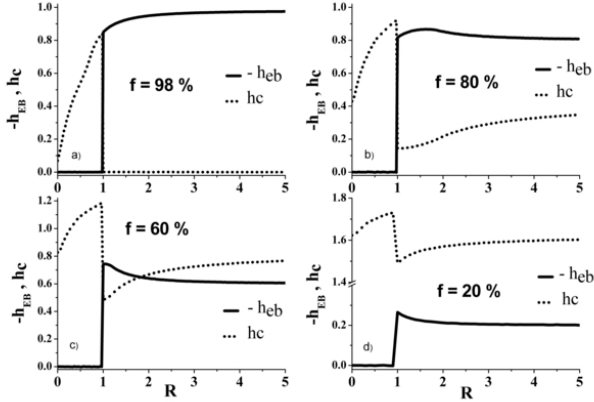

FIG. 29 The dependence of the reduced exchange bias field h_{eb} and the reduced coercive field h_c as a function of the R-ratio for four different values of the conversion factor f.

The reduced coercive field shown in Fig. 29 is defined:

$$h_c = \frac{H_c^{SG}}{\frac{J_{eb}^{eff}}{\mu_0 \, M_F \, t_F}},$$

where H_c^{SG} is the absolute value of the coercive field within the SG model. It has no relation to the coercive field of the M&B model because the coercive field within the M&B model is considered to be a constant when the exchange bias is finite.

C. Azimuthal dependence of exchange bias and coercive field within the spin glass model.

In this section, the azimuthal dependence of exchange bias and coercive fields within the SG model

are discussed and compared with experimental results of polycrystalline $Ir_{17}Mn_{83}(15\,nm)/Co_{70}Fe_{30}(30\,nm)$ exchange bias system (133).

In Fig. 30 calculated magnetization components are plotted together with the experimental data points, and in Fig. 31b the azimuthal dependence of the coercive field and exchange bias field are plotted and compared to the experimental data in Fig. 31a. The hysteresis loops were calculated by numerical minimizing the expressions in Eq. 48. The parameters used in the simulation $f = 80\%$, $R = 5.9/f$, $\gamma = 20°$ do best reproduce the experimental data. Furthermore, it is assumed that the AF layer has a uniaxial anisotropy. The MCA anisotropy of the F layer is neglected ($K_F = 0$). Therefore, the coercivity which appears in the simulations is not related to the F properties, but to the interfacial properties of the F/AF bilayer.
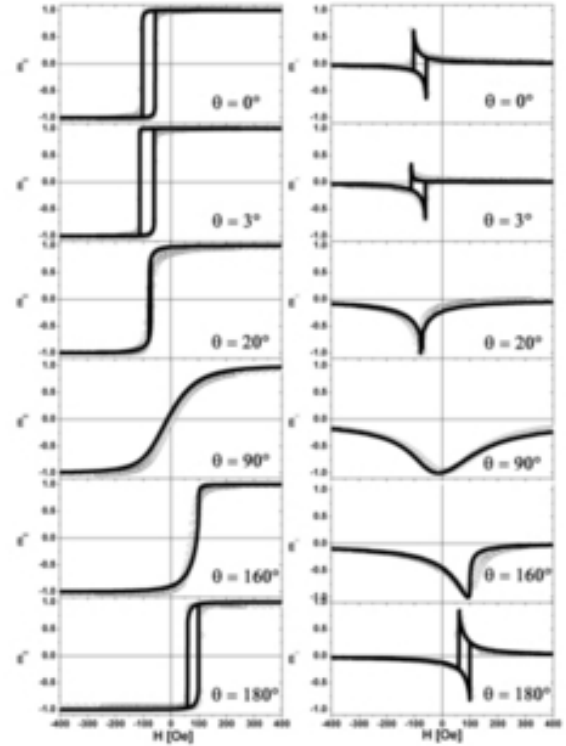

FIG. 30 Experimental (open circles) and simulated hysteresis loops (black lines) for different azimuthal angles. The simulated curves are calculated by the Eq. 48 with the following parameters: $f = 80\%$, $R = 5.9/f$, $\gamma = 20°$ (133).

First we discuss the hysteresis loops shown in Fig. 30. The system is cooled down in a field oriented parallel to the AF anisotropy direction. The hysteresis loops (solid lines) are simulated for different azimuthal angles θ of the applied field in respect to the field cooling orientation. In Fig. 30 representative hysteresis curves are shown for the longitudinal ($m_{\parallel}$) and transverse ($m_{\perp}$) magnetization.

At $\theta = 0°$, the magnetization curves are symmetric and shifted to negative fields. At $\theta = 180°$, the magnetization curves are also symmetric but shifted to positive fields. At $\theta = 3°$, however, the longitudinal hysteresis loop becomes asymmetric. The first reversal at H_{c1} is sharp and the reversal at H_{c2} is more rounded. This asymmetry is also seen in the transverse component of the magnetization. The F spins rotate asymmetrically: the values of the β angle depend on the external field scan direction, being different for swaps from negative to positive saturation as compared with swaps from positive to negative saturation. As the azimuthal angle increases, the coercive field becomes zero. For instance, at $\theta = 20°, 90°$ and $160°$ there is almost no coercivity. Also, the transverse component of the magnetization shows that the F spins do not follow a 360° path, but they rotate within the 180° angular space.
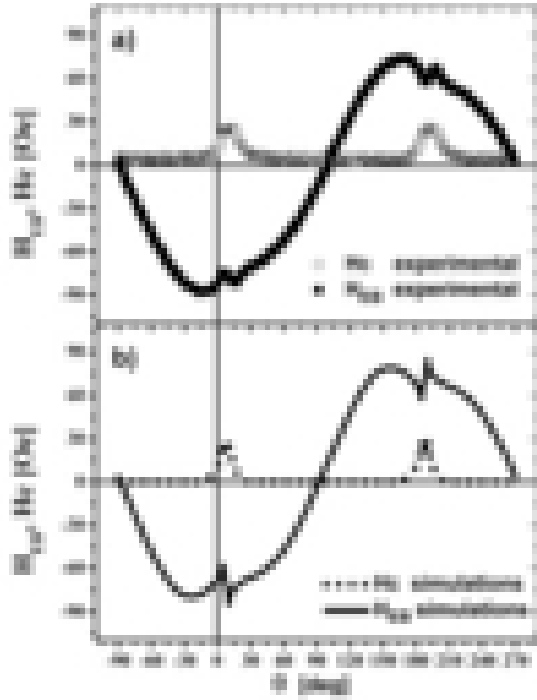

FIG. 31 a) The experimental coercive field (open symbols) and exchange bias (filled symbols) field as a function of the azimuthal angle θ.d) Simulated coercive field (dotted line) and exchange bias field (continuous line) as a function of the azimuthal angle (133).

In Fig. 31 the coercive field and the exchange bias field are extracted from the experimental and simulated hysteresis loops using Eq. 16. We distinguish the following characteristics of the H_c and H_{eb}: the unidirectional behavior ($\approx \cos(\theta)$) of the H_{eb} as a function of the azimuthal angle is (see Fig. 11) clearly visible; additionally, the behavior of the H_{eb} as a function of the azimuthal angle shows sharp modulations close to the orientation of

the AF uniaxial anisotropy; the coercive field H_c has a peak-like behavior close to the orientation of the AF uniaxial anisotropy, at $\theta = 0°$ and $\theta = 180°$. In all cases we find an astounding agreement between calculated curves and experimental data. It is remarkable, that the EB field and the coercive field are completely reproduced by the SG model

Experimentally the azimuthal dependence of the exchange bias field was first explored for NiFe/CoO bilayers (3). It was suggested that the experimental results can be better described with a cosine series expansions, with odd and even terms for H_{eb} and H_c , respectively, rather than being a simple sinusoidal function as initially suggested by Meiklejohn and Bean (92; 93).

The simulations shown in this section are different with respect to the previous reports on the angular dependence of exchange bias field (3; 39; 95; 156; 178). One difference is that the MCA anisotropy of the F is supposed to be negligible when compared with the coercive fields obtained experimentally, and the sharp features of the H_{eb} are reproduced numerically rather then being described by cosine series expansions. Recently, Camarero et. al (22) reports on very similar azimuthal dependent hysteresis loops as shown here. There, an elegant way based on asteroid curve is used to describe the intrinsic asymmetry of the hysteresis loops close to the 0° and 180° azimuthal angle. A unidirectional anisotropy displaces the asteroid critical curve from the origin. Therefore, if the applied field is not parallel to the unidirectional anisotropy, the field sweep line does not pass through the symmetry center of the asteroid critical curve leading to inequivalent switching fields and consequently asymmetric reversals (22).

D. Dependence of exchange bias field on the thickness of the antiferromagnetic layer

After a short inspection of the phase diagram of EB and coercive field (Fig. 29) we notice that there is a critical value for the R-ratio at which the exchange bias vanishes and the coercive field is enhanced. This critical value R=1 depends on four parameters: the anisotropy of the antiferromagnet, the interfacial exchange coupling parameter, the thickness of the ferromagnet, and the conversion factor. The conversion factor further depends on the AF domain and/or AF grain size, if any.

In Fig. 32 the normalized exchange bias field is plotted as a function of the AF thickness and for several conversion factors. The anisotropy of the AF layer (K_{AF}) and the J_{eb} parameter are assumed to be constant.We notice two main characteristics of the EB field dependence on the AF thickness: when f has high values close to unity, the EB field decreases with decreasing AF thickness. However, when f is reduced, a completely different behavior of the EB is observed. The EB field increases as the thickness of the AF decreases, developing a peak-like feature. This peak-like behavior for the EB field at criti-
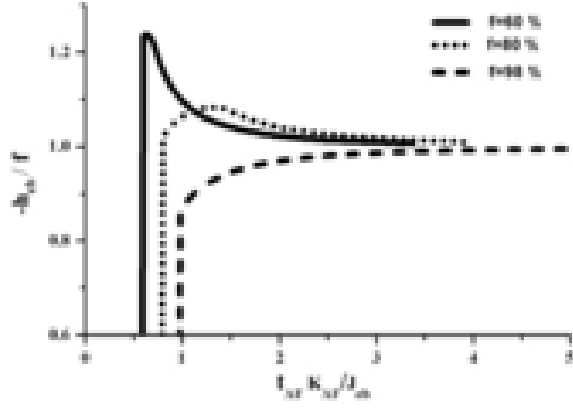
FIG. 32 The normalized exchange bias $h_{eb}/f = H_{eb}/H_{eb}^\infty$ as a function of the $t_{AF}K_{AF}/J_{eb}$ for different values of the conversion factor f. The anisotropy constant K_{AF} and J_{eb} are assumed to be constant as the AF thickness is being varied for each f. An asymmetric peak like behavior of the exchange bias field develops for high values of the conversion factor.

cal AF thickness is a result of enhanced coercivity which is accounted for by the f-factor. Also, an essential parameter is the α angle, which describes the rotation of the AF spins during the magnetization reversal. The critical thickness is preserved by the SG model, but it differs in magnitude as compared to the M&B model. Since some interfacial coupling energy is dissipated as coercivity, the critical thickness within SG model is lower as compared to the corresponding one given by the M&B model. The critical AF thickness within the SG model follows from the condition R = 1:

$$t_{AF,cr}^{SG} = \frac{f\, J_{eb}}{K_{AF}} = f\, t_{AF,cr}^{MB}, \qquad (49)$$

where $t_{AF,cr}^{SG}$ and $t_{AF,cr}^{MB}$ are the AF critical thickness predicted by the SG and M&B models, respectively.

Experimentally the R-ratio can be tuned by changing the thickness of the AF and keeping the other three parameters constant. As a result one observes a critical thickness of the AF layer for which the EB disappears (1; 11; 26; 46; 63; 75; 88). This AF critical thickness can be qualitatively understood within the MB model. When the hardness of the AF layer is reduced, the AF spins will rotate under the torque created by the F layer trough the interfacial coupling constant. The shape of the EB as function of AF thickness , however, can be different from one system to another depending on the other three parameters. The most prominent experimental feature of the EB dependence on the AF thickness is the development of a peak close to the critical thickness. Several proposals were made to describe the peculiar shapes of EB field dependence on AF thickness. According to the Malozemoff model, a change in the AF domain size as function of AF thickness results in a change

of exchange bias magnitude. Another influences on the AF dependence of the EB and coercive field are of structural origin (63; 75; 78). It has been shown by Kuch *et. al* (78) that at the microscopic level, the coupling between the AF an F layers depends on the atomic layer filling and on the morphology of the interface. The AF-F coupling was observed to vary by a factor of two between filled and half-filled interface. Moreover, islands and vacancy islands at the interface lead to a quite distinct coupling behavior. Therefore, structural configurations are indeed contributing to the EB-dependence as function of AF thickness.

The peak-like behavior of the EB field as function of the AF thickness is strongly dependent on temperature. An almost complete set of curves, showing a monotonous development of the AF peak from high to low temperatures was measured by Ali et al. (1). The data is reproduced in Fig. 33 together with the simulations based on DS model. Although the DS model does describe well some experimental observed features, some discrepancies still exists. For instance the development of the AF peak as well as the critical AF thickness as function of temperature are more pronounced in the experimental data as compared to the DS simulations.
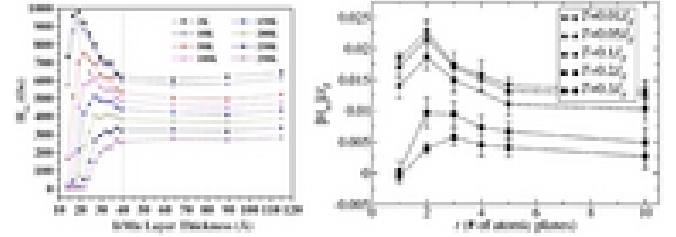

FIG. 33 Left: IrMn thickness dependence of the exchange bias field H_{eb} for a number of temperatures. Lines between the points are a guide to the eye. Right: Prediction of the DS model for the AF thickness dependence of the exchange bias field from the stability analysis of the interface AF domains at different temperatures. (from Ref. (1))

The SG model, through the conversion factor f, appears to be able to describe the evolution of the critical AF thickness(see Fig. 32 and Fig. 33 (left)). Also the shape of the EB dependence on the AF thickness, from an almost ideal M&B type at T=290 K to a pronounced peaked curve at T=2 K is qualitatively reproduced. Although not considered so far, the conversion factor seems to be temperature dependent. This can be understood if we consider the basic assumption of the SG model, namely the frustration at the interface. Temperature fluctuations acting on metastable spin states cause a variation of the SG anisotropy as function of temperature. We will not further speculate on the exact temperature dependence of the f-factor, but we mention that a numerical analysis for the EB dependencies shown in Fig. 33 would allow to untangle all the parameters in the R-ratio. The conversion factor is given by the shape of

the EB curves, fJ_{eb} can be extracted from the temperature dependence of the EB field at high AF thicknesses, and finally, the anisotropy constant will be deduced from the critical AF thickness. Note also, that the SG model has the potential to even describe the different temperature dependent shapes of the EB field, namely linear dependence versus more rounded shape: for an AF thickness close to the critical region, the temperature dependence of the EB bias will be clearly steeper (linear-like) as compared to the corresponding one at higher AF thicknesses(more rounded).

E. The blocking temperature for exchange bias

Experimentally it is found that the temperature where the exchange bias effect first occurs is usually lower than the Néel temperature of the AF layer (T_N) (109). This lower temperature is called blocking temperature (T_B). For thick AF layers $T_B \leq T_N$, whereas for thin AF layers $T_B \ll T_N$ (109). Furthermore, the coercive field increases starting just below T_N (with some exceptions) in contrast to the EB field, which appears only below T_B.

These three experimentally observed characteristic features can qualitatively be explained within the M&B and SG models. In order to have a non-vanishing EB field in the region with $R \geq 1$, the following condition has to be be fulfilled:

$$K_{AF} > \frac{fJ_{eb}}{t_{AF}} = K_{AF,crit}, \qquad (50)$$

where $K_{AF,crit}$ is the critical AF anisotropy for the onset of the EB field. For a fixed AF layer thickness, the condition above sets a critical value for the AF anisotropy for which the EB can exist. Considering that the AF anisotropy increases steadily below T_N, for large AF layer thicknesses the condition of Eq. 50 is fulfilled just below T_N, whereas for thinner AF layers this condition is fulfilled at a correspondingly lower temperature T_B. It is clear from the phase diagrams in Fig. 29 and in Fig. 32 that there is a region of anisotropy $0 < K_{AF} < K_{AF}^{crit}$ where the EB field is zero and the coercive field is enhanced. It follows that the enhancement of the coercive field should be observed above the blocking temperature and below the Néel temperature of the AF. This situation is indeed observed experimentally. For the case of CoO(25 Å)/Co layers the coercive field increases starting from the $T_N^{CoO} = 291\ K$, whereas the exchange bias field first appears below $T_B = 180\ K$ (130).

Further possible causes for a reduced blocking temperature and for the behavior of the EB and coercive fields as a function of temperature are discussed elsewhere: finite size effects(79), stoichiometry (168) or multiple phases (169), AF grains (53) and diluted AF (147).

XIII. TRAINING EFFECT

The training effect refers to the dramatic change of the hysteresis loop when sweeping consecutively the applied magnetic field of a system which is in a biased state. The coercive fields and the resulting exchange bias field versus n, where n is the nth measured hysteresis loop, displays a monotonic dependence (121; 142; 142; 143). The absolute value of H_{c1} and of the EB field decreases from an initial value at $n = 1$ to an equilibrium value at $n = \infty$. The absolute value of the coercive field H_{c2}, however, displays an opposite behavior, i.e. it increases with n. These features of the training effect is referred to as Type I by Zhang et. al.(182). The other case when both $|H_{c1}|$ and $|H_{c2}|$ decrease is called Type. II. In this section we deal only with the so-called Type I training effect. Several mechanisms were suggested as a possible cause of the effect. While it is widely accepted that the training effect is related to the unstable state of the AF layer and/or F/AF interface prepared by field cooling procedure, it is not yet well established what mechanisms are dominantly contributing to the training effect.

Néel (105) discussed the training effect as a tilting of the superficial magnetization of the AF domains. This would lead to a Type I training effect. Néel also discussed that a creeping effect could lead to a Type II training effect.

Micromagnetic simulations within the DS model (98; 117) show that the hysteresis curve is not closed after a complete loop. The lost magnetization is directly related to a partial loss of the superficial magnetization of the AF domains, which further leads to a decreased exchange bias.

Zhang et. al. (181) suggested that the training effect can be explained by incorporating into the Fulcomer and Charap's model (36) positive and negative exchange coupling between the grains constituting the AF layers.

In Ref. (56), the authors found direct evidence for the proportionality between the exchange bias and the total saturation moment of the heterostructure. The findings were related to the prediction of the phenomenological M&B approach, where a linear dependence of the exchange bias on the AF interface magnetization is expected.

Binek (14) suggested that the phenomenological origin of the training effect is a deviation of the AF interface magnetization from its equilibrium value. Analytical calculations in the framework of non-equilibrium thermodynamics leads to a recursive relation accounting for the dependence of the H_{eb} field on n.

Hoffmann (58) argues that only biaxial AF symmetry can lead to training effects, reproducing important features of the experimental data, while simulation with uniaxial AF symmetry show no difference between the first and second hysteresis loops.

Experiments performed by PNR, AMR and Kerr Microscopy (18; 47; 48; 90; 129; 130; 165; 174) also support the irreversible changes taking place at the F/AF inter-
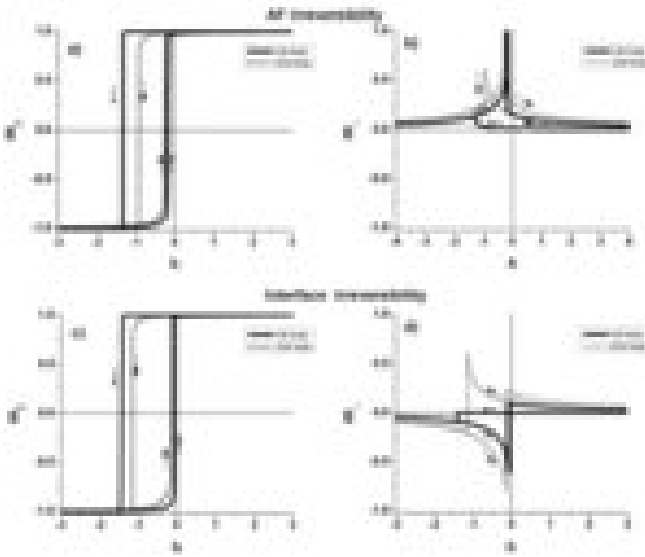
FIG. 34 Simulations of training effect within the SG model. Longitudinal a) and transverse b) components of magnetization for a scenario (see text) involving irreversible changes of the AF domain angle θ_{AF} during the magnetization reversal. Longitudinal c) and transverse d) components of magnetization for the case when only the interface disorder parameter γ increases and the AF state remains unchanged.

face and in the AF layer. It has been observed that during the very first reversal at H_{c1}, interfacial magnetic domains are formed and they do not disappear even in positive or negative "saturation". The interfacial domains serve as seeds for the subsequent magnetization reversals. These ferromagnetic domains at the interface have to be intimately related to the AF domain state (111). Therefore, the irreversible changes of the AF domain state are responsible for the training effect. Furthermore measurements have detected out-of-plane magnetic moments (132; 174) hinting at the existence of perpendicular domain walls in the AF layer, as originally suggested by Malozemoff. Therefore, irreversible changes of the AF magnetic domains and of the interfacial domains during the hysteresis loops play an important role for the training effect.

A. Interface disorder and the training effect

In the following we analyze the AF domains and interface contributions to the training effect. We assume that a gradual increase of the interfacial disorder of the F/AF system leads to a training effect. Within the SG model, the magnetic state of the F/AF interface can be mimiced through a unidirectional induced anisotropy K_{eff}, which is allowed to have an average direction γ, where γ is related to the spin disorder of the interface. Also, we will consider the influence of a progressive rotation of an AF domain anisotropy during the reversal. Both situations

will be treated below.

In Fig. 34a) and b) we show first and second hysteresis loops (longitudinal and transverse components of magnetization) calculated with the help of Eq. 48. In these calculations we set the conversion factor to $f = 60\%$ and $R = 62.5/f$. We consider a drastic change of an AF domain which progressively rotates its anisotropy axis during the magnetization reversal. This situation can be accounted for in the SG model by replacing the α angle in Eq. 48 with $\alpha - \theta_{AF}$, where the θ_{AF} is the orientation of the AF domain anisotropy. We also set the γ angle to be almost zero.

Following closely the experimental observations (129; 130), before the first reversal θ_{AF} is zero, and just after the first reversal θ_{AF} increases towards an equilibrium value. The first branch of the hysteresis loop appears rather sharp, therefore we assume that the AF spins and F spins are collinear immediately after cooling in a field ($\theta_{AF} = 0°$). For the second branch of the 1st hysteresis loop we consider that $\theta_{AF} = 20°$, therefore the second leg appears more rounded. The transition from $\theta_{AF} = 0°$ to $\theta_{AF} = 20°$ is assumed to happen right after or during the first reversal at H_{c1}. This is in accordance with the observation that for thin CoO layers (129; 130) where the disordered interface appears after the first reversal at H_{c1}. Now, the first branch of the second hysteresis loop is simulated with $\theta_{AF} = 20°$. At the third reversal, we again assume that the AF domain angle further increases. Therefore, the second branch of the hysteresis loop is simulated assuming a new value of $\theta_{AF} = 30°$.

The hysteresis loops bear all the features observed experimentally (51; 56; 128; 129; 143; 162; 181; 182). More strikingly, the transverse component of magnetization shows a small step increase at H_{c1} and larger increase at H_{c2}, on the reverse path. These are typical features observed experimentally by PNR (129; 130), AMR (18; 47; 48) and MOKE (90). Moreover, the transverse component at saturation behaves very close to recent observations of Brems *et al.* (18) on Co/CoO bilayers and lithographically nanostructured wires. After field cooling and before passing through the first magnetization reversal in the descending field branch, the resistance in saturation (which is proportional to the square of the orientation of transverse component of magnetization) reaches its maximum because all spins are oriented along the cooling field. After going through a complete hysteresis loop, the resistance at saturation is reduced, indicating that spins in the F are rotated away from the cooling field. After reversing the field back to positive saturation the resistance does not recover its initial value. Moreover, the untrained state can be partially reinduced by changing the orientation of the applied magnetic field (18) which can be interpreted as a further indication of AF domain rotation during the reversal.

Next, we consider only the interface disorder through a progressive change of γ angles. In Fig. 34b) and c) we show first and second hysteresis loops calculated with the help of Eq. 48. In these calculations we consider that

the AF is strong, $R = 62.5/f$. For the conversion factor we take a value of $f = 60\%$. Also, we assume the average AF orientation to be parallel to the field cooling orientation ($\theta_{AF} = 0$). Following closely the experimental observations, before the first reversal γ is zero, while just after the first reversal, γ increases towards an equilibrium value. The first branch of the hysteresis loop appears rather sharp, therefore we assume that the AF spins and F spins are collinear immediately after cooling in a field ($\gamma = 0$). For the second branch of the 1st hysteresis loop we consider that $\gamma = 10°$, therefore the second leg appears rather rounded. The transition from $\gamma = 0$ to $\gamma = 10°$ is assumed to happen right after or during the first reversal at H_{c1}. The first branch of the second hysteresis loop is simulated with $\gamma = 10°$. At the third reversal , we again assume that the disorder of the interface increases. Therefore, the second branch of the hysteresis loop (and right after during during the reversal at H_{c1} of the second loop) is simulated assuming a new value of $\gamma = 20°$.

The simulations above implies a viscosity-like behavior to the disordered interface (37). For example, when the F magnetization acquires an angle with respect to the unidirectional anisotropy, the torque exerted on the interfacial spins will drag them away from the initial direction set by the field cooling. Reversing the magnetization back to positive directions the K_{eff} spins will not follow (completely), they remain close to this position (viscosity). This is because the maximum torque exerted by the F spins was already acting at negative fields, while for positive fields it is much reduced. When measuring again the hysteresis loop, at negative coercive field, the K_{eff} spins will rotate even further and so on. Therefore, the angle of the K_{eff} anisotropy and/or of the AF domains increases after each hysteresis loop, similar to a rachet, causing a decreased exchange bias field.

Comparing the hysteresis curves shown in Fig. 34a) with the ones in Fig. 34c) one notices the same qualitative characteristics. This is not the case for the transverse magnetization curve. The F spins rotate only on the positive side for the first case, whereas for the second case the F magnetization rotation covers the entire 360° angular range. The anisotropic magnetoresistance (AMR) and PNR hides the chirality of the ferromagnetic spin rotation as they provide $\sin^2(\beta)$ information, whereas MOKE is sensitive to the chirality as it provides $\sin(\beta)$ information. Therefore, measuring both hysteresis components by MOKE, can help to distinguish between the dominant influence on the training effect: AF domain (or/and grain) rotation versus SG interface instability. The training effect is discussed furthermore in section XIII.B.

B. Empirical expression for the training effect

The very first empirical expression for training (121; 142) effects suggested a power law dependence of the coercive fields and the exchange bias field as a function of cycle index n:

$$H_{eb}^n = H_{eb}^\infty + \frac{k}{\sqrt{n}}, \qquad (51)$$

where k is an experimental constant. This expression follows well the experimental dependence of the EB field for $n \geq 2$, but when the very first point is included to the fit, then the agreement is poor.
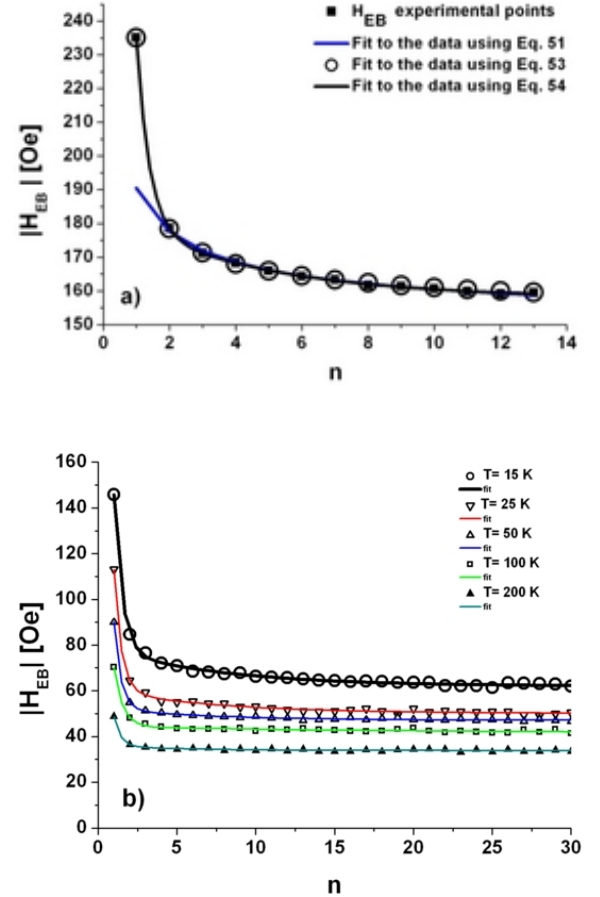

FIG. 35 a) Exchange bias as function of the loop index n. The gray line is the best fit to the data using Eq. 51. The open circles are the best fit (12) to the data using Eq. 53. The black line is the best fit to the data using Eq. 54. b)Temperature dependence of the training effect. The lines are the best fit to the data using Eq. 54

Binek (14) has shown by using non-equilibrium thermodynamics that using a recursive relation, the evolution of the EB field as a function of n, can be well reproduced for all cycle indexes ($n \geq 1$). The recursive expression reads:

$$H_{eb}^{n+1} - H_{eb}^n = -\Gamma \left(H_{eb}^n - H_{eb}^\infty\right)^3, \qquad (52)$$

where Γ is a physical parameter which, for $n \gg 1$, was directly related to the k parameter of Eq.51. It was shown

that a satisfactory agreement between the Eq. 51 and Eq. 52 is achieved for $n \geq 3$. Therefore the approach of Binek appears to provide the phenomenological origin of the hitherto unexplained power-law decay of the EB field with increasing loop index $n > 1$. The analytic expression (Eq. 52) was further tested for temperature dependent training effect (15).

More recently the Eq. 52 has been further refined by extending the free energy expansion with a correction of the leading term. The new equation for training effect reads (139):

$$H_{eb}^{n+1} - H_{eb}^n = -\gamma_b \left(H_{eb}^n - H_{eb}^\infty\right)^3 - \gamma_c \left(H_{eb}^n - H_{eb}^\infty\right)^5, \quad (53)$$

where the new γ_c parameter results from the higher order expansion of the free energy and hence $\gamma_c \ll \gamma_b$. The γ_b parameter is similar to the Γ in Eq. 52. Both parameters γ_b and γ_c exhibits a exponential dependence on the sweep rate for measuring the hysteresis loop. A number of three fit parameters is required for both Eq. 52 and Eq. 53, but the last equation provides better fitting results for moderate sweep rates.

In the following we analyze another type of expression which reproduces the dependence of the coercive field and exchange bias field as a function of the loop index n and for different temperatures. It is based on the simulations shown in the previous section. There it was argued that the training affect is related to the interfacial spin disorder. With each cycle the spin disorder increases slightly, thereby decreasing the exchange bias field. Additional effects are related to the AF domain size that also affects the magnitude of the EB and H_c fields. Both contributions cause a gradual decrease of exchange bias as a function of cycle n. They can be treated probabilistically. We suggest the following expression to simulate the decrease of the EB as a function of n:

$$H_{eb}^n = H_{eb}^\infty + A_f \exp(-n/P_f) + A_i \exp(-n/P_i), \quad (54)$$

where, H_{eb}^n is the exchange bias of the nth hysteresis loop, A_f and P_f are parameters related to the change of the frozen spins, A_i and P_i are parameters related to the evolution of the interfacial disorder. The A parameters have dimension of Oersted while the P parameters have no dimension but they are similar to a relaxation time, where the continuous variable "time" is replaced by a discrete variable n. We expect that the interfacial contribution sharply decreases with n as the anisotropy of the interfacial spins is reduced (low AF anisotropy spins), while the contribution from the "frozen" AF spins belonging to the AF domains ("frozen-in" uncompensated spins) appear as a long decreasing tail as they are intimately embedded into a much stiffer environment.

In the following we show fits to the "trained" exchange bias field. In Fig. 35a) The EB field of thirteen consecutive hysteresis loops were measured at T = 10 K and are plotted as a function of loop index for a CoO(40 Å)/Fe(150 Å)/Al$_2$O$_3$ bilayer. Three fits are

shown: one using the empirical relation Eq. 51, the second one is a fit performed by Binek (12) using the Eq. 53, and the third one using Eq. 54. We observe that the fit using the Eq. 51 ($H_{eb}^\infty = 146.6\,Oe, k = 44\,Oe$) follows well the experimental curve for $n \geq 2$. However, the best fits are obtained using Eq. 53 and Eq. 54. The best fit parameters using Eq. 53 are (12): $H_{eb}^\infty = 148.632\,Oe$, $\gamma_{eb}^b = 0.00029472$, and $\gamma_{eb}^c = -2.772\,10^{-8}$. The parameters obtained from fits to the data using the Eq. 54 are: $H_{eb}^\infty = 158\,Oe, A_f = 25.87\,Oe, P_i = 4.33, A_i = 739.14\,Oe, P_i = 0.39$. Within the SG approach, we distinguish, indeed, a sharp contribution due to low anisotropy AF spins at the interface and a much weaker decrease from the "frozen-in" uncompensated spins.

The temperature dependence of the training effect for a monocrystalline Fe(150 Å)(110)/CoO(300 Å)(111)/Al$_2$O$_3$ bilayer (113; 114; 134) is shown in Fig. 35b). The sample was field cooled in saturation to the measuring temperature where 31 consecutive hysteresis loops were measured. The fits to the data using Eq. 54 are shown as continues lines in Fig. 35b).

We distinguish three main characteristics related to the temperature dependence of the training effect:

- each curve shows two regimes, a fast changing one and a slowly decreasing tail;

- the "relaxation times" (P_i and P_f) do not visibly depend on the temperature;

- the interface transition towards the equilibrium state is approximatively ten times faster then the transition of the "frozen" spins towards their stable configuration.

XIV. FURTHER CHARACTERISTICS OF EB-SYSTEMS

A. Asymmetries of the hysteresis loop

A curios characteristic of EB systems is the often observed asymmetry between the two branches of the hysteresis loop for descending and ascending magnetic fields. The hysteresis loop shape of an isolated ferromagnet is with no exceptions symmetric with respect to the field and magnetization axis. This is not the case for an exchange bias system, where the unidirectional anisotropy and the stability of the AF can result in asymmetries of the hysteresis loops and of the magnetization reversal modes. One can distinguish two different classes of the hysteresis loop asymmetries. One of them can be assigned to intrinsic properties of the EB systems which lacks training effects, and the another one is intimately related to irreversible changes of the AF domain structure during the magnetization reversal.
i) In the first category we encounter four different situations of asymmetryic magnetization reversal all related to a stable interface without training effect:
a) the first branch of the hysteresis loop is much extended

compared to the ascending branch (see Fig. 36). This asymmetric hysteresis loop was observed in FeNi/FeMn bilayers (106). The underlying mechanism is related to a Mauri type mechanism for exchange bias where a parallel domain wall (exchange spring) is formed in the AF layer. The reversal is understood in terms of domain wall pinning in the antiferromagnet (45; 69; 106).
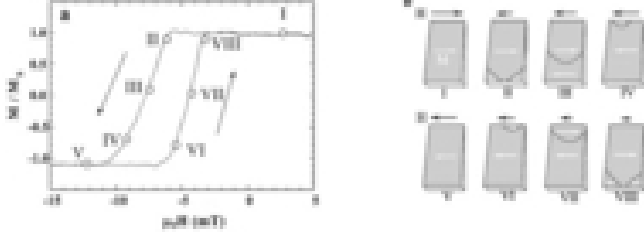

FIG. 36   a) Asymmetric hysteresis loop (a) of a NiFe/FeMn bilayer and schematics of domain structure at different stages of magnetization reversal (106).

b) coherent rotation during the first reversal at H_{c1}, domain wall nucleation and propagation at H_{c2} (see Fig. 37). Such asymmetric magnetization reversal has been observed by PNR in Fe/FeF$_2$ and Fe/MnF$_2$ systems (32). This asymmetry depends on the relative orientation of the field cooling direction with respect to the twin structure of the AF layer. The reversal asymmetry mentioned above takes place when the FC is parallel oriented with a direction bisecting the anisotropy axes of the two AF structural domains. When the field cooling orientation is parallel to the anisotropy axes of one AF domain, the reversal mechanism is symmetric, i. e. for both branches of the hysteresis loop magnetization rotation prevails.
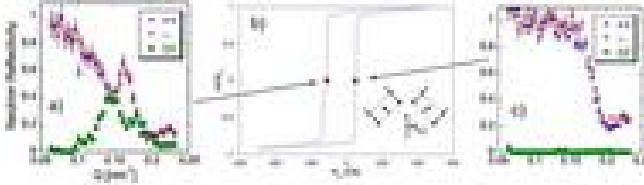

FIG. 37   a) Asymmetric hysteresis loop (b) of a Fe/MnF$_2$ bilayer and and the corresponding neutron reflectivity curves: a) the PNR curves recorded at the first coercive field, H_{c1} and c) the PNR curve recorded at H_{c2}. The lack of SF reflectivity at H_{c2} suggests that the reversal proceeds by domain wall nucleation and propagation, whereas at H_{c1} the magnetization reverses by rotation (31; 32).

c) sharp reversal on the descending branch and rounded reversal on the ascending one (see Fig. 38). This asymmetry has recently been clarified by studies of the azimuthal dependence of exchange bias in IrMn/F bilayers (22; 30; 133). It is an intrinsic property of the EB bilayer systems and it takes place whenever the measuring external field is offset with respect to the field cool-

ing orientation. By simply analyzing the geometrical asteroid solutions, it becomes obvious that the sweep line does not symmetrically cross the shifted asteroid when the field is not parallel to the unidirectional anisotropy. Actually, this is a peculiar case of asymmetry which can be understood even within the phenomenological model for exchange bias (22) which assumes a rigid AF spin structure. Within the SG and M&B model (133) such asymmetric reversals can be simulated over a wide range of AF thicknesses and anisotropies. Also, within the DS model (5; 6), the effect of an offset measuring field axis with respect to the anisotropy axes of the AF and F layer can result in asymmetric reversal modes.
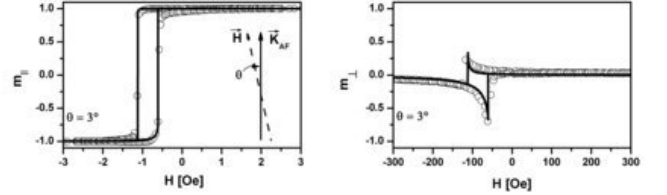

FIG. 38   Asymmetric hysteresis loop of a IrMn/CoFe bilayer along an offset $\theta = 3°$ angle (133).

d) the descending part is steeper, while the ascending branch is more rounded (see Fig. 39). This asymmetry of the hysteresis loop needs to be distinguished from the previous ones, since it occurs when the external field is oriented parallel with respect to the anisotropy axis. It is observed in EB bilayers with thin antiferromagnetic layers or for systems containing low anisotropy AF layers. We call these antiferromagnets weak antiferromagnets and characterize them by the R-ratio. When the R-ratio is slightly higher than one (weak AF layers), then the asymmetry of the hysteresis loop can be reproduced within the SG model. When the R-ratio is much higher than one (strong AF layers), then the hysteresis loops are symmetric as shown in Fig. 28. To account for the asymmetry we consider the following example where
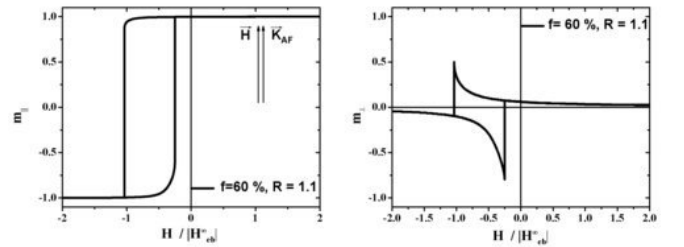

FIG. 39   Longitudinal (left) and transverse components (right) of the magnetization vector for an week antiferromagnet: $R = 1.1$. The hysteresis loop is asymmetric: the descending part is steeper than the ascending part. The asymmetry is clearly seen also in the transverse component of the magnetization.

it is essential that the AF layer is weak but the R ratio is

higher than 1: $R = 1.1$, $f = 60\%$, $\gamma = 5°$, and $\theta = 0°$. For these values the minimization of the free energy is evaluated numerically. The results are plotted in Fig. 39. The longitudinal and transverse components of the magnetization vector is shown as a function of the reduced field $h = H/|H_{eb}^{\infty}|$. We clearly recognize that the hysteresis loop is asymmetric: steeper on the descending leg and more rounded on the ascending leg. The asymmetry is due to the large rotation angle of the AF spins during the F magnetization reversal. This asymmetry has not received experimental recognition so far, therefore it remains a prediction of the SG model.

ii) The second class of asymmetric hysteresis loop is directly related to the training effect, and therefore to the stability of the AF layer and AF/F magnetic interface during the magnetization reversal.

a)sharp reversal at H_{c1} and more rounded reversal on the ascending branch, at H_{c2} (see Fig. 40). Measuring subsequent hysteresis loops, the rounded reversal character does not change but appears also at H_{c1}. This type of asymmetry, being related to the training effect, is frequently reported in different exchange bias systems (41; 51; 55; 56; 90; 121; 128; 129; 143; 162; 163; 165; 174; 181; 182). Its underlying microscopic origin, has been recently demonstrated to stem in irreversible changes that occurs in the AF layer. Polarised Neutron Reflectivity measurements have revealed that at H_{c1} the reversal proceeds by domain wall nucleation and propagation (40; 41; 80; 128; 129; 163; 165; 174). At the second coercive field , magnetization rotation is the reversal mechanism. Moreover, by analyzing the AF/F interface (128; 129), it has been observed experimentally that a transition from a collinear state to an non-collinear disorder state occurs. It suggests that the AF layer in (CoO thin layer)/F evolves from a single AF to a multiple AF domain state. In a AF layer that exhibits a domain state the anisotropy orientation in different domains is laterally distributed causing a reduced coercive and exchange bias field. Note that a thick CoO film is suggested to be already in a domain state (117) after field cooling, therefore one would expect a variation of the loop asymmetry (and training effect) with respect to the thickness of the AF layer.

B. Temperature dependence of the rotatable AF spins (coercivity)

We discuss here the temperature dependence of the interfacial properties. Experimentally this can best be studied by an element selective method (29; 131; 137; 141; 180) to distinguish between the hysteresis of the F and AF layer. Element specific hysteresis loops have been studied for Fe/CoO (131), which highlights the behavior of the rotatable interfacial AF spins.

The exchange bias hysteresis loops measured at the L_3 absorption edges of Co (E=780 eV, closed symbols) and Fe (E=708.2 eV, open symbols) and for different
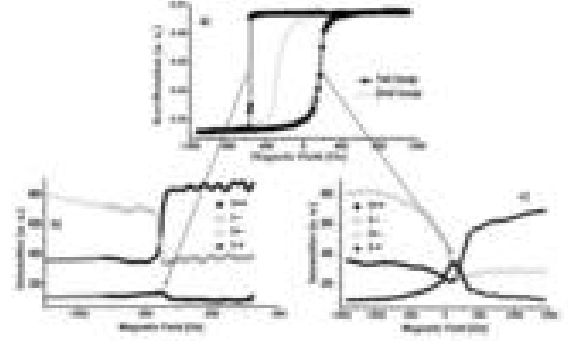

FIG. 40 (a) MOKE hysteresis loop of a CoO/Co bilayer after field cooling to 50 K in an external field of 2000 Oe. The black dots denote the first hysteresis loop, the dotted line the second loop. Any further loops are not significantly different from the second. (b) and (c) Hysteresis loops recorded by polarized neutrons from the same sample but at 10 K. I++, I−−, I+− and I−+ refer to non-spin flip and spin-flip intensities as a function of external magnetic field. (Ref. (129))
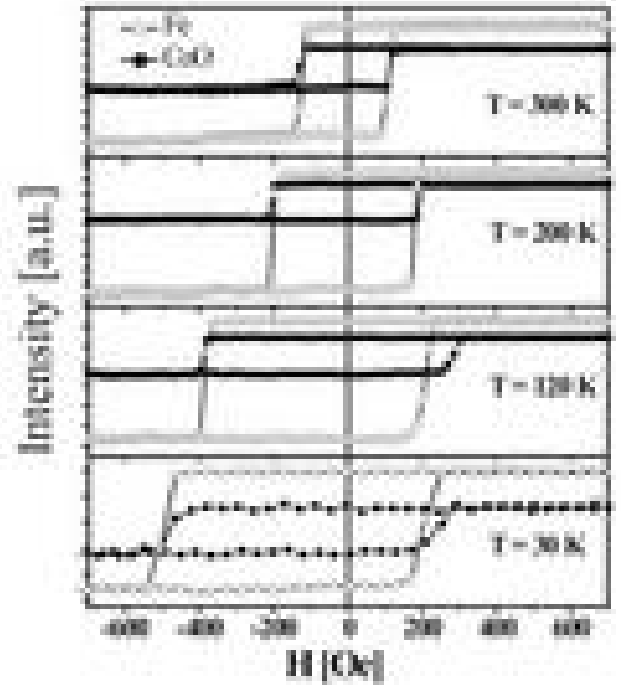

FIG. 41 The temperature dependence of the exchange biased hysteresis loops measured at L_3 absorption edges of Co (E=780 eV, closed symbols) and Fe (E=708.2 eV, open symbols). Scattering angle is $2\theta = 32°$ (131).

temperatures are shown in Fig. 41. After FC to 30 K, several hysteresis loops were measured in order to eliminate training effects. Subsequentially the temperature was raised stepwise, from low to high T. For each tem-

perature an element-specific hysteresis loop at the energies corresponding to Fe and CoO, respectively, was measured. The hysteresis loops of Fe as a function of temperature show a typical behavior. At low temperatures an increased coercive field and a shift of the hysteresis loop is observed. As the temperature is increased, the coercive field and the exchange bias decrease until the blocking temperature is reached. Here, the exchange bias vanishes and the coercive field shows little changes as the temperature is further increased.

A ferromagnetic hysteresis loop corresponding to the CoO layer is observed for all temperatures, following closely the hysteresis loop of Fe , with some notable differences. It appears that the ferromagnetic components of CoO develop higher coercive fields than Fe below the blocking temperature. This is an essential indication that the AF rotatable spins mediate coercivity between the AF layer and the F one, justifying the conversion factor introduced in the SG model. After careful analysis of the element specific reflectivity data (34; 131), one can conclude that a positive exchange coupling across the Fe/CoO interface. The ferromagnetic moment of CoO is present also above the Néel temperature. Here, the AF layer is in a paramagnetic state, therefore the coercive fields for the Fe and CoO rotatable spins are equal.

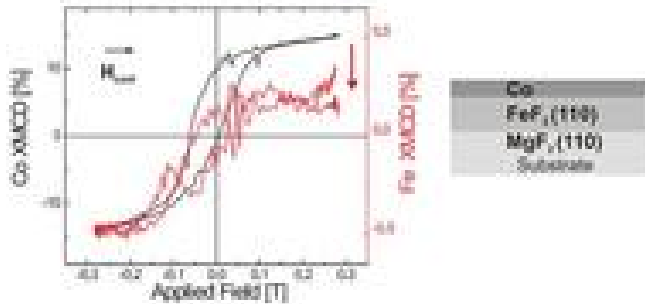## C. Vertical shift of magnetization curves (frozen AF spins)

FIG. 42 Element-specific Co (black) and Fe (gray) hysteresis loops acquired at T= 15 K after field cooling in +200 Oe along the FeF$_2$ [001] axis, parallel to the AF spin axis. The direction of the cooling field and the vertical shift of the Fe loop at T = 15 K is indicated by arrows. Reproduced from (120).

A vertical shift of magnetization has been observed frequently (56; 62; 62; 64; 66; 83; 103; 108; 110; 117; 119; 120; 122; 140) and is considered to have several origins related to the different mechanisms for exchange bias. Within the M&B model a AF monolayer in contact to the F layer is assumed to be uncompensated, but still being part of the AF lattice. At most one could expect a contribution to the macroscopic or microscopic magnetization equal to that of the net magnetization of an AF monolayer and this only by probing an AF layer consisting of an odd number of monolayers. The Mauri mecha-

nism for exchange bias is not likely to result in a vertical shift of the hysteresis loop, since the AF interface is compensated. Within the SG, Malozemoff, and DS models for EB, a small vertical shift is intrinsic. At the interface between the AF and F layer, a number of frozen AF spins will be uncompensated due to the proximity of the F layer. Their orientation is either parallel or antiparallel oriented with respect to the F spins, depending on the type of coupling(direct or indirect exchange). They contribute to the magnetization of the system. In case of an indirect exchange coupling mechanism, the hysteresis loop should be shifted downwards (107; 108), whereas in case of direct exchange coupling the magnetization curve should be shifted upwards. The other part of the interface magnetization, namely the rotatable AF spins, do not cause any shift since they rotate in phase with the F layer. Within the DS model AF domains cause an additional shift to the macroscopic magnetization curve along the magnetization axis (66; 117; 122).

To demonstrate the shift of the magnetization we discuss a recent experiment by Ohldag *et al.* (120) using XMCD (158). The evolution of the dichroic signal as function of the magnetic field, providing the element specific hysteresis loops, is shown Fig. 42.

The sample structure is Pd(2 nm)/Co(2.8 nm)/FeF$_2$(68 nm)(110)/MgF$_2$(110)/substrate and has been grown by via molecular beam epitaxy. The F layer is a polycrystalline Co whereas the AF layer is a FeF$_2$(110) untwined single crystalline layer. The system exhibits a positive exchange bias at large cooling fields (107). For weak cooling fields the exchange bias curve is shifted to the negative fields, as usual for all EB systems. The microscopic origin of the positive exchange bias is an antiferromagnetic coupling at the F/AF interface (107). Although, the mechanism was clearly demonstrated by magnetometery measurements, the microscopic investigation of the AF interface provides more detailed information.

The hysteresis loop of Co is typical and appears symmetric with respect to the magnetization axis (see Fig. 42). This is not the case for the AF interface magnetization which shows a twofold behavior: a) some interfacial AF spins are parallel oriented with respect to the F spins and both are rotating almost in phase; the AF hysteresis loop is shifted downwards with respect to the magnetization axis. This seems to be a direct proof of the preferred antiparallel coupling between the F Co and the AF Fe magnetization at the AF-F interface. The interfacial AF Fe moments are aligned during FC by the exchange interaction which acts as an effective field on the uncompensated spins, most likely confined to the interface (120). An AF uncompensated magnetization in FeF$_2$ can also occur due to piezomagnetism, which is allowed by symmetry in rutile-type AF compounds and may be induced by stresses occurring below the Néel temperature (12; 13).

These experimental observations can also be described by the SG model. During the field cooling procedure the

frozen-in spins depicted in Fig. 27 will be pointing opposite to the F spins as to fulfill the indirect exchange condition at the F/AF interface. The rotatable ones remain unchanged in the figure, being parallel aligned with the F spins. The orientation of the frozen spins is governed by the exchange interaction at the F/AF interface, whereas the rotatable spins are align by the F layer and the external field. Upon reversal the rotatable spins will follow the ferromagnet whereas the frozen spins remain pinned, leading to a shift downwards of the interfacial AF hysteresis loop. As the system described above does not exhibits training effects, no irreversible changes occurs during the magnetization reversal. In high enough cooling fields, the frozen-in spins will align parallel to the cooling field becoming also parallel with the rotatable AF and F spins. This will cause a positive shift of the hysteresis loop (positive exchange bias), since the orientation of the AF frozen spins is negative with respect to the coupling sign (107).

The experimental results described above could most likely be described also by DS model and the Malozemoff model if magnetic domains in the AF layer will be confirmed.

A relative vertical shift of the magnetization related to training effect is described by Hochstrat et al. (56) for a NiO(0001)/Fe(110) exchange bias system. The antiferromagnet is a single crystal NiO whereas the ferromagnetic material is an Fe layer deposited under ultrahigh vacuum condition. Upon successive reversals of the F layer a decreased of the total magnetization was observed by SQUID magnetometery. The variation of the vertical shift as a function of the hysteresis loop index n was correlated to a decrease of the AF magnetization. A linear correlation between the AF magnetization, deduced from the vertical shift, and the exchange bias field during training was found, suggesting that the training effect may be related to a reduced AF magnetization along the measuring field axis and as a function of the loop index.

In Fig. 43 we show another situation where a vertical shift is visible in macroscopic magnetization curves measured by SQUID magnetometery (17). The system is a polycrystalline CoO(2.5 nm)/Co(15 nm) bilayer grown by magnetron sputtering (18). The hysteresis loop at room temperature and along the easy magnetization axis of the F layer is symmetric with respect to the magnetization axis and shows a low coercive field. Upon field cooling the system through the Néel of the CoO layer ($T_N = 291~K$) to the measuring temperature T=4.2 K the system is set in an exchange bias state. Then, a hysteresis loop is measured by sweeping the field from 2000 Oe to -2000 Oe and back. By comparing this hysteresis loop with the one measured at room temperature one clearly observes a vertical shift up along the magnetization axis. Moreover, this up-shift is due to the ferromagnetic Co spins which do not fully saturate at -2000 Oe. Previous studies have shown that after the reversal at H_{c1}, the AF CoO layer breaks into AF domains exhibiting an anisotropy distribution. Due to the

strong coupling between the F and the AF domains, the F layer cannot easily be saturated. Next, after repeating the field cooling procedure, another hysteresis loop was measured by sweeping the external field to much larger negative value, namely to -9000 Oe. Now one observes that the hysteresis loop becomes more symmetric with respect to the magnetization axis. The saturation field, where the hysteresis loops closes, is about -8000 Oe.

The example above shows that a vertical shift of magnetization can be related to non a homogeneous state of the F layer due to non-collinearities at the AF/F interface. The relation to the training effect is clearly seen as different coercive fields H_{c2} depending on the strength of the applied fields. When a stronger field is applied in the negative direction, the exchange bias decreases due to a larger degree of irreversible changes into the AF layer.
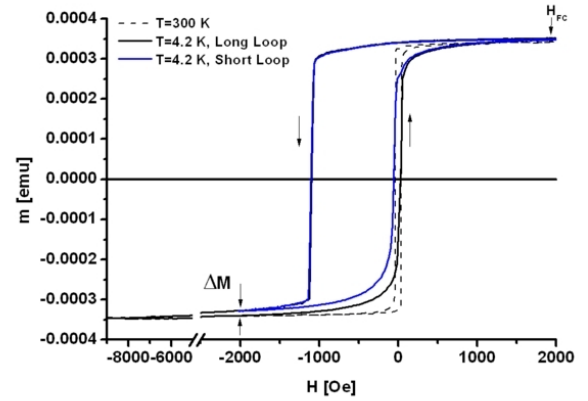

FIG. 43   Hysteresis loops of a CoO(25Å)/Co(180Å). The dashed line is the hysteresis loop recorded at 300 K which is above the Néel temperature of the CoO layer. After field cooling the system to 4.2 K, a hysteresis loop is recorded sweeping the applied field from 9000 to -9000 Oe and back to 9000 Oe (black line, long loop). A second loop is measured under the same conditions as the previous one, but the field range is shorter, namely between 2000 Oe to -2000 Oe and back to 2000 Oe. The cooling field was positive. A vertical shift of the hysteresis loop is clearly visible for the short loop, whereas the long loop appears to be centered with respect to magnetization axis.(Ref. (17))

A distinct class of vertical shifts is found in exchange bias systems where a diluted antiferromagnet (66; 112; 117; 122) acts as a pinning layer. As function of dilution of a CoO layer by Mg impurities, as well as, partial oxygen pressure during the deposition, the AF layer acquires an excess magnetization seen as a vertical shift of the hysteresis loop. This strongly supports the fact that the domain state in the AF layer as well as the EB effect is caused and controlled the defects (66; 122).

Vertical shifts in nanostructures and nanoparticles are often observed due to uncompensated AF spins. For a detailed discussion we refer to recent reviews by Nogues *et*

al. (110) and Iglesias *et al.* (62) and also recent papers on AF nanoparticles (103; 140).

XV. FURTHER EVIDENCE FOR SPIN-GLASS LIKE BEHAVIOR OBSERVED IN FINITE SIZE SYSTEMS

Although nanoparticles are not covered in this review, we, nevertheless, discuss two recent instances which in AF nanoparticles confirm the SG behavior. One is Co_3O_4 nanowires (140) and the other is CoO granular structure (50).
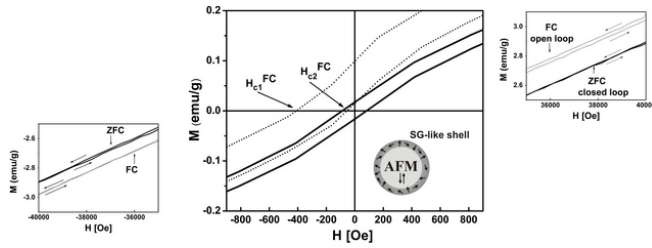
A. AF Nanoparticles

FIG. 44 Field cooled and zero field cooled hysteresis loops of Co_3O_4 nanowires. From Ref. (140)

Nanoparticles of antiferromagnetic materials have been predicted by Néel (104) to have a small net magnetic moment due to an unequal number of spins on the two sublattices as a result of the finite size (74). Hysteresis loops of AF nanoparticles have been observed and several suggestions were made to account for their weak ferromagnetism (74). One important finite size effect of AF magnetic nanoparticle is the breaking of a large number of exchange bonds for surface atoms. This can have a particularly strong effect on ionic materials, since the exchange interactions are superexchange interactions. The deficit of exchange bonds could lead to a spin disordered shell exhibiting spin-glass like behavior. The last effect is demonstrated most recently by Salabas *et al.* (140) and discussed further below.

In Fig. 44 two hysteresis loops of Co_3O_4 nanoparticles (8 nm diameter) prepared by a nanocasting route are shown (140). Both curves were measured at T = 2 K after cooling the system in zero field (ZFC hysteresis loop) and in an external applied field of +4 T(FC hysteresis loop). Whereas the ZFC loop shows typical weak ferromagnetic properties specific to AF particles, after FC a completely different behavior is observed. The hysteresis loop is exchange biased, it is vertically shifted and shows training effect. Moreover, the temperature dependence (not shown) of the coercive field and exchange bias field increases with decreasing temperature, which is also a usual behavior of EB systems. More strikingly the FC hysteresis loop does not close on the right side

at positive fields. This open hysteresis loop is a direct indication of a spin-glass like behavior, similar to the loops observed in pure spin glass systems (10). This behavior appears to support the SG model(Fig. 27), where a reduced anisotropy is assumed to occur at the F/AF interface. Both frozen-in spins and rotatable spins are directly seen in the FC hysteresis loop. Moreover, the irreversible changes of the surface AF spins are causing the open loop. A similar open loop is also predicted by the DS model. Within the DS model the hysteresis loop of the AF interface layer is not closed on the right hand side because the DS magnetization is lost partly during F reversal due to a rearrangement of the AF domain structure. The AF particles, however, are supposed to be single AF domains, therefore irreversible changes are due to surface effects rather than caused by AF domain kinetics. Certainly, at very large cooling fields, the bulk structure of the AF particle should be also affected. The spin-glass like behavior was also recently observed for cobalt ferrite nanoparticles (103), for $(Mn,Fe)_2O_{3-t}$ nanograins (123), and for a εFe_3NCrN nanocomposite system (38).

B. Extended granular AF film

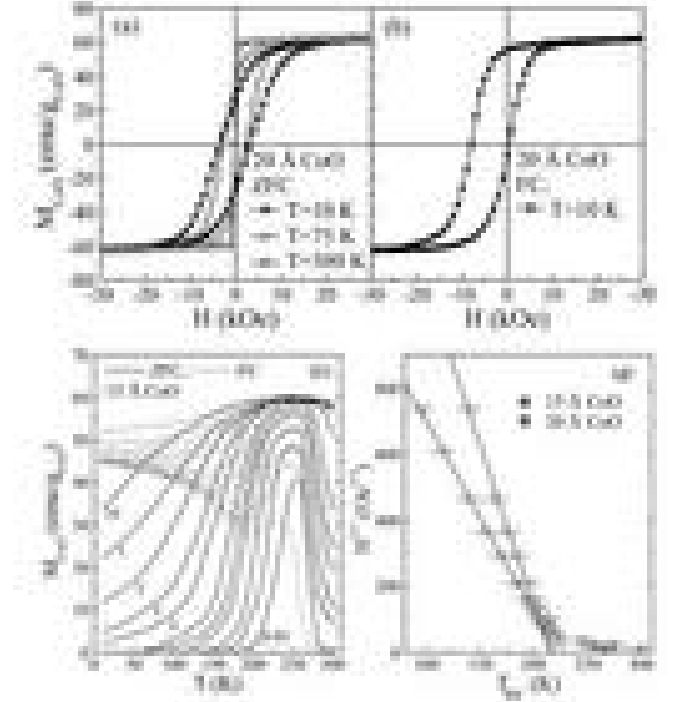FIG. 45 a) ZFC hysteresis loops of [CoO [x Å]/Au (60 Å)] multilayers. b) FC hysteresis loop of a [CoO [20 Å]/Au (60 Å)] multilayer. c) ZFC and FC magnetization curves as a function of increasing temperature T in different fields for a [CoO [15 Å]/Au (60 Å)] multilayer. d) Field dependence of T_{irr} raised to the 2/3 power for two different multilayers.(Ref. (50))

Another direct experimental evidence of a spin-glass

like behavior was observed by Gruyters (50) on CoO/Au multilayers, CoO/Cu/Fe trilayers, and CoO/Fe bilayers with granular structure. In Fig. 45a) the ZFC hysteresis loop of a CoO/Au multilayer and for different temperature is shown. One notices that the coercive field is enhanced at low temperatures, but no hysteresis shift develops. The FC hysteresis loop (see Fig. 45b)), however, is almost completely shifted to one side of the field axis. These observations are explained by Gruyters as an effect of the uncompensated AF spins of the granular film structure. The saturation magnetization of this granular CoO film is about 60-62 emu/g_{CoO} which would result in an enormous amount of uncompensated spins equivalent to 22% for the observed particles volume. No stoichiometry influences are considered to contribute to this value. Although the uncompensation level is unclear, the evidence of a spin-glass behavior is well demonstrated. In Fig. 45c) ZFC and FC magnetization curves are measured as function of temperature and for different external fields. Two main characteristic features are observed for these curves: an irreversibility temperature T_{irr}, where the ZFC and FC branches of M_{CoO}(T) coalesce, and a pronounced peak due to superparamagnetic blocking in the ZFC magnetization. The direct evidence of a spin-glass behavior is the field dependence of T_{irr} shown in Fig. 45d).The existence of critical lines spanned by the variables temperature and magnetic field can be explained by mean-field theory. One of these lines has been predicted by de Almeida and Thouless for Ising spin systems (50). The T_{irr} raised to 2/3 power as function of field exhibits a linear dependence in agreement with the predictions Almeida and Thouless.

C. Dependence of the exchange bias field on lateral size of the AF domains

The relation between the exchange bias and the reduced size effects due nano-structuring of the AF-F systems is important from both fundamental and technological points of view. From a fundamental point of view, the reduced lateral size of both F and AF objects induces significant changes of the exchange bias field, coercive fields and also the asymmetry of the hysteresis loops (4; 28; 33; 41; 42; 52; 57; 82; 124; 146; 150; 164; 179). In some systems an increased exchange bias field occurs for reduced lateral sizes, whereas in other cases an opposite behavior is reported, the exchange bias field decreases with decreasing the lateral length scales (110). We refer in the following to the last situation.

In Fig. 46 are depicted schematically several lateral systems which are commonly used to study the influences of the nano-structuring onto the exchange bias properties. A reduced lateral size of the ferromagnet (Fig. 46b) and Fig. 46c)) gives rise to additional shape anisotropies for the ferromagnet leading to a change of both coercive and exchange bias fields as well as a change of the hysteresis shape. In Fig. 46a) these additional anisotropies

are minimized and therefore the dependence of exchange bias as function of the AF lateral size is more transparent. For all three situations we can assume that at the borders defined by the geometrical nanostructures, there is an additional disorder extending to the interface. Even for the case b) where the F is nano-structured we may expect that the lithographic process will not always be stopped exactly at the interface but also affecting the AF layer around the dot.

Due to nano-structuring it is natural to expect that at the edges of the dot there are AF spins with reduced anisotropy. These spins will contribute to the coercivity at the expense of the interfacial exchange energy. The effective interfacial exchange energy can be written as: $J_{eb}^{eff} = FfJ_{eb}$, where F is a conversion factor related to size effects, similar to the f defined for the interface. It is easy to estimate the F-parameter, as the fraction of the outer shell area divided by the total dot area: $F \approx A1/A2 \approx (\pi(D-d)^2)/(\pi D^2) = 1 - 2d/D + d^2/D^2$, where d is the lateral thickness of the outer shell and D is the diameter of the dot itself. Assuming that $d << D$ and that d is constant, we obtain the general expression for the variation of the exchange bias field as D:

$$\frac{-H_{eb} + H_{eb}^{D \to \infty}}{H_{eb}^{D \to \infty}} \approx 1 - F \approx \frac{1}{D}, \qquad (55)$$

where $H_{eb}^{D \to \infty}$ is the exchange bias of an extended film. Within this simple model the exchange bias field decreases as the lateral size of the AF structure decreases. This 1/D dependence is often observed experimentally (110).

FIG. 46 A schematic view of different nanostructered systems used to study the finite size effects on the exchange bias properties.

The general behavior of the hysteresis loops as a function of the f-parameter is depicted in Fig. 28. We see that for high f corresponding to a large diameter AF dot, the coercive field is small and the exchange bias is high. When, however, the lateral size of a AF object becomes smaller, the f ratio decreases leading to an increased coercive field and reduced exchange bias field. Transition from the top hysteresis to the bottom hysteresis of Fig. 28 are usually observed due to nanostructuring of the AF layers (4; 28; 33; 110).

XVI. CONCLUSIONS

The results presented in this chapter provides an overview of the physics of a F/(Interface)/AF exchange

bias systems. Fundamental properties of the unidirectional anisotropy are considered and discussed. The Meiklejohn and Bean model as well as the Mauri model are considered in detail and compared, both analytically and numerically. The Néel approach, Malozemoff model, Domain State model and a model of Kim and Stamps are shown as they provide novel and fundamental ideas on the EB phenomenon. The Spin Glass model is discussed in even more details. Further experimental results touching the fundamentals of exchange bias are described.

We distinguish several outcomes of our overview:

- The exchange bias is an interface effect, as clearly proved by the $1/t_F$ dependence. Deviations from this law were observed in the literature, but fundamentally this expression is clearly well established.

- The AF anisotropies in the bulk of the AF layer and at the interface to a soft ferromagnetic layer give rise to an impressively rich behavior of the magnetic properties: the hysteresis loops can be shifted along both field and magnetization axis and in both positive and negative directions, the azimuthal dependence of exchange bias exhibits non-intuitive behavior such as a shift of its maximum with respect to the field cooling orientation, the hysteresis loops are asymmetrically shaped, etc. Some of the exchange bias characteristics mentioned above are not fully and consistently revealed experimentally which leaves an open window for further quests.

- The analytical formulae for the exchange bias within M&B model depends mainly on the properties of the AF layer, namely on its anisotropy and thickness.

- The peak-like increase of the EB close to the critical thickness of the AF layer can be reproduced by the SG model. This effect is also accounted for by the DS model.

- Azimuthal dependence of exchange bias could help to distinguish between two ideal mechanisms for exchange bias: Mauri versus M&B models.

- The SG model describes the conversion of coupling into coercivity.

List of acronyms

AMR	Anisotropic Magneto-Resistance
FC	Field Cooling
ZFC	Zero Field Cooling
EB	Exchange Bias
DS	Domain State Model
SG	Spin Glass Model
SW	Stoner-Wohlfarth Model
M&B	Meiklejohn and Bean Model
MCA	Magneto-Crystalline Anisotropy
MOKE	Magneto-Optical Kerr Effect
PNR	Polarized Neutron Reflectivity
SQUID	Superconducting Quantum Interference Device
AF	Antiferromagnet
F	Ferromagnet
MFM	Magnetic Force Microscopy
MRAM	Magnetic Random Access Memory
DAFF	Diluted Antiferromagnets in an External Magnetic Field
XMCD	Soft X-ray Resonant Magnetic Dichroism
XRMS	Soft X-ray Resonant Magnetic Scattering

References

[1] M. Ali, C. H. Marrows, M. Al-Jawad, B. J. Hickey, A. Misra, U. Nowak, and K. D. Usadel. Antiferromagnetic layer thickness dependence of the irmn/co exchange-bias system. Phys. Rev. B., 68(21):214420, 2003.

[2] Mannan Ali, Patrick Adie, Christopher H. Marrows, Denis Greig, Bryan J. Hickey, and Robert L. Stamps. Exchange bias using a spin glass. Nature Materials, 6:70, 2007.

[3] T. Ambrose, R. L. Sommer, and C. L. Chien. Angular dependence of exchange coupling in ferromagnet/antiferromagnet bilayers. Phys. Rev. B., 56:83, 1997.

[4] V. Baltz, J. Sort, B. Rodmacq, B. Dieny, and S. Landis. Size effects on exchange bias in sub 100 nm ferromagnetic antiferromagnetic dots deposited on prepatterned substrates. Appl. Phys. Lett., 84:4923, 2004.

[5] B. Beckmann, U. Nowak, and K. D. Usadel. Asymmetric reversal modes in ferromagnetic/antiferromagnetic multilayers. Phys. Rev. Lett., 91:187201, 2003.

[6] B. Beckmann, K. D. Usadel, and U. Nowak. Cooling-field dependence of asymmetric reversal modes for ferromagnetic/antiferromagnetic multilayers. Phys. Rev. B., 74(5):054431, 2006.

[7] A. Berger, A. Inomata, J. S. Jiang, J. E. Pearson, and S. D. Bader. Experimental observation of disorder-driven hysteresis-loop criticality. Phys. Rev. Lett., 85(19):4176–4179, Nov 2000.

[8] F. S. Bergeret, A. F. Volkov, and K. B. Efetov. Odd triplet superconductivity and related phenomena

in superconductor-ferromagnet structures. Rev. Mod. Phys., 77:1321, 2005.

[9] A. E. Berkowitz and K. Takano. Exchange anisotropy - a review. J. Magn. Magn. Mater., 200:552, 1999.

[10] K. Binder. Spin glasses: Experimental facts, theoretical concepts, and open questions. Rev. Mod. Phys., 58(4):801–976, October 1986.

[11] Ch. Binek, A. Hochstrat, and W. Kleemann. Exchange bias in a generalized meiklejohn-bean approach. J. Magn. Magn. Mater., 234:353, 2001.

[12] Christian Binek. page private communication.

[13] Christian Binek. Ising-type antiferromagnets. Springer Tracts in Modern Physics, 196, 2003.

[14] Christian Binek. Training of the exchange-bias effect: A simple analytic approach. Phys. Rev. B., 70:014421, 2004.

[15] Christian Binek, Xi He, and Srinivas Polisetty. Temperature dependence of the training effect in a co/coo exchange-bias layer. Phys. Rev. B., 72(5):054408, 2005.

[16] H.-B. Braun, J. Kyriakidiis, and D. Loss. Dynamic magnetic hysteresis and anomalous viscosity in exchange bias systems. Phys. Rev. B., 56:8129, 1997.

[17] Steven Brems, Dieter Buntinx, Kristiaan Temst, Chris Van Haesendonck, Florin Radu, and Hartmut Zabel. page unpublished, 2005.

[18] Steven Brems, Dieter Buntinx, Kristiaan Temst, Chris Van Haesendonck, Florin Radu, and Hartmut Zabel. Reversing the training effect in exchange biased coo/co bilayers. Phys. Rev. Lett., 95:157202, 2005.

[19] D. Bürgler, S. O. Demokritov, P. Grünberg, and M. T. Johnson. Interlayer exchange coupling in layered magnetic structures. in Handbook of Magnetic Materials K. H. J. Buschow, ed., Elsevier North-Holland, Amsterdam, 13, 2001.

[20] A. I. Buzdin. Proximity effects in superconductor-ferromagnet heterostructures. Rev. Mod. Phys., 77:935, 2005.

[21] J. Camarero, Y. Pennec, J. Vogel, S. Pizzini, M. Cartier, F. Fettar, F. Ernult, A. Tagliaferri, N. B. Brookes, and B. Dieny. Field dependent exchange coupling in nio/co bilayers. Phys. Rev. B., 67(2):020413, 2003.

[22] Julio Camarero, Jordi Sort, Axel Hoffmann, Jose Miguel García-Martín, Bernard Dieny, Rodolfo Miranda, and Josep Nogués. Origin of the asymmetric magnetization reversal behavior in exchange-biased systems: Competing anisotropies. Phys. Rev. Lett., 95:057204, 2005.

[23] C. Chappert, H. Bernas, J. Ferre, V. Kottler, J. P. Jamet, Y. Chen, E. Cambril, T. Devolder, F. Rousseaux, V. Mathet, and H. Launois. Planar patterned magnetic media obtained by ion irradiation. Science, 280:1919–1922, 1998.

[24] Xi Chen, Ch. Binek, A. Hochstrat, and W. Kleemann. Dilution-induced enhancement of the blocking temperature in exchange-bias heterosystems. Phys. Rev. B., 65(1):012415, Dec 2001.

[25] R. Coehoorn. Exchange anisotropy, stoner-wolhfarth model. Lecture Notes, Eindhoven University of Technology, page Eindhoven University of Technology, 2000-2001.

[26] R. Coehoorn, J. T. Kohlhepp, R. M. Jungblut, A. Reinders, and M. J. Dekker. Mesoscopic magnetism and the phenomenon of exchange anisotropy: Mbe grown cu(110)/ni$_{80}$fe$_{20}$/fe$_{50}$mn$_{50}$ bilayers with corrugated interfaces. Physica B: Condensed Matter, 319("1-

4"):"141–167", 2002.

[27] C. Daboo, R. J. Hicken, E. Gu, M. Gester, S. J. Gray, D. E. P. Eley, E. Ahmad, J. A. C. Bland, R. Ploessl, and J. N. Chapman. Anisotropy and orientational dependence of magnetization reversal processes in epitaxial ferromagnetic thin films. Phys. Rev. B., 51(22):15964–15973, Jun 1995.

[28] Johannes Eisenmenger, Zhi-Pan Li, Waldemar A. A. Macedo, and Ivan K. Schuller. Exchange bias and asymmetric reversal in nanostructured dot arrays. Phys. Rev. Lett., 94(5):057203, 2005.

[29] D. Engel, , H. Schmoranzer, A. Ehresmann, H. C. Mertins, D. Abramsohn, and W. Gudat. Soft x-ray resonant magnetic reflection investigations of femn/co/cu/co spin valves modified by he-ion bombardment. J. Magn. Magn. Mater., 345:185–188, 2004.

[30] J. McCord et al. page unpublished.

[31] M. R. Fitzsimmons, C. Leighton, A. Hoffmann, P. C. Yashar, J. Nogues, K. Liu, C. F. Majkrzak, J. A. Dura, H. Fritzsche, and I. K. Schuller. Influence of interfacial disorder and temperature on magnetization reversal in exchange-coupled bilayers. Phys. Rev. B., 64:104415, 2001.

[32] M. R. Fitzsimmons, P. Yashar, C. Leighton, Ivan K. Schuller, J. Nogues, C. F. Majkrzak, and J. A. Dura. Asymmetric magnetization reversal in exchange-biased hysteresis loops. Phys. Rev. Lett., 84:3986, 2000.

[33] M. Fraune, U. Rüdiger, G. Güntherodt, S. Cardoso, and P. Freitas. Size dependence of the exchange bias field in nio/ni nanostructures. Appl. Phys. Lett., 77:3815–3817, 2000.

[34] J. W. Freeland, V. Chakarian, Y. U. Idzerda, S. Doherty, J. G. Zhu, J.-H. Park, and C.-C. Kao. Identifying layer switching in magnetic multilayers with x-ray resonant magnetic scattering. Appl. Phys. Lett., 71(2):"276–278", 1997.

[35] H. Fujiwara, C. Hou, M. Sun, and H. S. Cho. Effect of exchange coupling of polycrystalline antiferromagnetic layers on the magnetization behavior of soft magnetic layers. IEEE Transactions on Magnetics, 35(5):3082, 1999.

[36] E. Fulcomer and S. H. Charap. Temperature and frequency dependence of exchange anisotropy effects in oxidized nife films. J. Appl. Phys., 43:4184, 1972.

[37] E. Fulcomer and S. H. Charap. Thermal fluctuation aftereffect model for some systems with ferromagnetic-antiferromagnetic couplings. J. Appl. Phys., 43:4190, 1972.

[38] N. S. Gajbhiye and Sayan Bhattacharyya. Exchange bias and spin-glass-like ordering in εFe$_3$NCrN nanocomposites. Japanese Journal of Applied Physics, 46(3A):980–987, 2007.

[39] J. Geshev, L. G. Pereira, and J. E. Schmidt. Angular dependence of the exchange bias obtained from magnetization and ferromagnetic resonance measurements in exchange-coupled bilayers. Phys. Rev. B., 64:184411, 2001.

[40] M. Gierlings, M.J. Prandolini, H. Fritzsche, M. Gruyters, and D. Riegel. Change and asymmetry of magnetization reversal for a co/coo exchange-bias system. Phys. Rev. B., 74:092407, 2002.

[41] E. Girgis, R. D. Portugal, M. J. Van Bael, K. Temst, and C. Van Haesendonck. Asymmetric magnetization reversal in exchange-biased nife/coo submicron-sized struc-

tures. J. Appl. Phys., 97(10):103911, 2005.

[42] E. Girgis, R. D. Portugal, H. Loosvelt, M. J. Van Bael, I. Gordon, M. Malfait, K. Temst, C. Van Haesendonck, L. H. A. Leunissen, and R. Jonckheere. Enhanced asymmetric magnetization reversal in nanoscale co/coo arrays: Competition between exchange bias and magnetostatic coupling. Phys. Rev. Lett., 91:187202, 2003.

[43] N. J. Gökemeijer, T. Ambrose, and C. L. Chien. Long-range exchange bias across a spacer layer. Phys. Rev. Lett., 79:4270, 1997.

[44] N. J. Gökemeijer, R. L. Penn, D. R. Veblen, and C. L. Chien. Exchange coupling in epitaxial coo/nife bilayers with compensated and uncompensated interfacial spin structures. Phys. Rev. B., 63:174422, 2001.

[45] V. S. Gornakov, Yu. P. Kabanov, O. A. Tikhomirov, V. I. Nikitenko, S. V. Urazhdin, F. Y. Yang, C. L. Chien, A. J. Shapiro, and R. D. Shull. Experimental study of the microscopic mechanisms of magnetization reversal in feni/femn exchange-biased ferromagnet/antiferromagnet polycrystalline bilayers using the magneto-optical indicator film technique. Phys. Rev. B., 73:184428, 2006.

[46] T. Gredig, I. N. Krivorotov, and D. Dahlberg. Magnetization reversal in exchange biased co/coo probed with anisotropic magnetoresistance. J. Appl. Phys., 91(10):7760, 2002.

[47] T. Gredig, I. N. Krivorotov, and E. Dan Dahlberg. Temperature dependence of magnetization reversal and angular torque in co/coo. Phys. Rev. B., 74:094431, 2006.

[48] T. Gredig, I. N. Krivorotov, P. Eames, and D. Dahlberg. Unidirectional coercivity enhancement in exchange-biased co/coo. Appl. Phys. Lett., 81:1270, 2002.

[49] P. Grünberg, R. Schreiber, Y. Pang, M.B. Brodsky, and H. Sowers. Layered magnetic structures: Evidence for antiferromagnetic coupling of fe-layers across cr-interlayers. Phys. Rev. Lett., 57:2442, 1986.

[50] M. Gruyters. Spin-glass-like behavior in coo nanoparticles and the origin of exchange bias in layered coo/ferromagnet structures. Phys. Rev. Lett., 95(7):077204, 2005.

[51] M. Gruyters and D. Riegel. Strong exchange bias by a single layer of independent antiferromagnetic grains: The coo/co model system. Phys. Rev. B., 63:052401, 2000.

[52] Z. B. Guo, K. B. Li, G. C. Han, Z. Y. Liu, P. Luo, and Y. H. Wu. Exchange bias in patterned femn/nife bilayers. J. Magn. Magn. Mater., 251:323, 2002.

[53] Jing guo Hu, Guojun Jin, An Hu, and Yu qiang Ma. Temperature dependence of exchange bias and coercivity in ferromagnetic/antiferromagnetic bilayers. Eur. Phys. J. B, 40:265–271, 2004.

[54] T. Hauet, J. A. Borchers, Ph. Mangin, Y. Henry, and S. Mangin. Training effect in an exchange bias system: The role of interfacial domain walls. Phys. Rev. Lett., 96(6):067207, 2006.

[55] O. Hellwig, S. Maat, J. B. Kortright, and Eric E. Fullerton. Magnetic reversal of perpendicularly-biased co/pt multilayers. Phys. Rev. B., 65(14):144418, 2002.

[56] A. Hochstrat, Ch. Binek, and W. Kleemann. Training of the exchange-bias effect in nio/fe heterostructures. Phys. Rev. B., 66:092409, 2002.

[57] A. Hoffman, M. Grimsditch, J. E. Pearson, J. Nogues, W. A. A. Macedo, and I. K. Schuller. Tailoring the exchange bias via shape anisotropy in ferromagnetic/antiferromagnetic exchange-coupled systems. Phys. Rev. B., 67:220406, 2003.

[58] A. Hoffmann. Symmetry driven irreversibilities at ferromagnetic-antiferromagnetic interfaces. Phys. Rev. Lett., 93:097203, 2004.

[59] V. Hoink, M. D. Sacher, J. Schmalhorst, G. Reiss, D. Engel, D. Junk, and A. Ehresmann. Postannealing of magnetic tunnel junctions with ion-bombardment-modified exchange bias. Appl. Phys. Lett., 86(15):152102, 2005.

[60] Jung-Il Hong, Titus Leo, David J. Smith, and Ami E. Berkowitz. Enhancing exchange bias with diluted antiferromagnets. Phys. Rev. Lett., 96(11):117204, 2006.

[61] T. M. Hong. Simple mechanism for a positive exchange bias. Phys. Rev. B., 58:97, 1998.

[62] Oscar Iglesias, Amilcar Labarta, and Xavier Batlle. Exhange bias phenomenolgy and models of core/shell naopartiles. arXiv:cond-mat/0607716, 2006.

[63] R. Jungblut, R. Coehoorn, M. T. Johnson, J. aan de Stegge, and A. Reinders. Orientational dependence of the exchange biasing in molecular-beam-epitaxy-grown ni_80fe_20/fe_50mn_50 bilayers. J. Appl. Phys., 75:6659, 1994.

[64] B. Kagerer, C. Binek, and W. Kleemann. Freezing field dependence of the exchange bias in uniaxial fef_2-copt heterosystems with perpendicular anisotropy. J. Magn. Magn. Mater., 217(1-3):139–146, 2000.

[65] P. Kappenberger, S. Martin, Y. Pellmont, H. J. Hug, J. B. Kortright, O. Hellwig, and Eric E. Fullerton. Direct imaging and determination of the uncompensated spin density in exchange-biased coo/(copt) multilayers. Phys. Rev. Lett., 91:267202, 2005.

[66] J. Keller, P. Miltényi, B. Beschoten, G. Güntherodt, U. Nowak, and K. D. Usadel. Domain state model for exchange bias. ii. experiments. Phys. Rev. B., 66:014431, 2002.

[67] Joo-Von Kim and R. L. Stamps. Defect-modified exchange bias. Appl. Phys. Lett., 79(17):2785–2787, 2001.

[68] Joo-Von Kim and R. L. Stamps. Theory of long-wavelength spin waves in exchange biased bilayers. J. Appl. Phys., 89(11):7651–7653, 2001.

[69] Joo-Von Kim and R. L. Stamps. Hysteresis from antiferromagnet domain-wall processes in exchange-biased systems: Magnetic defects and thermal effects. Phys. Rev. B., 71(9):094405, 2005.

[70] Joo-Von Kim, R. L. Stamps, B. V. McGrath, and R. E. Camley. Angular dependence and interfacial roughness in exchange-biased ferromagnetic/antiferromagnetic bilayers. Phys. Rev. B., 61(13):8888–8894, 2000.

[71] T. L. Kirk, O. Hellwig, and E. E. Fullerton. Coercivity mechanisms in positive exchange-biased co films and co/pt multilayers. Phys. Rev. B., 65:224426, 2002.

[72] M. Kiwi. Exchange bias theory. J. Magn. Magn. Mater., 234:584–595, 2001.

[73] S. A. Koch, G. Palasantzas, T. Vystavel, J. Th. M. De Hosson, C. Binns, and S. Louch. Magnetic and structural properties of co nanocluster thin films. Phys. Rev. B., 71(8):085410, 2005.

[74] R. H. Kodama. Magnetic nanoparticles. J. Magn. Magn. Mater., 200:359, 1999.

[75] J. T. Kohlhepp and W. J. M. de Jonge. Stabilization of metastable expanded face-centered-tetragonal manganese. Phys. Rev. Lett., 96(23):237201, 2006.

[76] N. C. Koon. Calculations of exchange bias in thin films

with ferromagnetic/antiferromagnetic interfaces. Phys. Rev. Lett., 78:4865–4868, 1997.

[77] Ilya N. Krivorotov, Hongwei Yan, E. Dan Dahlberg, and Andreas Stein. Exchange bias in macroporous co/coo. J. Magn. Magn. Mater., 226-230:1800–1802, 2001.

[78] W. Kuch, F. Offi L. I. Chelaru, M. Kotsugi J. Wang, and J. Kirschner. Tuning the magnetic coupling across ultrathin antiferromagnetic films by controlling atomic-scale roughness. Nature Materials, 5:128–133, 2006.

[79] D. Lederman, C.A. Ramos, V. Jaccarino, and J.L. Cardy. Finite-size scaling in fef2/znf2 superlattices. Phys. Rev. B., 48:8365, 1993.

[80] W.-T. Lee, S. G. E. te Velthuis, G. P. Felcher, F. Klose, T. Gredig, and E. D. Dahlberg. Ferromagnetic domain distribution in thin films during magnetization reversal. Phys. Rev. B., 65:224417, 2002.

[81] C. Leighton, J. Nogues, H. Suhl, and I. K. Schuller. Competing interfacial exchange and zeeman energies in exchange biased bilayers. Phys. Rev. B., 60:12837, 1999.

[82] K. Liu, S. M. Baker, M. Tuominen, T. P. Russell, and I. K. Schuller. Tailoring exchange bias with magnetic nanostructures. Phys. Rev. B., 63:060403, 2001.

[83] Z. Y. Liu. Exchange bias and vertical loop shifts in a co(32 å)/nio(10 å)/[co(4 å)/pt(6 å)]$_4$ multilayer. Appl. Phys. Lett., 85(21):4971–4973, 2004.

[84] A. P. Malozemoff. Random-field model of exchange anisotropy at rough ferromagnetic-antiferromagnetic interfaces. Phys. Rev. B., 35:3679, 1987.

[85] A. P. Malozemoff. Heisenberg-to-ising crossover in a random-field model with uniaxial anisotropy. Phys. Rev. B., 37(13):7673–7679, 1988.

[86] A. P. Malozemoff. Mechanisms of exchange anisotropy (invited). J. Appl. Phys., 63(8):3874–3879, 1988.

[87] C. Martinez-Boubeta, K. Simeonidis, M. Angelakeris, N. Pazos-Perez, M. Giersig, A. Delimitis, L. Nalbandian, V. Alexandrakis, and D. Niarchos. Critical radius for exchange bias in naturally oxidized fe nanoparticles. Phys. Rev. B., 74(5):054430, 2006.

[88] D. Mauri, E. Kay, D. Scholl, and J. K. Howard. Novel method for determining the anisotropy constant of mnfe in a nife/mnfe sandwich. J. Appl. Phys., 62:2929, 1987.

[89] D. Mauri, H. C. Siegmann, P. S. Bagus, and E. Kay. Simple model for thin ferromagnetic films exchange coupled to an antiferromagnetic substrate. J. Appl. Phys., 62:3047, 1987.

[90] J. McCord, R. Mattheis, and R. Schäfer. Kerr observations of asymmetric magnetization reversal processes in cofe/irmn bilayer systems. J. Appl. Phys., 93:5491, 2003.

[91] W. H. Meiklejohn. Exchange anisotropy - a review. J. Appl. Phys., 33:1328, 1962.

[92] W. H. Meiklejohn and C. P. Bean. New magnetig anisotropy. Phys. Rev., 102:1413, 1956.

[93] W. H. Meiklejohn and C. P. Bean. New magnetig anisotropy. Phys. Rev., 105:904, 1957.

[94] T. Mewes, R. Lopusnik, J. Fassbender, B. Hillebrands, M. Jung, D. Engel, A. Ehresmann, and H. Schmoranzer. Suppression of exchange bias by ion irradiation. Appl. Phys. Lett., 76(8):1057–1059, 2000.

[95] T. Mewes, H. Nembach, M. Rickart, S. O. Demokritov, J. Fassbender, and B. Hillebrands. Angular dependence and phase diagrams of exchange-coupled epitaxial $ni_{81}fe_{19}/fe_{50}mn_{50}$(001) bilayers. Phys. Rev. B., 65(22):224423, Jun 2002.

[96] R. P. Michel, A. Chaiken, C. T. Wang, and L. E. Johnson. Exchange anisotropy in epitaxial and polycrystalline nio/nife bilayers. Phys. Rev. B, 58(13):8566–8573, Oct 1998.

[97] B. H. Miller and E. Dan Dahlberg. Use of the anisotropic magnetoresistance to measure exchange anisotropy in co/coo bilayers. Appl. Phys. Lett., 69:3932, 1996.

[98] P. Miltényi, M. Gierlings, J. Keller, B. Beschoten, G. Güntherodt, U. Nowak, and K. D. Usadel. Diluted antiferromagnets in exchange bias: Proof of the domain state model. Phys. Rev. Lett., 84(18):4224–4227, 2000.

[99] Peter Miltényi. Mikroskopischer ursprung der austauschkopplung in ferromagnetischen/antiferromagnetischen schichten. PHD Thesis, Aachen, 2000.

[100] A. Misra, U. Nowak, and K. D. Usadel. Control of exchange bias by diluting the antiferromagnetic layer. J. Appl. Phys., 93(10):6593–6595, 2003.

[101] A. Misra, U. Nowak, and K. D. Usadel. Structure of domains in an exchange-bias model. J. Appl. Phys., 95(3):1357–1363, 2004.

[102] A. Mougin, T. Mewes, M. Jung, D. Engel, A. Ehresmann, H. Schmoranzer, J. Fassbender, and B. Hillebrands. Local manipulation and reversal of the exchange bias field by ion irradiation in feni/femn double layers. Phys. Rev. B., 63:060409, 2001.

[103] A. Mumtaz, K. Maaz, B. Janjua, S. K. Hasanain, and Massimo F. Bertino. Exchange bias and vertical shift in cofe2o4 nanoparticles. J. Magn. Magn. Mater., 313:266–272, 2007.

[104] L. Néel. in: C. Dewitt, B. Dreyfus, P.D. de Gennes (Eds.), Low Temperature Physics. "Gordon and Beach, New York", 1962.

[105] L. Néel. Etude théorique du couplage ferro-antiferromagn´etique dans les couches minces. Ann. Phys. (Paris), 2:61, 1967.

[106] V. I. Nikitenko, V. S. Gornakov, A. J. Shapiro, R. D. Shull, K. Liu, S. M. Zhou, , and C. L. Chien. Asymmetry in elementary events of magnetization reversal in a ferromagnetic/antiferromagnetic bilayer. Phys. Rev. Lett., 84:765, 2000.

[107] J. Nogues, D. Lederman, T. J. Moran, and Ivan K. Schuller. Positive exchange bias in fef$_2$-fe bilayers. Phys. Rev. Lett., 76:4624, 1996.

[108] J. Nogues, C. Leighton, and Ivan K. Schuller. Correlation between antiferromagnetic interface coupling and positive exchange bias. Phys. Rev. B., 61(2):1315–1317, 2000.

[109] J. Nogues and I. K. Schuller. Exchange bias. J. Magn. Magn. Mater., 192:203, 1999.

[110] J. Nogués, J. Sort, V. Langlais, V. Skumryev, S. Suriñach, J. S. Muñoz, and M.D. Barób. Exchange bias in nanostructures. Physics Reports, 422(3):65, 2005.

[111] F. Nolting, A. Scholl, J. Stöhr, J. W. Seo, J. Fompeyrine, H. Siegwart, J.-P. Locquet, S. Anders, J. Lüning, E. E. Fullerton, M. F. Toney, M. R. Scheinfeink, and H. A. Padmore. Direct observation of the alignment of ferromagnetic spins by antiferromagnetic spins. Nature, 405:767, 2000.

[112] P. Nordblad, J. Mattsson, and W. Kleemann. Low field excess magnetisation in fe0.7mg0.3cl2. J. Magn. Magn. Mater., 140-144:1553–1554, 1995.

[113] G. Nowak. Diploma Thesis, Bochum, 2004.

[114] G. Nowak, A. Remhof, F. Radu, A. Nefedov, H.-W. Becker, and H. Zabel. Structural and magnetic properties of stoichiometric epitaxial coo/fe exchange bias bilayers. Phys. Rev. B., 75:174405, 2007.

[115] U. Nowak, A. Misra, and K. D. Usadel. Domain state model for exchange bias. J. Appl. Phys., 89(11):7269–7271, 2001.

[116] U. Nowak, A. Misra, and K. D. Usadel. Modeling exchange bias microscopically. J. Magn. Magn. Mater., 240(1-3):243–247, 2002.

[117] U. Nowak, K. D. Usadel, J. Keller, P. Miltényi, B. Beschoten, and G. Güntherodt. Domain state model for exchange bias. i. theory. Phys. Rev. B., 66:014430, 2002.

[118] H. Ohldag, T. J. Regan, J. Stöhr, A. Scholl, F. Nolting, J. Lüning, C. Stamm, S. Anders, and R. L. White. Spectroscopic identification and direct imaging of interfacial magnetic spins. Phys. Rev. Lett., 87(24):247201, Nov 2001.

[119] H. Ohldag, A. Scholl, F. Nolting, E. Arenholz, S. Maat, A. T. Young, M. Carey, and J. Stohr. Correlation between exchange bias and pinned interfacial spins. Phys. Rev. Lett., 91(1):017203, 2003.

[120] Hendrik Ohldag, Hongtao Shi, Elke Arenholz, Joachim Stöhr, and David Lederman. Parallel versus antiparallel interfacial coupling in exchange biased co/fef$_2$. Phys. Rev. Lett., 96(2):027203, 2006.

[121] D. Paccard, C. Schlenker, O. Massenet, R. Montmory, and A. Yelon. A new property of ferromagnetic-antiferromagnetic coupling. Phys. Status Solidi, 16:301, 1966.

[122] Cristian Papusoi, Jan Hauch, Marian Fecioru-Morariu, and Gernot Guntherodt. Tuning the exchange bias of soft metallic antiferromagnets by inserting nonmagnetic defects. J. Appl. Phys., 99(12):123902, 2006.

[123] E.C. Passamani, C. Larica, C. Marques, A.Y. Takeuchi, J.R. Proveti, and E. Favre-Nicolin. Large vertical loop shifts in mechanically synthesized (mn,fe)$_2$o$_{3-t}$ nanograins. J. Magn. Magn. Mater., 314:21–20, 2007.

[124] A. Paul, E. Kentzinger, U. Rücker, D. E. Bürgler, and P. Grünberg. Sequence, symmetry, and magnetic fluctuations of the magnetization reversal in exchange-biased multilayers. Phys. Rev. B., 70:224410, 2004.

[125] Li Pi, Shixiong Zhang, Shun Tan, and Yuheng Zhang. Exchange bias-like phenomenon in srruo3. Appl. Phys. Lett., 88:102502, 2006.

[126] C. Prados, E. Pina, A. Hernando, and A. Montone. Reversal of exchange bias in nanocrystalline antiferromagnetic-ferromagnetic bilayers. J. Phys.: Condens. Matter, 14:10063, 2002.

[127] Zoran Radović, Marko Ledvij, Ljiljana Dobrosavljević-Grujić, A. I. Buzdin, and John R. Clem. Transition temperatures of superconductor-ferromagnet superlattices. Phys. Rev. B., 44:759, 1991.

[128] F. Radu, M. Etzkorn, V. Leiner, T. Schmitte, A. Schreyer, K. Westerholt, and H. Zabel. Polarised neutron reflectometry study of co/coo exchange biased multilayers. Appl. Phys. A, 74:"S1570", 2002.

[129] F. Radu, M. Etzkorn, T. Schmitte, R. Siebrecht, A. Schreyer, K. Westerholt, and H. Zabel. Asymmetric magnetization reversal on exchange bias coo/co bilayers. J. Magn. Magn. Mater., 240:251, 2002.

[130] F. Radu, M. Etzkorn, R. Siebrecht, T. Schmitte, K. Westerholt, and H. Zabel. Interfacial domain formation during magnetization reversal in exchange-biased coo/co bilayers. Phys. Rev. B., 67:134409, 2003.

[131] F. Radu, A. Nefedov, J. Grabis, G. Nowak, A. Bergmann, and H. Zabel. Soft x-ray magnetic scattering studies on fe/coo exchange bias bilayers. J. Magn. Magn. Mater., 200:206, 2006.

[132] F. Radu, A. Vorobiev, J. Major, H. Humblot, K. Westerholt, and H. Zabel. Spin-resolved off-specular neutron scattering from magnetic domain walls using the polarized ^{3}he gas spin filter. Physica B, 335:63–67, 2003.

[133] F. Radu, A. Westphalen, K. Theis-Bröhl, and H. Zabel. Quantitative description of the azimuthal dependence of the exchange bias effect. J. Phys.: Condens. Matter, 18:L29–L36, 2006.

[134] Florin Radu. Fundamental aspects of exchange bias effect. PhD thesis, Ruhr-University Bochum, 2005.

[135] M. D. Rechtin and B. L. Averbach. Long-range magnetic order in coo. Phys. Rev. B., 6:4294, 1972.

[136] T. J. Regan, H. Ohldag, C. Stamm, F. Nolting, J. Lüning, J. Stöhr, and R. L. White. Chemical effects at metal/oxide interfaces studied by x-ray-absorption spectroscopy. Phys. Rev. B., 64(21):214422, Nov 2001.

[137] S. Roy, M. R. Fitzsimmons, S. Park, M. Dorn, O. Petracic, Igor V. Roshchin, Zhi-Pan Li, X. Batlle, R. Morales, A. Misra, X. Zhang, K. Chesnel, J. B. Kortright, S. K. Sinha, and Ivan K. Schuller. Depth profile of uncompensated spins in an exchange bias system. Phys. Rev. Lett., 95(4):047201, 2005.

[138] Mark Rubinstein, Peter Lubitz, and Shu-Fan Cheng. Ferromagnetic-resonance field shift in an exchange-biased coo/ni80fe20 bilayer. J. Magn. Magn. Mater., 195:299–306, 1999.

[139] S. Sahoo, S. Polisetty, Ch. Binek, and A. Berger. Dynamic enhancement of the exchange bias training effect. J. Appl. Phys., 101(5):053902, 2007.

[140] Elena-Lorena Salabas, Anja Rumplecker, Freddy Kleitz, Florin Radu, and Ferdi Schüth. Exchange anisotropy in nanocasted co3o4 nanowires. Nano Letters, 6(12):2977–2981, 2006.

[141] C. Sanchez-Hanke and C. C. Kao. An element-sensitive hysteresis loop study of an exchange-biased co/nio bilayer. J. Magn. Magn. Mater., 226-230:1803, 2001.

[142] C. Schlenker and D. Paccard. Couplages ferromagnétiques-antiferromagnétiques: étude des contractions de cycles dhystérésis a láide dún traceur de cycle trés basses fréquences. J. Phys., 28:611, 1967.

[143] C. Schlenker, S. S. P. Parkin, J. C. Scott, and K. Howard. Magnetic disorder in the exchange bias bilayered feni-femn system. J. Magn. Magn. Mater., 54-57:801, 1986.

[144] Till Schmitte. Bragg-moke and vector-moke investigations: Magnetic reversal of patterned microstripes. PhD thesis, Ruhr-University Bochum, 2002.

[145] A. Scholl, M. Liberati, E. Arenholz, H. Ohldag, and J. Stöhr. Creation of an antiferromagnetic exchange spring. Phys. Rev. Lett., 92:247201, 2004.

[146] A. Scholl, F. Nolting, J. W. Seo, H. Ohldag, J. Stöhr, S. Raoux, J.-P. Locquet, and J. Fompeyrine. Domain-size-dependent exchange bias in co/lafeo$_3$. Appl. Phys. Lett., 85:174428, 2004.

[147] G. Scholten, K. D. Usadel, and U. Nowak. Coercivity and exchange bias of ferromagnetic/antiferromagnetic multilayers. Phys. Rev. B., 71(6):064413, 2005.

[148] T. C. Schulthess and W. H. Butler. Consequences of spin-flop coupling in exchange biased films. Phys. Rev. Lett., 81(20):4516–4519, 1998.

[149] T. C. Schulthess and W. H. Butler. Coupling mechanisms in exchange biased films (invited). J. Appl. Phys., 85(8):5510–5515, 1999.

[150] Y. Shen, Y. Wu, H. Xie, K. Li, J. Qiu, , and Z. Guo. Exchange bias of patterned nife/irmn film. J. Appl. Phys., 91:8001, 2002.

[151] Hongtao Shi, David Lederman, and Eric E. Fullerton. Exchange bias in $fe_xzn_{1-x}f_2$/co bilayers. JAP, 91(10):7763–7765, 2002.

[152] Hongtao Shi, Zhongyuan Liu, and David Lederman. Exchange bias of polycrystalline co on single-crystalline fe[sub x]zn[sub 1 - x]f[sub 2] thin films. Phys. Rev. B., 72(22):224417, 2005.

[153] J. C. Slonczewski. In: Research Memorandum RM 003.111.224, IBM Research Center Poughkeepsie, unpublished, 1956.

[154] R. L. Stamps. Dynamic magnetic hysteresis and anomalous viscosity in exchange bias systems. Phys. Rev. B., 61(18):12174–12180, 2000.

[155] R. L. Stamps. Mechanisms for exchange bias. J. Phys. D:Appl. Phys., 33:R247, 2000.

[156] K. Steenbeck, R. Mattheis, and M. Diegel. Antiferromagnetic energy loss and exchange coupling of irmn/cofe films: experiments and simulations. J. Magn. Magn. Mater., 279:317, 2004.

[157] W. Stoecklein, S. S. P. Parkin, and J. C. Scott. Ferromagnetic resonance studies of exchange-biased permalloy thin films. Phys. Rev. B, 38(10):6847–6854, Oct 1988.

[158] J. Stöhr. Nexafs spectroscopy, volume 25 of Springer Series in Surface Sciences. ”Springer, Heidelberg”, 1992.

[159] E. C. Stoner and E. P. Wohlfarth. Interpretation of high coercivity in ferromagnetic materials. Nature, 160:650, 1947.

[160] E. C. Stoner and E. P. Wohlfarth. A mechanism of magnetic hysteresis in heterogeneous alloys. Philosophical Transactions of the Royal Society of London. Series A, Mathematical and Physical Sciences, 240(826):599–642, 1948.

[161] Kentaro Takano, R. H. Kodama, A. E. Berkowitz, W. Cao, and G. Thomas. Interfacial uncompensated antiferromagnetic spins: Role in unidirectional anisotropy in polycrystalline $ni_{81}fe_{19}$/coo bilayers. Phys. Rev. Lett., 79(6):1130–1133, 1997.

[162] S. G. E. te Velthuis, A. Berger, G. P. Felcher, B. K. Hill, and E. Dan Dahlberg. Training effects and the microscopic magnetic structure of exchange biased co/coo bilayers. J. Appl. Phys., 87:5046, 2000.

[163] K. Temst, M.J. Van Bael, J. Swerts, H. Loosvelt, E. Popova, D. Buntinx, J. Bekaert, C. Van Haesendonck, Y. Bruynseraede, R. Jonckheere, and H. Fritzsche. Polarized neutron reflectometry on lithographically patterned thin film structures. Superlattices and Microstructures, 34:87, 2003.

[164] K. Temst, E. Girgis, R. D. Portugal, H. Loosvelt, E. Popova, M.J. Van Bael, C. Van Haesendonck, H. Fritzsche, M. Gierlings, L. H.A. Leunissen, and R. Jonckheere. Mmagnetization and polarized neutron reflectivity experiments on patterned exchange bias structures. Eur. Phys. J. B, 45:261–266, 2005.

[165] K. Temst, E. Popova, H. Loosvelt, M. J. Van Bael, S. Brems, Y. Bruynseraede, C. Van Haesendonck, H. Fritzsche, M. Gierlings, L. H. A. Leunissen, and R. Jonckheere. The influence of finite size and shape anisotropy on exchange bias: A study of patterned co/coo nanostructures. J. Magn. Magn. Mater., 304:”14–18”, 2006.

[166] André Thiaville. Extensions of the geometric solution of the two dimensional coherent magnetization rotation model. J. Magn. Magn. Mater., 182(1-2):5, 1998.

[167] C. Tsang, N. Heiman, and K. Lee. Exchange induced unidirectional anisotropy at femn-ni_80fe_20 interfaces. J. Appl. Phys, 52:2471, 1981.

[168] Y. Tsuchiya, K. Kosuge, S. Yamaguchi, and N. Nakayama. Exchange anisotropy of crnx/feny/crnx trilayer thin films prepared by reactive sputtering. Mater. Trans. JIM, 38:91, 1997.

[169] M. Tsunoda, Y. Tsuchiya, M. Konoto, and M. Takahashi. Microstructure of antiferromagnetic layer affecting on magnetic exchange coupling in trilayered ni-fe/25 at J. Magn. Magn. Mater., 171:29, 1997.

[170] C. Tusche, H. L. Meyerheim, F. U. Hillebrecht, and J. Kirschner. Evidence for a mixed conio layer at the co/nio(001) interface from surface x-ray diffraction. Phys. Rev. B., 73(12):125401, 2006.

[171] S. Urazhdin and C. L. Chien. Effects of antiferromagnetic spin rotation on the anisotropy of ferromagnetic/antiferromagnetic bilayers. Phys. Rev. B., 71(22):220410, 2005.

[172] V. K. Valev, M. Gruyters, A. Kirilyuk, and Th. Rasing. Direct observation of exchange bias related uncompensated spins at the coo/cu interface. Phys. Rev. Lett., 96(6):067206, 2006.

[173] H. Wang, T. Zhu, K. Zhao, W. N. Wang, C. S. Wang, Y. J. Wang, and W. S. Zhan. Surface spin glass and exchange bias in fe[sub 3]o[sub 4] nanoparticles compacted under high pressure. Phys. Rev. B., 70(9):092409, 2004.

[174] U. Welp, S. G. E. te Velthuis, G. P. Felcher, T. Gredig, and E. D. Dahlberg. Domain formation in exchange biased co/coo bilayers. J. Appl. Phys., 93:7726, 2003.

[175] N. R. Werthamer. Theory of the superconducting transition temperature and energy gap function of superposed metal films. Phys. Rev., 132:2440, 1963.

[176] K. Westerholt, U. Geiersbach, and A. Bergmann. Exchange bias in $[co2mnge/au]_n$, $[co2mnge/cr]_n$ and $[co2mnge/cu2mnal]_n$ multilayers. J. Magn. Magn. Mater., 257:239, 2003.

[177] Haiwen Xi and Robert M. White. Antiferromagnetic thickness dependence of exchange biasing. Phys. Rev. B, 61(1):80–83, Jan 2000.

[178] Yong-Goo Yoo, Mun-Cheol Paeka, Seong-Gi Min, and Seong-Cho Yu. Angular dependence of exchange coupling in nife/spacer/irmn trilayer structures. J. Magn. Magn. Mater., 290-291:198, 2005.

[179] J. Yu, A. D. Kent, and S. S. P. Parkin. Exchange biasing in polycrystalline thin film microstructures. J. Appl. Phys., 87:5049, 2000.

[180] O. Zaharko, P. M. Oppeneer, H. Grimmer, M. Horisberger, H.-Ch. Mertins, D. Abramsohn, F. Schäfers, A. Bill, and H.-B. Braun. Exchange coupling in fe/nio/co film studied by soft x-ray resonant magnetic reflectivity. Phys. Rev. B., 66(13):134406, Oct 2002.

[181] K. Zhang, T. Zhao, and F. Fujiwara. Training effect of exchange biased iron-oxide/ferromagnet systems. J. Appl. Phys., 89:6910, 2001.

[182] K. Zhang, T. Zhao, and F. Fujiwara. Training effect in ferro (f)/antiferromagnetic (af) exchange coupled systems: Dependence on af thickness. <u>J. Appl. Phys.</u>, 91:6902, 2002.